

Lattice Fokker Planck Method for Complex Fluids

A Thesis
Submitted for the Degree of
DOCTOR OF PHILOSOPHY

by
SHIWANI SINGH



ENGINEERING MECHANICS UNIT
JAWAHARLAL NEHRU CENTRE FOR ADVANCED SCIENTIFIC RESEARCH
(A Deemed University)
Bangalore – 560 064

MARCH 2015

Dedicated to my parents

DECLARATION

I hereby declare that the matter embodied in the thesis entitled “**Lattice Fokker Planck Method for Complex Fluids**” is the result of investigations carried out by me at the Engineering Mechanics Unit, Jawaharlal Nehru Centre for Advanced Scientific Research, Bangalore, India under the supervision of **Prof. Santosh Ansumali** and that it has not been submitted elsewhere for the award of any degree or diploma.

In keeping with the general practice in reporting scientific observations, due acknowledgment has been made whenever the work described is based on the findings of other investigators.

Shiwani Singh

CERTIFICATE

I hereby certify that the matter embodied in this thesis entitled “**Lattice Fokker Planck Method for Complex Fluids**” has been carried out by **Ms. Shiwani Singh** at the Engineering Mechanics Unit, Jawaharlal Nehru Centre for Advanced Scientific Research, Bangalore, India under my supervision and that it has not been submitted elsewhere for the award of any degree or diploma.

Prof. Santosh Ansumali
(Research Supervisor)

Acknowledgements

I would like to express my sincere gratitude to Prof. Santosh Ansumali for his constant support and encouragement during the course of my Ph. D. It was a pleasure to learn the intricacies of kinetic theory and lattice Boltzmann method from him. I am also grateful to Prof. Ganesh Subramanian for his invaluable comments and discussions. His insightful suggestions helped me a lot in understanding the polymer dynamics better.

I have learned a lot from the courses taught by Prof. Rama Govindarajan, Prof. Meheboob Alam and Prof. Rajesh Ganapathy. The discussions with Prof. H. C. Öttinger, Prof. Sauro Succi and Prof. Martin Kröger were very enlightening. I would like to extend my gratitude to Dhiraj, Siddharth and Chakri for helping me on various computational issues from time to time.

I thank my EMU-mates especially Sumesh, Ponnu, Anubhab, Harish, Ratul, Dhiraj, Srikanth and Saikishan who helped me on numerous issues during the initial phase of my Ph. D. I enjoyed discussions on various topics with my other lab-mates: Reddy, Vicky and Rashmi.

I am indebted to Manasa and Garima for their immense support through my highs and lows. Special thanks to my friends Manjusha, Chandan, Palak, Ashvini and Shiny who made my life enjoyable in JNC. I thank our administrative officer, A. Jayachandra, Dr. Princy, library, complab, hostel and other admin staff for their cooperation.

Finally, I wish to thank my parents, brother and Deepak for their unconditional support and encouragement.

Abstract

The constitutive relations used in numerical modeling of coupled polymeric solution are mostly obtained by a pre-averaging approximation of the underlying micro-mechanical model for polymer. However, in time-dependent elongational flows, such models are known to deviate from the predictions obtained by the original micro-mechanical models. An alternate approach, where one couples the macroscopic flow solver with microscopic Brownian dynamics simulations, is increasingly being used. In such an approach, the ensemble-averaged configuration statistics are obtained by solving the system of Langevin equations for the polymer which are then coupled with the Navier-Stokes description for the solvent.

An approach is developed where both the polymer and the solvent are modeled at the kinetic level. It is argued that although one is interested in the slow dynamics of configuration distribution function, invoking the inertia of the polymer can be useful to develop efficient numerical schemes. Basically, in the inertial framework, there is a wide separation between the time scale associated with the rapid momentum relaxation of the beads comprising a polymer molecule and the slow time scale associated with the restoring action of spring force. Hence, the precise nature of the short-time momentum relaxation process of individual polymer molecule does not affect the slow dynamics in configuration space. Thus, for numerical convenience, the actual diffusive dynamics in momentum space, and described by Fokker Planck equation, can be replaced by relaxation dynamics of the BGK type. The BGK-type kinetic model is further modified in such a way that the effects of the hydrodynamic interaction are recovered. Applying the lattice Boltzmann formulation to the resulting kinetic equations with a BGK relaxation term, we determine the bulk rheological properties for two canonical flow situations viz. simple shear and extensional flows.

Finally, in order to extend the scheme for non-homogeneous flows, the system is modeled as two component mixture consisting of FENE dumbbells and solvent gas. This system is contrasted with the gaseous mixture case where the Boltzmann type kinetic models are well developed. An extension of two component Boltzmann equations and associated models are developed for polymer-solvent mixture case. The model is then validated numerically for the case of one way coupling with the imposed plane Poiseuille flow.

List of Figures

3.1	Discrete velocity sets.	22
3.2	Schematic of D2Q9 velocity set on two dimensional grid.	23
3.3	The stream-function for grid size of 312×312 for lid driven cavity.	24
3.4	Variation of density with time in LB simulation at the center of domain for $Re=50$, $Ma=0.1$ and grid-size = 700×700	28
3.5	L_1 and L_2 norm for velocity in x direction at $Re=250$ and $Ma=0.05$ for Taylor-Green vortex as a function of grid size	28
3.6	L_1 and L_2 norm for velocity in x direction at $Re = 4000$ and $Ma = 0.05$ for Taylor-Green vortex with different grid size	29
3.7	Streamline plot of cavity flow for grid-size= 200×200 . The isothermal model (left) is patently unstable, while the energy-conserving one (right) shows no sign of instability.	30
3.8	Streamline plot of cavity flow for grid-size= 256×256 . The isothermal model is still unstable, although to a less extent than for the case 200×200 . The energy-conserving one shows also a small improvement over the 200×200 , especially around the top-left corner	31
3.9	Streamline plot of cavity flow for grid-size= 312×312	31
3.10	Scheme showing the relaxation of f to f^{eq} through a quasi-equilibrium state f^*	33
3.11	Vorticity field at convection time= 1 on 200×200 grid.	34
4.1	Schematic of the three elementary structures used in velocity-space models.	36
4.2	Schematic of D2Q9 velocity set on two dimensional physical grid.	37
4.3	2D cross-section of real 3D simulation domain with bounce-back boundary condition	38
4.4	2D implementation of the bounce-back boundary condition. Circle are nodes inside the FENE sphere and filled squares are the nodes outside the sphere	38
4.5	Steady state value of the shear viscosity and the first normal stress coefficient for different Wi for an extensibility parameter $b=50$. Circles, present scheme with 24^3 as the number of grid points; filled diamonds symbols, present scheme with 32^3 as the number of grid points; square, Brownian Dynamics (Herrchen & Öttinger 1997); dashed line denotes the small Wi -expansion for FENE dumbbells, while the solid line denotes the predictions of the FENE-p model.	40

4.6	Time evolution of the shear viscosity and the first normal stress coefficient for $Wi=1.0$. Dashed lines, present scheme with 32^3 as the number of grid points; dots connected with lines, Brownian Dynamics for FENE dumbbells (Herrchen & Öttinger 1997); continuous lines, numerical solution for FENE-p (Herrchen & Öttinger 1997).	41
4.7	Time evolution of the shear viscosity and the first normal stress coefficient for $Wi=10.0$. Dashed lines, present scheme with 32^3 as the number of grid points; dots connected with lines, Brownian Dynamics for FENE dumbbells (Herrchen & Öttinger 1997); continuous lines, numerical solution for FENE-p (Herrchen & Öttinger 1997).	42
4.8	Time evolution of the second normal stress coefficient for $Wi=1,3,10$. Continuous lines, present scheme with 32^3 as the number of grid points; dots connected with lines, Brownian Dynamics for FENE (Herrchen & Öttinger 1997).	42
4.9	Steady state value of the shear viscosity and first normal stress coefficient at $Wi=1$ and 10 for $b=50$ with the grid spacing dX defined as $L/(\text{Number of grid points in each direction})$	43
4.10	Percentage error in shear viscosity and first normal stress coefficient for different Wi with two different grid sizes ($b=50$).	45
4.11	Probability density $\psi(\mathbf{Q})$, as a function of $ \mathbf{Q} $, at steady state for simple shear flow for different Wi ($b=50$).	46
4.12	Time evolution of the second normal stress coefficient for $Wi=1.0$ and $Wi=10.0$ for different grid sizes. Dashed lines, present scheme with 32^3 as the number of grid points; continuous lines, present scheme with 24^3 as the number of grid points; dots connected with lines, Brownian Dynamics for FENE (Herrchen & Öttinger 1997).	47
4.13	Percentage error in the steady state value of shear viscosity and first normal stress coefficient coefficient for different LB models for 24^3 grid points for $b=50$	48
4.14	Time evolution of the second normal stress coefficient for $Wi=1.0$ for three different LB models with 24^3 and 32^3 grid points for $b=50$	48
4.15	Time evolution of the second normal stress coefficient for $Wi=10.0$ for three different LB models with 24^3 and 32^3 grid points for $b=50$	49
4.16	Steady state value of extensional viscosity with different Wi for extensibility parameter $b=50$. Circle, present scheme with 24^3 as the number of grid points; plus symbol, present scheme with 32^3 as the number of grid points; diamond symbols, present scheme with 50^3 as the number of grid points; hexagon symbol, present scheme with 75^3 as the number of grid points; square, Brownian Dynamics (Herrchen & Öttinger 1997); dashed lines asymptotic expansion for FENE and continuous line expansion for FENE-p.	50
4.17	Probability density $\psi(\mathbf{Q})$ at steady state with different $ \mathbf{Q} $, and the root mean square extension as a function of Wi , showing the coil-stretch transition. ($b=50$)	50
4.18	Steady state value of the extensional viscosity with respect to dX at $Wi = 0.3$ and 3.0 and $b=50$	51

4.19	Percentage error in the steady state value of extensional viscosity for two different grid sizes. ($b=50$)	52
4.20	Time evolution of the extensional viscosity for $Wi=0.3$. Dashed lines, present scheme with 32^3 as the number of grid points; dots connected with lines, Brownian Dynamics for FENE (Herrchen & Öttinger 1997)) continuous lines, numerical solution for FENE-p (Herrchen & Öttinger 1997).	52
4.21	Time evolution of the extensional viscosity for $Wi=3.0$. Dashed lines, present scheme with 50^3 as the number of grid points; dots connected with lines, Brownian Dynamics for FENE (Herrchen & Öttinger 1997); continuous lines, numerical solution for FENE-p (Herrchen & Öttinger 1997).	52
4.22	Time evolution of the extensional viscosity and mean square extension, as well as polymer stress, with respect to mean square extension at $Wi=2,4,6$ for $b=50$	53
4.23	Time evolution of the (a) extensional viscosity and (b) mean square extension and (c) extensional viscosity with respect to mean square extension for $Wi=6.0$ and $b=50$. Dashed lines, present scheme; dots connected with lines, predictor corrector stochastic simulation for FENE (Lielens <i>et al.</i> 1999); continuous lines, numerical solution for FENE-p (Lielens <i>et al.</i> 1999).	54
4.24	Simulation time required to reach $t/\tau_R = 1$ with respect to the number of grid points in each direction.	55
5.1	(Color online) Steady state value of the shear viscosity and the first normal stress coefficient with different Wi for an extensibility parameter $b = 50$ and $h^* = 0.15$	62
5.2	Steady state value of the second normal stress coefficient with different Wi for an extensibility parameter $b = 50$ and $h^* = 0.15$	62
5.3	Time evolution of the shear viscosity and the first normal stress coefficient for $Wi = 1.0$ and 10 ($b = 50, h^* = 0.15$).	63
5.4	Time evolution of the second normal stress coefficient for $Wi = 1.0$ and 10 ($b = 50, h^* = 0.15$).	63
5.5	(Color online) Steady state value of the shear viscosity and the first normal stress coefficient with respect to different h^* as function of Wi for extensibility parameter $b = 50$. These calculations have been performed with 32 grid points in each direction.	63
5.6	Steady state value of the root mean square extension and shear viscosity as function of Wi for two values of $h^* = 0$ and 0.25 with extensibility parameter $b = 50$	64
5.7	Time evolution of first normal stress coefficient at $Wi=0.1$ and $h^* = 0.15$ at different resolution of present scheme as well as different number of trajectories for BD.	65
6.1	Scheme showing the relaxation of f to f^{eq} through a quasi-equilibrium state f^*	73
7.1	Schematic showing the polymer modeled as a dumbbell and solvent as a structureless particle.	77
7.2	Schematic of polymer configuration	79
7.3	Schematic showing different types of collision in binary gas mixture	79

7.4	Possible cross collision between solvent molecule and polymer dumbbell at location \mathbf{x}	80
7.5	Four dimensional configuration space for polymer dumbbell	89
7.6	The polymer density profiles at $Wi= 0.5, 1$ and 2 in plane Poiseuille flow in a channel of width $L= 10 \times l_0$ and a given x . The polymer density ρ_P is scaled by its value at the centerline of the channel ρ_c . The number of grid point taken in Q-space is 20×20	90

List of Tables

3.1	Comparison of the primary vortex and on the lower right secondary vortex. . .	24
3.2	Error as a function of wavenumber	30
3.3	Percentage error in stream function value at center vortex at $Ma = 0.05$ and $Re = 5000$	32
3.4	Percentage error in stream function value at center vortex at $Ma = 0.087$ and $Re = 5000$	32
4.1	Steady state value of shear viscosity and first normal stress-coefficient at $Wi=1.0$ and 10.0 for $b=50$ with different grid sizes	44
4.2	Weights for different velocity-space models	46
5.1	CPU time required to reach $t = \tau_R$ at different resolution of present scheme as well as different number of trajectories for BD at fixed $dt=0.001$ ($Wi=0.1$, $b=50$ and $h^* = 0.15$).	65
7.1	Discrete velocity set	89

Contents

Abstract	vii
List of Figures	xii
List of Tables	xiii
1 Introduction	1
1.1 Introduction	1
1.2 Outline of the thesis	3
2 Fokker Planck for dilute polymer solution	5
2.1 Introduction	5
2.2 Smoluchowski Equation	6
2.3 Fokker Planck Equation for inertial dynamics	9
2.4 BGK Model for inertial Fokker Planck equation	12
2.5 Outlook	14
3 Lattice Boltzmann method	15
3.1 Introduction	15
3.2 Boltzmann Equation for Dilute Gases	16
3.3 Maxwell-Boltzmann Distribution	17
3.4 Bhatnager-Gross-Krook Collision Model	19
3.5 Lattice Boltzmann scheme for BGK Model	20
3.6 Time and space discretization scheme	22
3.7 Benchmarking of Isothermal case	24
3.8 Entropic Construction of the Equilibrium	24
3.8.1 Energy Conserving Discrete Equilibrium	25
3.9 Sound Propagation in Lattice Boltzmann Method	26
3.10 Taylor-Green vortex and convergence of Lattice Boltzmann	27
3.11 Cavity Flow	29
3.12 Quasi-equilibrium LB	32
3.12.1 Bench-marking via Doubly periodic Shear Layer	33
3.13 Outlook	34

4	Lattice Fokker Planck Method	35
4.1	Introduction	35
4.2	Discrete Polymer Kinetic Theory	35
4.2.1	Boundary condition	37
4.3	Results	39
4.3.1	Shear flow	39
4.3.2	Extensional Flow	47
4.4	Outlook	54
5	Lattice Fokker Planck Method with hydrodynamic interaction	57
5.1	Introduction	57
5.2	Hydrodynamic interaction	58
5.3	Boltzmann BGK formulation for inclusion of hydrodynamic interaction	60
5.4	Discrete formulation	61
5.5	Results	61
5.6	Outlook	64
6	Mixture hydrodynamics and kinetic models	67
6.1	Introduction	67
6.2	Two fluid continuum model for binary mixture	68
6.3	Kinetic Theory for gas mixture	69
6.3.1	BGK collision term	72
6.3.2	Quasi-equilibrium Model	73
7	Two fluid kinetic theory for polymer solution	75
7.1	Introduction	75
7.2	Polymer solution as a two component mixture	76
7.3	Kinetic Description	77
7.3.1	Collision in binary gas mixture	79
7.4	Collision in polymer-solvent mixture	80
7.4.1	Mass and Momentum Conservation Laws	82
7.5	Collision Modeling for polymer-solvent mixture	84
7.6	Numerical validation via one way coupling	87
7.6.1	Discrete formulation	88
7.6.2	Results	90
7.7	Conclusion	90
7.8	Appendix A: Chapman-Enskog Expansion	91
8	Outlook	95
	References	97

Chapter 1

Introduction

1.1 Introduction

The numerical modeling involving flow of complex fluids such as polymeric liquids often relies on coupling approximate constitutive relations for the stress tensor, typically obtained via approximate representations of underlying micro-mechanical model for the individual polymer molecules (Bird *et al.* 1987*a,b*; Larson 1988; Keunings 1997; Lielens *et al.* 1998, 1999) with a Navier-Stokes description for the solvent. For example, the FENE-p constitutive model obtained via a pre-averaging approximation applied to a non-interacting finitely extensible non-linearly elastic (FENE) dumbbells, serving as mechanical models for the polymer molecules, is often used for simulating turbulence in dilute polymer solutions (Sureshkumar *et al.* 1997; Dimitropoulos *et al.* 2005; Chokshi & Kumaran 2007). However, such constitutive models are not only cumbersome to solve numerically, their validity itself is questionable in case of the unsteady strong (extensional) flows (Keunings 1997; Doyle *et al.* 1998; Lielens *et al.* 1999). An approach, termed as CONNFESSIT (The Calculation of Non-Newtonian Flow: Finite Elements and Stochastic Simulation Technique), that combines the Finite Element method for solving fluid with stochastic method for polymer was introduced by Öttinger (Laso & Öttinger 1993; Feigl *et al.* 1995). This approach provides a means to incorporate various molecular models for polymer without having a closed form constitutive equation. Later this approach was extended by using the variance reduction method and now such a macro-micro coupling is routinely used (Hulsen *et al.* 1997; Öttinger *et al.* 1997; Bonvin & Picasso 1999; Jendrejack *et al.* 2004). In most of these approaches the macroscopic flow solver is coupled with microscopic Brownian dynamics simulations where one solves the system of Langevin equations for the polymer molecules to obtain ensemble-averaged configuration statistics (Öttinger 1996; Hulsen *et al.* 1997; Ma & Graham 2005).

In recent years mesoscale solvers based on the LB formulation have emerged as an alternative to direct solvers of Navier-Stokes equations (Chen & Doolen 1998; Succi 2001; Aidun & Clausen 2010). Due to the efficiency of such solvers, instead of macro-micro coupling, meso-micro coupling is increasingly being used for describing dilute polymer solutions wherein (LB) flow solvers replace macroscopic flow solvers (Ahlrichs & Dünweg 1998; Jendrejack *et al.* 2004; Pham *et al.* 2009; Ahlrichs & Dünweg 1999; Jain *et al.* 2012).

However, in the coupled simulation for polymer and solvent, a large part of the computational resources are spent in the polymer solver rather than the solvent solver (Somasi *et al.* 2002; Koppol *et al.* 2007). Therefore, it is desirable to devise an alternate direct approach to solve the underlying Smoluchowski equation for the configuration probability density for polymer (Risken 1996; Lozinski & Chauvière 2003; Chauvière & Lozinski 2004).

With this objective in mind, one may choose to directly discretize the corresponding Fokker

Planck (FP) collision operator by expanding it in terms of orthogonal polynomials (Moroni *et al.* 2006*a,b*; Melchionna *et al.* 2006). However, such approaches would be limited to extremely weak flows, since, for strong flows, a similar expansion of the distribution function would require the inclusion of a large number of terms with an increasing departure from equilibrium.

Other attempts to incorporate viscoelasticity at kinetic level revolved around the addition of a body force to the generalized Boltzmann/Bhatnagar-Gross-Krook (BGK) description (Giraud *et al.* 1998; Ispolatov & Grant 2002). However, it was shown by Wagner (2001) that such approaches are not expected to give the correct nonlinear rheology (the nonlinearity inherent in the convected derivatives that are an integral part of the constitutive equations for polymer solutions).

An alternate way to approach the same problem is to introduce the inertia of the beads. This inherently introduces a large separation of time scales in the system because there exists a fast time scale associated with momentum relaxation of the beads and a slow time scale associated with the restoring action of the spring force (Schieber & Öttinger 1988). Though one is interested in the slow dynamics of configuration probability, the inertial framework can be utilized to develop efficient numerical schemes. In this thesis, it is shown that the actual diffusive dynamics governing the momentum relaxation of a polymer molecule, and described by a Fokker-Planck operator, may be replaced by a BGK (Bhatnagar, Gross and Krook) type relaxation dynamics without affecting the slow (Smoluchowski) dynamics in configuration space. Essentially, due to the wide separation in time scales between the rapid momentum relaxation of the beads comprising a polymer molecule (modeled as a FENE-dumbbell) and that for a change in the corresponding configuration coordinates, the dynamics in configuration space is insensitive to the precise nature of the short-time momentum relaxation processes of individual polymer molecules. Thus, the actual diffusive dynamics in momentum space can be replaced by relaxation dynamics of the BGK type. This BGK type framework is used to develop numerical schemes similar to lattice Boltzmann (LB) method.

This thesis, takes the viewpoint that the LB method is an approximate technique for solving Boltzmann BGK equation using a discrete velocity set (Succi *et al.* 1992; Chen & Doolen 1998; Succi 2001; Aidun & Clausen 2010). The LB method is extended in this thesis for solving the relaxation dynamics of polymer molecule in phase space (Singh *et al.* 2011, 2013*b*). Similar to this thesis and associated publications (Singh *et al.* 2011, 2013*b*), Ammar (2010) independently developed solver for Smoluchowski equation without hydrodynamic interaction. The scheme is further developed to include the effects of hydrodynamic interaction between the beads which are known to affect the bulk rheological properties (for instance, they lead to a nonzero second normal stress difference in the FENE model). Unlike BD simulations where the inclusion of hydrodynamic interaction requires long computational time due to the calculation of square-root of diffusion tensor, the present deterministic solver is quite fast.

The efficiency of the discrete Fokker-Planck solver for homogeneous flows suggests that it might be quite advantageous to extend this approach to inhomogeneous systems. The kinetic models for binary gas mixture that properly account for the cross collisional exchange of momentum between the components of the mixture, are well established (Gross & Krook 1956; Hamel 1965; Garzó *et al.* 1989; Levermore *et al.* 1988; Goldman & Sirovich 2004; Arcidiacono *et al.*

2006). Though Curtiss & Bird (1996) has made an initial attempt to create a rigorous kinetic framework for polymer solution, the development of full phase space kinetic theory of polymer solution is still in elementary stage. The most difficult part in such kinetic framework is the asymmetry in the description appearing due to non-local nature of polymer micro-mechanical models. The reason behind this is that the structure-less solvent particles are governed by the one particle distribution function whereas the polymer modeled as dumbbell are governed by two particle distribution function. In this asymmetric description, the collision mechanism and hence the cross-collisional transfer of momentum is not straightforward. Other technical difficulties are how does polymeric stress arise in this kinetic description and for the two-particle distribution for polymer, what is the best way to define moments at a given location? Therefore, starting from Boltzmann description of collision between the polymer dumbbell and solvent molecule, a BGK type collision model for polymer-solvent mixture is proposed that can reproduce the desired continuum dynamics. It is emphasized the single relaxation BGK type model is not sufficient to reproduce independent transport coefficients. Therefore, similar to binary gas mixture, a quasi equilibrium based collision model is preferred which has tunable diffusivity as well as viscosity.

1.2 Outline of the thesis

Chapter 2 is organized as follows: For FENE dumbbells, the Langevin equation and the equivalent probabilistic description in terms of Smoluchowski equation is discussed. It is being pointed out that an alternate description for FENE dumbbell is a phase-space description of the inertial dynamics in terms of the Fokker-Planck equation. It is argued that existence of time scale separation and the fact that one is interested in only the slow dynamics provides an opportunity to create kinetic theory based deterministic solvers. Furthermore, it is shown that the actual diffusive dynamics of the Fokker-Planck equation, governing the momentum relaxation of a polymer molecule can be replaced by a BGK-type relaxation dynamics without affecting the slow (Smoluchowski) dynamics in configuration space.

In Chapter 3, a brief description of Boltzmann equation for dilute gases is provided. Bhatnager-Gross-Krook (BGK) approximation to the collision term is introduced and is justified by listing qualitative features of the Boltzmann collision term. The LB method, a successful method to solve BGK equation in low Mach number limit (ratio of flow speed and sound speed), is reviewed in this chapter. Furthermore, a variant of LB method where the energy conservation law is kept intact is discussed and shown to be more stable to the existing LB method. In this chapter, it is also shown that the energy conserving model created via entropic route of LB method leads to correct sound dynamics. The numerical simulations presented in this chapter also suggest that, as compared to the conventional isothermal models, the numerical stability range for energy conserving models is better.

In Chapter 4, a discrete formulation, similar to the lattice Boltzmann method is developed for the Fokker Planck equation. This formulation, termed as lattice Fokker Planck, is rigorously benchmarked by determining the bulk rheological properties for both steady as well as time-dependent shear and extensional flows at moderate to large Weissenberg numbers and are contrasted with the Brownian dynamics simulations.

In Chapter 5, this BGK-type kinetic model is further modified in such a way that the effects of the hydrodynamic interaction are recovered. Using shear flow, this extension of the scheme is tested where it is shown to reproduce the desired effects caused by hydrodynamic interaction on the bulk rheological properties. In contrary to its stochastic counter-part, where one needs to calculate the square root of diffusion tensor matrix at every time step, the proposed method is simple to implement as well as at least an order of magnitude faster than Brownian dynamics simulations.

In Chapter 6, with the objective to extend the scheme for non-homogeneous flows, binary gas mixture models are reviewed. At kinetic level, the single relaxation time BGK model is not adequate for gas mixture due to the fact that Schmidt number is not an independent parameter in such a model. Therefore, one needs a multi-relaxation time approach, based on the quasi-equilibrium models, to describe gas mixtures.

A Boltzmann type description is given for the collision between the solvent molecule and polymer dumbbell at kinetic level. A two-fluid model, based on quasi-equilibrium relaxation kinetic model, to couple the polymer phase with solvent phase is proposed in Chapter 7. The model is shown to recover the desired continuum description. The model is then validated numerically, for the case of one way coupling, with the imposed plane Poiseuille flow. The numerical formulation is done via LB method in four dimensional polymeric configuration space. The preliminary results show that the present scheme is indeed capable of capturing the inhomogeneous effects in terms of polymer migration towards the center of the channel.

In Chapter 8, the development of lattice Fokker Planck method is summarized. Future application of this formulation for inhomogeneous flows is discussed. The limitations and involved trade-off of the present formulation is also discussed. Finally, other possible extensions of present approach are discussed.

Chapter 2

Fokker Planck for dilute polymer solution

2.1 Introduction

Viscoelastic liquids such as polymer solutions exhibit striking differences compared to Newtonian fluids in a variety of flow situations. Even for very small disturbance, the polymer molecules are easily distorted and in high velocity fields they stretch to many times their undisturbed coiled state. Despite their ubiquity and importance, modeling the flows of polymeric liquids remains a challenge. The solution of the equations of motion for a polymeric fluid is not straightforward due to the absence of a generally valid constitutive relation between the polymeric stress tensor and the imposed rate of strain. Such a relation is derivable only in the linear response regime when the elastic behavior at the molecular level may be modeled as an ensemble of Hookean springs. The Hookean approximation breaks down in strong flows, where the polymer molecules are stretched significantly (Larson 1988), and the resulting non-linear elastic response precludes a closed-form constitutive relation (Bird *et al.* 1987*b*; Herrchen & Öttinger 1997). As a result, a formulation in terms of macroscopic fields alone requires closure approximations. While the simplest closures (Bird *et al.* 1980; Chilcott & Rallison 1988) are adequate for steady flows, even the most sophisticated ones are not quantitatively correct in unsteady flows with a complex stretch history (Lielens *et al.* 1998, 1999). In such cases, it is necessary to solve the equations of motion at the kinetic level.

One such approach for solving flexible polymers at kinetic level is BD simulations where one simulates the associated system of stochastic differential equations in the inertia-less limit (Laso & Öttinger 1993). The BD simulations of model micro-mechanical systems such as bead-spring models constitute an elegant tool for quantitative description of the polymer dynamics, even in highly non-equilibrium flow conditions. These simulations are based on numerical integration of the underlying stochastic differential equations describing the motion of individual beads of a single chain molecule. This methodology provides a rigorous and powerful tool, which is straightforward too, for investigating various linear and nonlinear effects such as emergence of the first normal stress coefficient, hydrodynamic interaction, excluded volume, or finite polymer extensibility (Öttinger 1994). In recent years, a micro-macro simulation of polymer dynamics, where the momentum balance equation of the solvent is solved together with the stochastic differential equations of motion for the configurations of polymer molecules, is regularly used. Since these simulations require the trajectories of very large ensembles of polymer chains, the development of an efficient simulation alternate to BD is needed for enhancing the capabilities of direct numerical simulation of complex phenomena such as polymeric drag reduction. Furthermore, since the statistical error in BD simulation is inversely proportion to the square-root

of the trajectory required, the method becomes highly expensive in the limit of weak flows.

An alternate approach is to directly discretize the underlying Smoluchowski Equation. However, such schemes are often cumbersome and are not very efficient. Another approach where one could expand the Fokker-Planck collision term in a truncated sequence of orthogonal is proposed in Ref. Moroni *et al.* (2006*a,b*). However, an analogous approach for polymer molecules would be limited to weak flows, since a similar expansion of the configuration distribution function would require the inclusion of a prohibitively large number of terms with an increasing departure from equilibrium (strong flows). The reason behind this is the absence of smallness parameter.

A model where the inertia of the beads is included in the equations of motion is proposed in Ref. Schieber & Öttinger (1988). The corresponding deterministic equation in this case is the FP equation in the phase space which has an attractive feature that there exist a large separation of characteristic time scales between the one associated with the momentum relaxation of the beads and the other associated with the restoring action of the spring force. Such FP equation appears very often in modeling of complex fluid as well as in other branches of physics and engineering. Most of numerical methods to solve these equations rely on the association with equivalent Langevin equation which leads to a stochastic solver via BD. A direct solver of FP (for low-dimensional problems) is desirable from the point of view of possible increase in speed from deterministic formulation.

In this Chapter, it is argued that due to the presence of wide separation in the time scales, the precise nature of short time dynamics of momentum relaxation does not affect the slow dynamics of the configuration probability density. A common feature in applications is that, one is often interested in the slow dynamics only. Hence, the short time diffusive dynamics of momentum relaxation can be modeled via relaxation mechanism of BGK type with the motivation to develop an efficient numerical scheme.

This chapter is organized as follows: In Sec.2.2, a review of the inertia-less Langevin equation and the equivalent description based on the configuration-space Smoluchowski equation for the dynamics of FENE dumbbells is presented. In Sec.2.3, the inertial dynamics of a polymer molecule in phase-space in terms of the FP equation is discussed. In Sec.2.4, a BGK-type relaxation mechanism is proposed as an alternate to the actual FP model, and it is shown that either models lead to the same governing equation for the configuration probability density at leading order. Finally, the Chapter is concluded in Sec.2.5.

2.2 Smoluchowski Equation

The mechanical model of a polymer molecule, developed in terms of a dumbbell consisting of two beads of equal mass m_B and friction constants ζ , and located at \mathbf{R}_1 and \mathbf{R}_2 in an incompressible homogeneous flow field, is briefly reviewed. The evolution equation for the i^{th} bead ($i = 1, 2$) in this model is given by

$$m_B \frac{d}{dt} \dot{\mathbf{R}}_i(t) = \mathbf{F}_i^c(t) - \underbrace{\zeta (\dot{\mathbf{R}}_i(t) - \mathbf{u}_i(t))}_{\mathbf{F}_i^D(t)} + \mathbf{F}_i^B(t), \quad (2.1)$$

where \mathbf{F}_i^c is the entropic spring force, \mathbf{F}_i^B is the Brownian force and \mathbf{F}_i^D is the drag force (Bird *et al.* 1987*b*). The fluid velocity at the location of the beads is given by $\mathbf{u}_i(t) = \mathbf{u}_0(t) + \boldsymbol{\kappa} \cdot \mathbf{R}_i(t)$ with $\mathbf{u}_0(t)$ being the mean velocity corresponding to the center of mass of the dumbbell and $\boldsymbol{\kappa}$ as the transpose of the velocity gradient tensor. Here, the length of the dumbbell is assumed to be much smaller than that characterizing the ambient flow; thus the flow is homogeneous and the elements of $\boldsymbol{\kappa}$ are therefore taken as constants. The Brownian force \mathbf{F}_i^B , due to the random collision of solvent molecules with the beads of the dumbbell, follows Gaussian statistics with the mean and the variance as

$$\langle F_{i\alpha}^B(t) \rangle = \mathbf{0}, \quad \langle F_{i\alpha}^B(t) F_{j\beta}^B(t') \rangle = 2k_B T \zeta \delta_{ij} \delta(t - t') \delta_{\alpha\beta}, \quad (2.2)$$

where k_B is the Boltzmann constant and T is the constant temperature. It is convenient to describe such a dynamics in terms of the center of mass coordinate $\mathbf{R} = (\mathbf{R}_1 + \mathbf{R}_2)/2$ and the end-to-end vector $\mathbf{Q} = \mathbf{R}_2 - \mathbf{R}_1$. The magnitude of the entropic spring force for a freely jointed bead-rod chain consisting of N beads is given by the inverse Langevin function (Bird *et al.* 1987*b*). In this work, a well known approximation for the inverse Langevin function, a simpler empirical form of the force law also referred to as the FENE (finitely extensible nonlinear elastic) spring force (Warner 1972), is used. In explicit form, the FENE spring force is

$$\mathbf{F}_1^c = -\mathbf{F}_2^c = \mathbf{F}^c = \frac{H\mathbf{Q}}{[1 - Q^2/Q_0^2]}, \quad (2.3)$$

where H is the Hookean spring constant and $Q_0 = \sqrt{b}$ is the length at full extension. The stochastic differential equations which describe the evolution of center of mass as well as relative motion is:

$$\begin{aligned} \frac{m_B}{\zeta} d\dot{\mathbf{R}}(t) &= \left[-\dot{\mathbf{R}} + \mathbf{u}_0(t) + \boldsymbol{\kappa}(t) \cdot \mathbf{R}(t) \right] dt + \sqrt{\frac{k_B T}{2\zeta}} [dW_2(t) + dW_1(t)], \\ \frac{m_B}{\zeta} d\dot{\mathbf{Q}}(t) &= \left[-\dot{\mathbf{Q}} + \boldsymbol{\kappa}(t) \cdot \mathbf{Q}(t) - \frac{2}{\zeta} \mathbf{F}^c(t) \right] dt + \sqrt{\frac{2k_B T}{\zeta}} [dW_2(t) - dW_1(t)]. \end{aligned} \quad (2.4)$$

where W_μ ($\mu = 1, 2$) are the standard Wiener process (Van Kampen 1992; Öttinger 1996). In the inertia-less limit ($m_B/\zeta \rightarrow 0$), Eq. (2.4) simplifies as:

$$\begin{aligned} d\mathbf{R}(t) &= [\mathbf{u}_0(t) + \boldsymbol{\kappa}(t) \cdot \mathbf{R}(t)] dt + \sqrt{\frac{k_B T}{2\zeta}} [dW_2(t) + dW_1(t)], \\ d\mathbf{Q}(t) &= \left[\boldsymbol{\kappa}(t) \cdot \mathbf{Q}(t) - \frac{2}{\zeta} \mathbf{F}^c(t) \right] dt + \sqrt{\frac{2k_B T}{\zeta}} [dW_2(t) - dW_1(t)]. \end{aligned} \quad (2.5)$$

In order to understand the dynamics of the polymeric stress, it is convenient to represent the Langevin dynamics in terms of the equivalent Smoluchowski description (Doi & Edwards 1988). The Smoluchowski equation governing the dynamics of configuration probability density $\psi(\mathbf{Q}, t)$

is

$$\frac{\partial \psi}{\partial t} + \frac{\partial}{\partial Q_\alpha} \left(\kappa_{\alpha\beta} Q_\beta \psi - \frac{2}{\zeta} F_\alpha^c \psi \right) = \frac{2k_B T}{\zeta} \frac{\partial^2 \psi}{\partial Q^2}. \quad (2.6)$$

The dumbbell contributes to the stress via an intra-molecular force of tension or compression which is transmitted through the connector \mathbf{Q} . The expression for stress was provided by Kramer as (Kramers 1944, 1946):

$$\sigma_{\alpha\beta}^P = nH \left\langle \frac{Q_\alpha Q_\beta}{1 - Q^2/Q_0^2} \right\rangle - nk_B T \delta_{\alpha\beta}, \quad (2.7)$$

which is proportional to the conformation tensor $A_{\alpha\beta} = n \langle Q_\alpha Q_\beta \rangle$ in the limit of Hookean dumbbells ($Q_0 \rightarrow \infty$). Here, n is the number of polymer molecules per unit volume and the angular brackets denote an ensemble average of a quantity $\phi(\mathbf{Q})$ with respect to $\psi(\mathbf{Q}, t)$, being given as $\langle \phi \rangle = \int \phi \psi(\mathbf{Q}, t) d\mathbf{Q}$. By taking the required non-linear moment of Eq. (2.6), the equation governing the stress tensor may be derived as

$$\begin{aligned} \frac{\partial \sigma_{\alpha\beta}^P}{\partial t} - \left[\kappa_{\alpha\theta} \sigma_{\theta\beta}^P + \kappa_{\beta\theta} \sigma_{\theta\alpha}^P + nk_B T_0 (\kappa_{\alpha\beta} + \kappa_{\beta\alpha}) - \frac{2Hn}{Q_0^2} \kappa_{\gamma\theta} R_{\alpha\beta\gamma\theta} \right] \\ + \left[\frac{4H^2 n}{\zeta} Z_{\alpha\beta} - \frac{4H^2 n}{Q_0^2 \zeta} N_{\alpha\beta} \right] = \frac{2Hnk_B T_0}{\zeta} \left[\frac{\delta_{\alpha\beta}}{(1 - \frac{A_{\theta\theta}}{Q_0^2})} - \frac{(D+4)}{Q_0^2} Z_{\alpha\beta} + \frac{2}{Q_0^4} N_{\alpha\beta} \right]. \end{aligned} \quad (2.8)$$

It should be noted that the dynamics of the stress, given by Eq. (2.8), is not closed, and involves both the conformation tensor $A_{\alpha\beta}$ and a few other higher order moments defined as:

$$Z_{\alpha\beta} = \left\langle \frac{Q_\alpha Q_\beta}{(1 - \frac{Q^2}{Q_0^2})^2} \right\rangle, \quad R_{\alpha\beta\gamma\theta} = \left\langle \frac{Q_\alpha Q_\beta Q_\gamma Q_\theta}{(1 - \frac{Q^2}{Q_0^2})^2} \right\rangle \text{ and } N_{\alpha\beta} = \left\langle \frac{Q^2 Q_\alpha Q_\beta}{(1 - \frac{Q^2}{Q_0^2})^3} \right\rangle. \quad (2.9)$$

The dynamics of these quantities can themselves be framed using Eq. (2.6). For example the evolution equation for the conformation tensor is

$$\frac{\partial A_{\alpha\beta}}{\partial t} - \kappa_{\alpha\theta} A_{\theta\beta} - \kappa_{\beta\theta} A_{\theta\alpha} + \frac{4}{\zeta n} \sigma_{\alpha\beta}^P = 0. \quad (2.10)$$

Similarly, one can write the evolution equation for $Z_{\alpha\beta}$ and other high order moments too. However, as is typical of kinetic equations for the probability density (for instance, those encountered in the kinetic theory of gases or turbulence), the evolution equations for these moments will involve other higher-order moments, and the resulting moment hierarchy is not closed.

A widely used closure at the level of second moments, the so-called pre-averaging approximation that leads to the FENE-p (finite elastic nonlinear extensibility-Peterlin) force, is

$$\mathbf{F}_{\text{FENE-p}}^c = \frac{H\mathbf{Q}}{1 - \langle \frac{Q^2}{Q_0^2} \rangle}. \quad (2.11)$$

This approximation physically corresponds to only constraining the mean-squared length of the polymer molecules to be less than a certain maximum value, while still allowing for a Gaussian distribution of polymer configurations that include individual molecules of an extension

that can exceed the aforementioned maximum by an arbitrary amount. Such an interpretation is not unique. For example, the FENE-p approximation implies that the stress is entirely determined in terms of the set of second moments $\langle QQ \rangle$, and one could, in principle, have multiple configurational distributions that lead to the same second moments (Öttinger 1987). This pre-averaging approximation allows one to write polymeric stress as

$$\sigma_{\alpha\beta}^P = \frac{nHA_{\alpha\beta}}{1 - A_{\theta\theta}/Q_0^2} - nk_B T_0 \delta_{\alpha\beta}, \quad (2.12)$$

which is completely defined in terms of the conformation tensor alone. Although widely used in rheological modeling, FENE-P closure does not capture some of the complex rheological properties, like the transient second normal stress coefficient in unsteady simple shear flow (Herrchen & Öttinger 1997). This closure also fails in unsteady extension, predicting too fast a growth in the stress (Keunings 1997). Moreover, the computational methods used for solving FENE-P model (Eq. (2.10)) often require an artificial diffusivity for numerical stability (Sureshkumar *et al.* 1997; Chokshi & Kumaran 2007).

2.3 Fokker Planck Equation for inertial dynamics

A more elaborate description of the dumbbell can be provided in terms of the phase space probability density $f(\mathbf{Q}, \dot{\mathbf{Q}}, t)$ where $\dot{\mathbf{Q}}$ denotes the velocity degrees of freedom (Bird *et al.* 1987b; Schieber & Öttinger 1988; Degond *et al.* 2009). The configurational probability density ψ can be computed in terms of f as

$$\psi(\mathbf{Q}, t) = \int f(\mathbf{Q}, \dot{\mathbf{Q}}, t) d\dot{\mathbf{Q}}, \quad (2.13)$$

and provides a coarse grained description. The evolution equation of $f(\mathbf{Q}, \dot{\mathbf{Q}}, t)$ is given in terms of the Fokker Planck equation (Degond *et al.* 2009) as

$$\frac{\partial}{\partial t} f(\mathbf{Q}, \dot{\mathbf{Q}}, t) + \dot{Q}_\alpha \frac{\partial}{\partial Q_\alpha} f(\mathbf{Q}, \dot{\mathbf{Q}}, t) = \frac{\partial}{\partial \dot{Q}_\alpha} \left[\frac{2}{m_B} F_\alpha^c + \frac{\zeta}{m_B} (\dot{Q}_\alpha - U_\alpha) + \frac{2k_B T \zeta}{m_B^2} \frac{\partial}{\partial \dot{Q}_\alpha} \right] f(\mathbf{Q}, \dot{\mathbf{Q}}, t), \quad (2.14)$$

where $U_\alpha = \kappa_{\alpha\beta} Q_\beta$ and the diffusive dynamics is now in velocity space with the velocity-space diffusivity being proportional to $k_B T \zeta / m_B^2$. It can be seen that, apart from the time $\tau_R = \zeta / 4H$ characterizing the restoring action of the spring force, an additional time-scale $\tau_I = m_B / \zeta$ related to the momentum relaxation of the beads is also present in the system. A distinct feature of such a description in the inertia-less limit ($m_B / \zeta \rightarrow 0$) is the presence of a large separation in time scales as $\tau_I \ll \tau_R$. This becomes apparent if one introduces two non-dimensional parameters, $\epsilon = \tau_I / \tau_R$, and the Weissenberg number $Wi = \kappa \tau_R$ (where κ is a characteristic shear rate defined such that $\kappa_{\alpha\beta} = \kappa \hat{\kappa}_{\alpha\beta}$ with $\hat{\kappa}_{\alpha\beta}$ being the non-dimensional form of the transpose of the velocity gradient tensor). In terms of these parameterization, Eq. (2.14) may be written in the

dimensionless form

$$\left[\frac{\partial f}{\partial \hat{t}} + \hat{Q}_\alpha \frac{\partial f}{\partial \hat{Q}_\alpha} \right] = \frac{1}{\epsilon} \underbrace{\left(\frac{\partial}{\partial \hat{Q}_\alpha} \left[\frac{1}{2} \hat{F}_\alpha^c + (\hat{Q}_\alpha - \text{Wi} \hat{U}_\alpha) + \frac{\partial}{\partial \hat{Q}_\alpha} \right] f \right)}_{\Omega}, \quad (2.15)$$

where the non-dimensional quantities are

$$\hat{t} = \frac{t}{\tau_R}, \quad \hat{Q} = \frac{\dot{Q}}{\sqrt{\frac{2k_B T}{m_B}}}, \quad \hat{Q} = \frac{Q}{\sqrt{\frac{2k_B T}{m_B}} \tau_R}, \quad \hat{F}^c = \frac{\dot{Q}}{1 - \frac{\dot{Q}^2}{2b\epsilon}} \text{ and } \hat{U} = \hat{\kappa}_{\alpha\beta} \hat{Q}_\beta, \quad (2.16)$$

and $b = HQ_0^2/k_B T$. Note that the time in Eq. (2.15) has been scaled with τ_R to emphasize the slower relaxation processes in configuration space. The dimensionless parameter ϵ which is the ratio of microscopic (inertial) to macroscopic time scales, may also be interpreted as the corresponding ratio of length scales, in the following manner:

$$\epsilon = \frac{\tau_I}{\tau_R} = \frac{4Hm_B}{\zeta^2} = 2 \left(\frac{\lambda_{MFP}}{l_0} \right)^2, \quad (2.17)$$

where the mean free path, the microscopic length scale $\lambda_{MFP} = (\sqrt{2k_B T/m_B})(m_B/\zeta)$ and $l_0 = \sqrt{(k_B T/H)}$. Thus, ratio ϵ is analogous to Kn^2 with Kn , the Knudsen number, defined as the ratio of the mean free path and a ‘‘macroscopic’’ length scale which is l_0 in the present context. Further, the solution of Eq. (2.15), at leading order is

$$\Omega = 0 \implies f^{\text{eq}}(\mathbf{Q}, \dot{\mathbf{Q}}, t) \rightarrow \psi(\mathbf{Q}, t) \left(\frac{1}{2\pi} \right)^{\frac{3}{2}} \exp \left[-\frac{\{\dot{Q}_\alpha - (\text{Wi} U_\alpha - F_\alpha^c/2)\}^2}{2} \right], \quad (2.18)$$

which reflects the rapid equilibration of the velocity degrees of freedom towards a mean that is sum of the imposed flow field and velocity due to the entropic spring force. Here onwards, the hat is removed for simplicity. One may also analyze the dynamics in terms of the configuration probability density ψ and other higher moments ψu_α , $P_{\alpha\beta}$ and the third order moment $M_{\alpha\beta\gamma}(\mathbf{Q}, t)$ defined as

$$\psi u_\alpha(\mathbf{Q}, t) = \int \dot{Q}_\alpha f d\dot{\mathbf{Q}}, \quad P_{\alpha\beta}(\mathbf{Q}, t) = \int \dot{Q}_\alpha \dot{Q}_\beta f d\dot{\mathbf{Q}}, \quad M_{\alpha\beta\gamma}(\mathbf{Q}, t) = \int \dot{Q}_\alpha \dot{Q}_\beta \dot{Q}_\gamma f d\dot{\mathbf{Q}}. \quad (2.19)$$

The evolution equations for these moments are given by

$$\begin{aligned} \frac{\partial}{\partial t} \psi + \frac{\partial}{\partial Q_\alpha} (\psi u_\alpha) &= 0, \\ \frac{\partial}{\partial t} (\psi u_\alpha) + \frac{\partial}{\partial Q_\beta} (P_{\alpha\beta}) &= \frac{1}{\epsilon} (\psi \bar{v}_\alpha^* - \psi u_\alpha), \\ \frac{\partial}{\partial t} P_{\alpha\beta} + \frac{\partial}{\partial Q_\alpha} (M_{\alpha\beta\gamma}) &= \frac{2}{\epsilon} (\bar{P}_{\alpha\beta}^{\text{eq}} - P_{\alpha\beta}), \end{aligned} \quad (2.20)$$

with

$$\bar{v}_\alpha^* = \text{Wi} U_\alpha - \frac{F_\alpha^c}{2}, \quad \bar{P}_{\alpha\beta}^{\text{eq}} = \psi \delta_{\alpha\beta} + \frac{\psi}{2} (\bar{v}_\alpha^* u_\beta + \bar{v}_\beta^* u_\alpha), \quad (2.21)$$

where, the similarity with the conservation laws of hydrodynamics is apparent. In Eq.(2.20), the limit $\epsilon \ll 1$ leads to $u_\alpha = \bar{v}_\alpha^*$, which corresponds to an instantaneous momentum equilibration. As indicated earlier, one notes from the above system that the equation for the n^{th} order moment contains the $(n+1)^{\text{th}}$ order moment, necessitating a closure approximation. The detailed derivation of the required Smoluchowski equation from the FP equation for the polymeric case, using the above mentioned facts, can be found in Schieber & Öttinger (1988); Degond *et al.* (2009). Later in this chapter (see Sec. 2.4), it is shown that a Chapman-Enskog expansion of the kinetic equation results in the same Smoluchowski equation at the leading order. At this stage, it is worth pointing out, few important similarities and differences between the the present moment chain and the moment chains encountered in hydrodynamics as well as in the case of a diffusing Brownian particle.

- The space co-ordinates \mathbf{x} and the velocity coordinates \mathbf{v} for the case of hydrodynamics correspond, respectively, to the to end-to-end vector \mathbf{Q} and its time derivative $\dot{\mathbf{Q}}$ in the polymeric case.
- Unlike hydrodynamics, momentum is not a conserved variable for polymer dynamics. This is expected because momentum will be conserved for the fluid-polymer system as a whole and not for the polymer itself. An important consequence of absence of conservation law is that the zeroth moment, the configuration probability density ψ (which is a conserved quantity), is the only slow variable.
- The other dimensionless parameter, Weissenberg number, may be written as,

$$\text{Wi} = \kappa \tau_R \equiv \frac{\bar{v}^* \tau_R}{l_0} \equiv \frac{\text{Ma}}{\frac{2\sqrt{2Hm_B}}{\zeta}} \equiv \text{Re}, \quad (2.22)$$

where, the Mach number is defined as $\text{Ma} = \bar{v}^* / \sqrt{(2k_B T / m_B)}$. The Wi number in polymer dynamics is thus analogous to the Reynold number (Re) for hydrodynamics, where the latter characterizes the ratio of inertial force to viscous force (in hydrodynamics $\text{Re} = \text{Ma} / \text{Kn}$).

- A separation in time scales, corresponding to the configurational and momentum degrees of freedom, analogous to the above scenario exists for the case of a Brownian particle (Titulaer 1978; Subramanian & Brady 2004). In this case, the longer time scale corresponding to spatial diffusion, which for the Brownian particle with a characteristic dimension a , is a^2/D , D being the Stokes-Einstein diffusivity; thus, the analog of ϵ is the ratio $(m_B/\zeta)/(a^2/D)$, which may be written in the form $(m_B\kappa/\zeta)/(\kappa a^2/D) = \text{St}/\text{Pe}$ where $\text{St} = m_B\kappa/\zeta$ is the Stokes number. Thus, $\sqrt{(\text{St}/\text{Pe})}$ is the analog of ϵ (or Kn), while $\text{Pe} = \kappa a^2/D$ is the analog of the Weissenberg number. A systematic multiple-scale (or a Chapman-Enskog) procedure can then be employed, in the limit of small St/Pe , to obtain the physical-space

Smoluchowski equation from the phase-space Fokker-Planck (or Kramers-Chandrasekhar) equation for the Brownian particle. Interestingly, in the absence of flow there are no corrections to the diffusive dynamics in physical space at any order in St/Pe . In the presence of flow, the first correction is $O(St/Pe)$, and takes the form of an off-diagonal diffusivity (Subramanian & Brady 2004).

2.4 BGK Model for inertial Fokker Planck equation

The moment chain presented in the previous section suggests that the replacement of the Fokker Planck kernel with the simplified relaxational term of BGK type will not affect the slow dynamics. Thus, a kinetic equation of the BGK form

$$\frac{\partial f}{\partial t} + \dot{Q}_\alpha \frac{\partial f}{\partial Q_\alpha} = \frac{1}{\epsilon} (f^{eq}(\psi, \bar{\mathbf{v}}^*) - f), \quad (2.23)$$

is chosen, where the equilibrium distribution is

$$f^{eq} = \psi \left(\frac{1}{2\pi} \right)^{\frac{3}{2}} \exp \left[-\frac{(\dot{Q}_\alpha - \bar{v}_\alpha^*)^2}{2} \right], \quad (2.24)$$

and \bar{v}_α^* is still given by Eq. (2.21). The moment chain associated with Eq. (2.23) is

$$\begin{aligned} \frac{\partial \psi}{\partial t} + \frac{\partial(\psi u_\alpha)}{\partial Q_\alpha} &= 0, \\ \frac{\partial(\psi u_\alpha)}{\partial t} + \frac{\partial P_{\alpha\beta}}{\partial Q_\beta} &= \frac{1}{\epsilon} (\psi \bar{v}_\alpha^* - \psi u_\alpha), \\ \frac{\partial P_{\alpha\beta}}{\partial t} + \frac{\partial M_{\alpha\beta\gamma}}{\partial Q_\gamma} &= \frac{1}{\epsilon} (\hat{P}_{\alpha\beta}^{eq} - P_{\alpha\beta}), \end{aligned} \quad (2.25)$$

where $\hat{P}_{\alpha\beta}^{eq} = \psi \delta_{\alpha\beta} + \psi \bar{v}_\alpha^* \bar{v}_\beta^*$. As was the case for the the moment hierarchy obtained from the Fokker-Planck dynamics, given by Eq. (2.20), the momentum is no longer a conserved variable in Eq. (2.25). One may also see that the relaxation rates for the higher-order moments, starting from the second, do not match in the BGK and Fokker-Planck descriptions. This arises from the distinct eigenspectra of the respective velocity-space operators. While the spatially homogeneous Fokker-Planck operator leads to a countable infinity of distinct eigenvalues, in turn leading to distinct relaxation rates for successive moments in Eq. (2.20), the BGK-operator is (trivially) characterized by a single relaxation rate, and leads to successive higher-order moments in (26) relaxing at the same rate. However, as one is interested only in the slow dynamics this distinction between the two approaches is irrelevant for the present discussion. The $O(1/\epsilon)$ dynamics from Eq. (2.23) represents $f \approx f^{eq}(\psi, \bar{\mathbf{v}}^*)$. It is shown in what follows that by doing a Chapman-Enskog expansion (Chapman & Cowling 1991), the dynamics at $O(1)$ (Euler level), gives the desired Smoluchowski equation for the probability density of polymer configurations. In the usual Chapman-Enskog procedure, f is expanded as

$$f = f^{eq}(\psi) + \epsilon f^{(1)} + \epsilon^2 f^{(2)} + \dots, \quad (2.26)$$

such that $\int f^{(n)} d\mathbf{Q} = 0$ for $n > 1$. The consequence of this is that the non-conserved moments are also expanded in powers of ϵ around their equilibrium values. For example the momentum and the second-order moments are expanded as

$$\begin{aligned}\psi u_\alpha &= \psi \bar{v}_\alpha^* + \epsilon \psi u_\alpha^{(1)} + \epsilon^2 \psi u_\alpha^{(2)}, \\ P_{\alpha\beta} &= \hat{P}_{\alpha\beta}^{eq} + \epsilon P_{\alpha\beta}^{(1)} + \epsilon^2 P_{\alpha\beta}^{(2)}.\end{aligned}\quad (2.27)$$

Further, the time derivative operator for any quantity ϕ is expanded in powers of ϵ as

$$\frac{\partial \phi(\psi)}{\partial t} = \sum_{N=0}^{\infty} \epsilon^N \frac{\partial^{(N)} \psi}{\partial t} \frac{\partial \phi}{\partial \psi}, \quad (2.28)$$

with $(\partial^{(0)}/\partial t)$ for the probability density is obtained via continuity equation

$$\frac{\partial^{(0)} \psi}{\partial t} + \frac{\partial(\psi \bar{v}_\alpha^*)}{\partial Q_\alpha} = 0. \quad (2.29)$$

Similarly $(\partial^{(1)}/\partial t)$ for the probability density equation obtained via continuity equation is

$$\frac{\partial^{(1)} \psi}{\partial t} + \frac{\partial(\psi u_\alpha^{(1)})}{\partial Q_\alpha} = 0. \quad (2.30)$$

At $O(1)$, momentum density equation is

$$\frac{\partial^{(0)} \psi \bar{v}_\alpha^*}{\partial t} + \frac{\partial \hat{P}_{\alpha\beta}^{eq}}{\partial Q_\beta} = -\psi \bar{u}_\alpha^{(1)}. \quad (2.31)$$

Finally,

$$\psi u_\alpha = \psi \bar{v}_\alpha^* - \epsilon \left(\frac{\partial \psi}{\partial Q_\alpha} + \psi \bar{v}_\gamma^* \frac{\partial \bar{v}_\alpha^*}{\partial Q_\gamma} \right). \quad (2.32)$$

On substituting the above expression in equation Eq. (2.25), following equation is obtained

$$\frac{\partial \psi}{\partial t} + \frac{\partial(\psi \bar{v}_\alpha^*)}{\partial Q_\alpha} = \epsilon \frac{\partial^2 \psi}{\partial Q^2} + \underbrace{\epsilon \frac{\partial}{\partial Q_\alpha} \left(\psi \bar{v}_\gamma^* \frac{\partial \bar{v}_\alpha^*}{\partial Q_\gamma} \right)}_{\text{error}}, \quad (2.33)$$

where the underbrace term is the leading-order error in the present formulation and is $O(\epsilon \text{Ma}^2)$. For sufficiently small Ma , this scheme will reproduce the desired dynamics with greater accuracy as

$$\frac{\partial \psi}{\partial t} + \frac{\partial(\psi \bar{v}_\alpha^*)}{\partial Q_\alpha} = \epsilon \frac{\partial^2 \psi}{\partial Q^2}. \quad (2.34)$$

In the non-dimensional form where the relevant length scale is the equilibrium extension l_0 , Eq. (2.34) is

$$\frac{\partial \psi}{\partial t} + \nabla_{\mathbf{Q}} \cdot \left[\left(\text{Wi} \boldsymbol{\kappa} \cdot \mathbf{Q} - \frac{\hat{\mathbf{F}}^c(\mathbf{Q})}{2} \right) \psi \right] = \frac{1}{2} \nabla_{\mathbf{Q}}^2 \psi, \quad (2.35)$$

with $\hat{\mathbf{F}}^c = \mathbf{Q}/(1-Q^2/b)$. Hence, it has been shown that on assuming a local relaxation mechanism, instead of the actual diffusion mechanism at the kinetic level, the same slow dynamics is obtained

via BGK description.

2.5 Outlook

In this chapter, the Langevin equation and the corresponding probabilistic description in terms of Smoluchowski equation governing the dynamics of polymer modeled as FENE dumbbell are discussed. A phase space kinetic formulation based on the BGK approximation is proposed for dilute polymer solution. It is shown via Chapman-Enskog expansion that the correct slow dynamics in configuration space is recovered in this framework. The main objective now is to formulate a discrete formulation on the lines of LB method for the aforementioned mechanism.

Chapter 3

Lattice Boltzmann method

3.1 Introduction

In Chapter 2, a mechanism which only relies on BGK relaxation description to reproduce viscoelastic behavior, is introduced. In the subsequent chapters, a numerical scheme for such a mechanism, on the lines of lattice Boltzmann method, was introduced. Before going into the details of such formulation, the lattice Boltzmann method is briefly reviewed in this chapter. Furthermore, a variant of the lattice Boltzmann method, where the energy conservation law is kept intact is discussed and shown to be more stable than the existing LBM.

In the last two decades, the lattice Boltzmann method (LBM) has emerged as an alternate tool to simulate the hydrodynamics of Newtonian fluids (Succi *et al.* 1992; Chen & Doolen 1998; Succi 2001; Aidun & Clausen 2010). The lattice Boltzmann method can be understood as approximate technique for solving Boltzmann BGK equation using a discrete velocity set (Abe 1997; He & Luo 1997*a,b*; Shan & He 1998; Ansumali & Karlin 2002; Ansumali *et al.* 2003; Yudistiawan *et al.* 2010). It was shown in Ref. (Shan & He 1998) that the LB method approximates the Boltzmann BGK equation in terms of the Hermite polynomial. Later, this idea was refined to formulate the LB method in a thermodynamically consistent manner (Ansumali *et al.* 2003; Ansumali & Karlin 2005).

The lattice Boltzmann is largely used as a tool for isothermal dynamics. Though the method is weakly compressible, the sound speed is not correctly predicted by the method. The reason for wrong sound speed is that the isothermal LBM predicts that sound dynamics is isothermal rather than isentropic. Thus, the method, in its standard form, can't be used for describing sound dynamics in a physically consistent manner. In this chapter, it is shown that the energy conserving model created via entropic route also leads to correct sound dynamics. Numerical simulations also suggest that as compared to the isothermal models, numerical stability range for the energy conserving models is also better.

The chapter is organized as follows. The Boltzmann equation for dilute gases is introduced in Sec.3.2 which is followed by a brief discussion on Maxwell-Boltzmann distribution function in Sec.3.3. The single relaxation approximation for Boltzmann collision operator, known as Bhatnager-Gross-Krook (BGK) approximation is introduced in Sec.3.4. The lattice Boltzmann model in isothermal case is then reviewed in Sec.3.5. The time and space discretization scheme for the same is presented in Sec.3.6 followed by an example of lid-driven cavity in Sec.3.7 to show the usefulness of LBM in fluid dynamics simulation. A thermodynamically consistent LB scheme is introduced in Sec.3.8 which ensures the positive definiteness of equilibrium value of probability distribution function and a variant of LB where energy conservation is kept intact is presented in Sec.3.8.1. In Sec.3.9, via an example it is shown that energy conserving model indeed manages to reproduce adiabatic sound propagation correctly. In Sec.3.10 and 3.11, the energy conserving

model is compared with isothermal model for the set up of Taylor-Green vortex and cavity flow respectively. In Sec.3.12, a further modification on lattice Boltzmann method to have a tunable Pr number is introduced and shown to be numerically more stable than isothermal as well as energy conserving model. Finally, the chapter is summarized in Sec.3.13.

3.2 Boltzmann Equation for Dilute Gases

In the kinetic theory of gases, fluid is modeled as an N -point particle system, where individual particles are in constant, random motion. In this description of fluid, the fundamental quantity of interest is the single particle distribution function f , where $f(\mathbf{x}, \mathbf{c}, t)d\mathbf{c}d\mathbf{x}$ provides the probability of finding a particle with velocity in the range \mathbf{c} to $\mathbf{c} + d\mathbf{c}$ and position in the range of \mathbf{x} to $\mathbf{x} + d\mathbf{x}$. The macroscopic quantities such as mass density ρ , momentum density $j = \rho\mathbf{u}$ and energy density $E = \rho\mathbf{u}^2/2 + e\rho$ (e is the internal energy) are lower order moment of f defined as

$$\rho = \langle 1, f \rangle, \quad \rho\mathbf{u} = \langle \mathbf{c}, f \rangle, \quad e = \left\langle \frac{\xi^2}{2}, f \right\rangle, \quad (3.1)$$

where $\xi = \mathbf{c} - \mathbf{u}$ is the peculiar velocity and \mathbf{u} represents the mean velocity and angular bracket denotes the inner product defined as

$$\langle \phi_1, \phi_2 \rangle = \int_{-\infty}^{\infty} \int_{-\infty}^{\infty} \int_{-\infty}^{\infty} d\mathbf{c} \phi_1 \phi_2. \quad (3.2)$$

The temperature T of the gas can be defined in terms of the internal energy as $e = 3k_B T/(2m)$, where k_B is the Boltzmann constant and m is mass of a gaseous particle. Here onwards the reduced temperature θ defined as $\theta = k_B T/m$, is used. In dilute limit, the dynamics of single particle distribution f is governed by the Boltzmann equation (Cercignani 1988):

$$\partial_t f + c_\alpha \partial_\alpha f = \Omega^B(f, f), \quad (3.3)$$

where Ω^B is a bi-linear function of f such that it obeys the following properties.

1. **Collisional Invariants:** The mass, the momentum and the energy are not altered by collision term (Ω^B), which implies

$$\langle \Omega^B, \{1, c_\alpha, \mathbf{c}^2\} \rangle = 0. \quad (3.4)$$

2. **Zero of Collision:** The Maxwell Boltzmann distribution f^{MB}

$$f^{\text{MB}} = \frac{\rho}{(2\pi\theta)^{3/2}} \exp\left(-\frac{(c-u)^2}{2\theta}\right), \quad (3.5)$$

is the zero of the collision term, i.e.,

$$\Omega^B(f, f) = 0 \iff f = f^{\text{MB}}. \quad (3.6)$$

3. **H-theorem:** Boltzmann collision term is such that

$$\langle \Omega^{\text{B}}, \ln f \rangle \leq 0. \quad (3.7)$$

Thus, the H -function defined as

$$H = \int d\mathbf{c} (f \ln f - f), \quad (3.8)$$

is the non-equilibrium generalization of the entropy (Cercignani 1988). This can be seen by writing evolution equation for the H function by multiplying Eq.(3.3) with $\ln f$ and integrating with respect to velocity (\mathbf{c}), which gives

$$\partial_t H + \partial_\alpha J_\alpha^{\text{H}} = -\Sigma^{(\text{B})}, \quad (3.9)$$

where entropy flux term and production term are

$$J_\alpha^{\text{H}} = \int d\mathbf{c} c_\alpha (f \ln f - f), \quad \Sigma^{(\text{B})} = -\langle \Omega^{\text{B}}, \ln f \rangle. \quad (3.10)$$

Thus, the Boltzmann equation ensures that the entropy production $\Sigma^{(\text{B})} \geq 0$ and is zero only when $f = f^{\text{MB}}$.

4. **Conservation Laws:** By taking appropriate moments of the Boltzmann equation Eq.(3.3), it is evident that macroscopic conservation laws have expected form:

$$\begin{aligned} \partial_t \rho + \partial_\alpha j_\alpha &= 0, \\ \partial_t j_\alpha + \partial_\beta (\rho u_\alpha u_\beta + p \delta_{\alpha\beta}) + \partial_\beta \sigma_{\alpha\beta} &= 0, \\ \partial_t E + \partial_\alpha ((E + p)u_\alpha + \sigma_{\alpha\gamma} u_\gamma) + \partial_\alpha q_\alpha &= 0, \end{aligned} \quad (3.11)$$

where the pressure $p = \rho\theta$ is that of an ideal gas and the stress tensor $\sigma_{\alpha\beta}$ and the heat flux q_α are defined as

$$\sigma_{\alpha\beta} = \langle \overline{\xi_\alpha \xi_\beta} \rangle, \quad q_\alpha = \left\langle \xi_\alpha \frac{\xi^2}{2} \right\rangle, \quad (3.12)$$

where for any second order tensor $A_{\alpha\beta}$, its traceless part $\overline{A}_{\alpha\beta}$ is

$$\overline{A}_{\alpha\beta} = \frac{1}{2}(A_{\alpha\beta} + A_{\beta\alpha}) - \frac{1}{D} A_{\gamma\gamma} \delta_{\alpha\beta}. \quad (3.13)$$

Thus, it can be seen that the conservation laws obtained from the Boltzmann equation are consistent with the continuum mechanics.

3.3 Maxwell-Boltzmann Distribution

In last section, it was highlighted that Maxwell-Boltzmann distribution is the zero of the collision term Eq.(3.6) and the H -function decreases until the Maxwell-Boltzmann distribution is

attained. These two key features of the Boltzmann equation, also permit a variational interpretation of the Maxwell-Boltzmann distribution. In this variational interpretation, the Maxwell-Boltzmann distribution is obtained via minimization of the H -function

$$H = \int d\mathbf{c} f(\log f - 1), \quad (3.14)$$

under the constraints of fixed value of mass, momentum and energy density (Eq.3.1). This constrained minimization is conveniently done as an absolute minimization of the thermodynamic potential Ξ defined as

$$\Xi = \int d\mathbf{c} [f(\log f - 1) + \alpha f + \beta_k c_k f + \gamma c^2 f], \quad (3.15)$$

where α, β_k and γ are the Lagrange multipliers associated with the mass, momentum and energy conservation respectively. The minimizer of this potential is obtained by taking extremum of Ξ

$$\frac{\partial \Xi}{\partial f} = 0, \quad (3.16)$$

which provides the formal solution as

$$f^{\text{eq}} = \exp [-(\alpha + \beta_k c_k + \gamma c^2)], \quad (3.17)$$

where the Lagrange multipliers are obtained by using the constraints

$$\left\langle \left\{ 1, \mathbf{c}, \frac{c^2}{2} \right\}, f^{\text{eq}} \right\rangle = \left\{ \rho, \rho \mathbf{u}, \frac{D}{2} \rho \frac{k_B T}{m} + \frac{1}{2} \rho u^2 \right\}. \quad (3.18)$$

Upon inversion, one gets the Lagrange multipliers in explicit form as

$$\alpha = -\log \rho + \frac{3}{2} \log 2\pi\theta + u^2, \quad \beta_k = -\frac{u_k}{\theta}, \quad \gamma = \frac{1}{2\theta}, \quad (3.19)$$

which shows that the Lagrange multiplier γ ensures energy conservation via temperature variation. Similarly, the linear momentum conservation is imposed by β_k through variation in velocity and the Lagrange multiplier α can be associated with the chemical potential μ and is responsible for conservation of mass. The explicit solution for f^{eq} is given by the Maxwell-Boltzmann distribution function (Eq. (3.5)). Thus, we see that the knowledge of the thermodynamic potential Ξ is sufficient to describe the equilibrium state as well as the slow moments, which can be understood as the derivative of the potential with respect to the Lagrange multipliers, i.e.,

$$\rho = \frac{\partial \Xi}{\partial \alpha}, \quad \rho u_k = \frac{\partial \Xi}{\partial \beta_k}, \quad \frac{D}{2} \rho \frac{k_B T}{m} + \frac{1}{2} \rho u^2 = \frac{\partial \Xi}{\partial \gamma}. \quad (3.20)$$

Indeed, the potential Ξ is the generator of the time dynamics. This is evident if one writes the Boltzmann collision term as:

$$\Omega^{\text{Boltzmann}} = \int d\mathbf{c}_1 \int d\boldsymbol{\omega} B(|\mathbf{c}-\mathbf{c}_1|, \boldsymbol{\omega}) \left[\exp\left(\frac{\partial \Xi}{\partial f(\mathbf{c})}\right) \exp\left(\frac{\partial \Xi}{\partial f_1(\mathbf{c}_1)}\right) - \exp\left(\frac{\partial \Xi}{\partial f'(\mathbf{c}')}\right) \exp\left(\frac{\partial \Xi}{\partial f'_1(\mathbf{c}'_1)}\right) \right], \quad (3.21)$$

where \mathbf{c}, \mathbf{c}_1 are the pre-collisional and $\mathbf{c}', \mathbf{c}'_1$ are the post-collisional velocity of two colliding particles. The function B represents the redistribution of velocities which depends crucially on the binary molecular interaction and ω gives the angle and relative strength of collision. This information can be used to create a variational discretization scheme for the kinetic equations.

3.4 Bhatnager-Gross-Krook Collision Model

Due to complexity of Boltzmann collision operator, a simplified description in terms of BGK collision term (Bhatnagar *et al.* 1954)

$$\Omega^{\text{BGK}} = \frac{1}{\tau} (f^{\text{MB}} - f), \quad (3.22)$$

is often used and where τ is the mean free time. This implies that evolution equation for the distribution function is

$$\partial_t f + c_\alpha \partial_\alpha f = \frac{1}{\tau} (f^{\text{MB}} - f). \quad (3.23)$$

Using Eq.(3.18), we can see that collisional invariant for the present model is same as the Boltzmann equation. It is also evident that zero of the collision term is Maxwell-Boltzmann distribution for this collision model too. The H -theorem for this model can be seen by writing the evolution equation for H -function using Eq.(3.23) as

$$\partial_t H + \partial_\alpha J_\alpha^H = \Sigma^{\text{BGK}}, \quad (3.24)$$

where

$$\Sigma^{\text{BGK}} = \frac{1}{\tau} \int dc (f^{\text{MB}} - f) \log \left(\frac{f}{f^{\text{MB}}} \right) + \frac{1}{\tau} \int dc (f^{\text{MB}} - f) \log f^{\text{MB}}, \quad (3.25)$$

which can be simplified further as

$$\Sigma^{\text{BGK}} = \frac{1}{\tau} \int dc (f^{\text{MB}} - f) \log \left(\frac{f}{f^{\text{eq}}} \right) \leq 0. \quad (3.26)$$

Here, Eq.(3.18) and inequality $\log x/y(x - y) \leq 0$ have been used. For any arbitrary kinetic model, whenever the collision term conserves mass, momentum and energy irrespective of the form of collision term, the conservation laws (Eqs.(3.11)) remain the same. Therefore, the BGK model leads to the same set of conservation laws as Boltzmann equation. Thus, BGK model preserves all of the qualitative properties of the collision operator mentioned in previous section. As this model provides qualitatively correct representation of the Boltzmann equation, it is widely used in the applications. However, quantitative comparison is often not possible due to the fact that this model predicts Prandtl number of the mono-atomic gas to be $\text{Pr} = 1$ instead of $\text{Pr} = 2/3$. Various extension of BGK model do exist where the aim is to obtain the correct Prandtl number (Cercignani 1988). This thesis will not deal with such corrections of BGK model. In next section, a numerical scheme based on lattice Boltzmann method will be introduced for the Boltzmann BGK equation.

3.5 Lattice Boltzmann scheme for BGK Model

In recent years, lattice Boltzmann method has emerged as a convenient solver for Boltzmann-BGK equation in low Mach number limit. In typical LBM formulations, one works with a set of discrete populations $f = \{f_i\}$, corresponding to predefined discrete velocities \mathbf{c}_i ($i = 1, \dots, N$). The natural choice for the set of discrete velocities are the nodes of a Gauss-Hermite quadrature. However, unlike conventional finite difference discretization of partial differential equation (PDE), no attempts are made to point-wise approximate the PDE on the discrete velocity set. The reason behind this is that if one chooses point-wise discretization of velocity space with finite number of discrete velocities, the moments of the equilibrium distribution is not the same as that of distribution function, i.e.,

$$\rho \equiv \sum_i^N f_i \neq \sum_i^N f_i^{\text{MB}}, \quad \rho \mathbf{u} \neq \sum_i^N f_i^{\text{MB}} \mathbf{c}_i. \quad (3.27)$$

Thus, violation in the conservation laws, due to this discretization error, can be minimized only by keeping very large number of discrete velocities. However, one would like to keep N to be as low as possible.

In lattice Boltzmann, this problem is eliminated by first projecting the Maxwell-Boltzmann distribution in a subspace spanned by the leading Hermite polynomials (Shan & He 1998). In other words, for low Mach number case, the Maxwell Boltzmann distribution with local velocity and local temperature is expanded around a global Maxwellian ($\mathbf{u} = \mathbf{0}, \theta = \theta_0$) corresponding to the rest state. The approximate equilibrium \tilde{f}^{MB} is then

$$\tilde{f}^{\text{MB}} \approx \underbrace{\frac{\rho}{(2\pi\theta_0)^{3/2}} \exp\left(-\frac{c^2}{2\theta_0}\right)}_{\omega(\mathbf{c})} \left(\sum_k^{N_1} \frac{1}{k!} a^{(k)} H^k\left(\frac{\mathbf{c}}{\sqrt{\theta_0}}\right) \right), \quad (3.28)$$

where $H^k(\mathbf{c}/\sqrt{\theta_0})$ are the orthogonal Hermite tensors and N_1 is the order of expansion. It is necessary to take $N_1 \geq 2$ if the momentum equation is to be obtained and $N_1 \geq 3$ if the energy conservation equation is needed. The coefficient of expansion $a^{(k)}$ are the functions of mass, momentum and energy density and are computed using the condition that lower order moments should be same for the expanded version of the equilibrium. For example,

$$\begin{aligned} a^{(0)} &= \int \tilde{f}^{\text{MB}} d\mathbf{c} = \rho, \\ a_{\alpha}^{(1)} &= \int \tilde{f}^{\text{MB}} \frac{c_{\alpha}}{\sqrt{\theta_0}} d\mathbf{c} = \frac{\rho u_{\alpha}}{\sqrt{\theta_0}} \\ a_{\alpha\beta}^{(2)} &= \int \tilde{f}^{\text{MB}} \frac{(c_{\alpha}c_{\beta} - \theta_0\delta_{\alpha\beta})}{\theta_0} d\mathbf{c} = \frac{\rho u_{\alpha}u_{\beta} + (\theta - \theta_0)\delta_{\alpha\beta}}{\theta_0}. \end{aligned} \quad (3.29)$$

It should be reminded that the first few Hermite polynomials are $H^{(0)} = 1$, $H_{\alpha}^{(1)}(\mathbf{c}/\sqrt{\theta_0}) = c_{\alpha}/\sqrt{\theta_0}$ and $H_{\alpha\beta}^{(2)}(\mathbf{c}/\sqrt{\theta_0}) = (c_{\alpha}c_{\beta} - \theta_0\delta_{\alpha\beta})/\theta_0$. The explicit form of discrete equilibrium for

the isothermal case, where $\theta = \theta_0$ (Grad 1949), is

$$\tilde{f}^{\text{MB}}(\rho, \mathbf{u}, \theta_0) \approx \frac{\rho}{(2\pi\theta_0)^{3/2}} \exp\left(-\frac{\mathbf{c}^2}{2\theta_0}\right) \left[1 + \frac{\mathbf{c}_\alpha u_\alpha}{\theta_0} + \frac{u_\alpha u_\beta}{2\theta_0^2} (c_\alpha c_\beta - \theta_0 \delta_{\alpha\beta})\right]. \quad (3.30)$$

Once the equilibrium is projected on the finite subspace spanned by the lower order Hermite polynomial, one works with the discrete velocity \mathbf{c}_i with $i = 1, \dots, N$ taken as the nodes and ω_i , as the associated weights of Gauss-Hermite quadrature. The Gaussian quadrature approximation of any integral is (Shan & He 1998)

$$\int d\mathbf{c} \phi(\mathbf{c}) \omega(\mathbf{c}) = \sum_i^N \omega_i \phi(\mathbf{c}_i). \quad (3.31)$$

Since $\tilde{f}^{\text{MB}} H^{(n)}/\omega$ is such a polynomial if $n \leq N$, therefore, the Hermite coefficients of \tilde{f}^{MB} can be written as

$$a^{(n)} = \sum_i^N \frac{\omega_i \tilde{f}_i^{\text{MB}} H^{(n)}(\mathbf{c}_i)}{\omega(\mathbf{c}_i)} \quad (3.32)$$

where $\tilde{f}_i^{\text{MB}} = \tilde{f}^{\text{MB}}(\mathbf{c}_i)$. In LB literature for convenience, the discrete form of Maxwell-Boltzmann distribution function is defined as:

$$f_i^{\text{MB}} = \frac{\omega_i \tilde{f}_i^{\text{MB}}}{\omega(\mathbf{c}_i)}. \quad (3.33)$$

Hence the Hermite coefficients becomes

$$a^{(n)} = \sum_i^N f_i^{\text{MB}} H^{(n)}(\mathbf{c}_i). \quad (3.34)$$

Thus, the discrete approximation to the moments in terms of discrete equilibrium is

$$\rho = \sum_i^N f_i^{\text{MB}}, \quad \rho u_\alpha = \sum_i^N f_i^{\text{MB}} \mathbf{c}_i, \quad \rho u_\alpha u_\beta + \rho \theta_0 \delta_{\alpha\beta} = \sum_i^N f_i^{\text{MB}} c_{i\alpha} c_{i\beta}. \quad (3.35)$$

The discrete form of Maxwell-Boltzmann distribution function till second order in Mach number (Ma) is:

$$f_i^{\text{MB}} = w_i \rho \left[1 + \frac{u_\alpha c_{i\alpha}}{\theta_0} + \frac{u_\alpha u_\beta}{2\theta_0^2} (c_{i\alpha} c_{i\beta} - \theta_0 \delta_{\alpha\beta})\right]. \quad (3.36)$$

The most commonly used discrete velocity sets are D1Q3, D2Q9, D2Q7, D3Q15, D3Q19 and D3Q27 as shown in the Fig. 3.1. Here, all the lattices are labeled by indicating the number of physical dimensions (D) and the number of microscopic discrete velocities (Q). However, the discrete equilibrium distribution of the form given by Eq. (3.36) has a drawback that it is not positive-definite. It is often indicated that this lack of positivity manifest itself in terms of numerical instability. Therefore, one needs to find f_i^{eq} in a thermodynamically consistent manner so that the positiveness of f_i^{eq} is ensured. In entropic formulation of LB (discussed in Sec. 3.8), this defect of the method is removed.

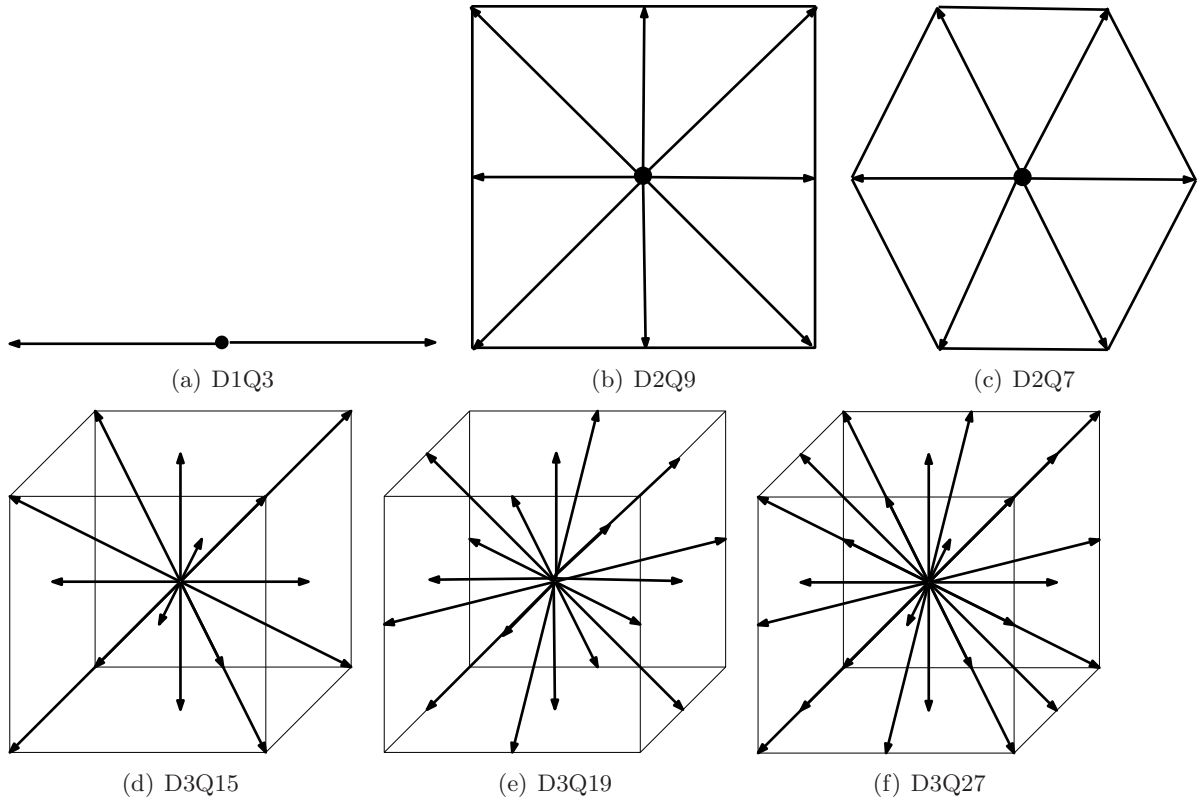


Figure 3.1: Discrete velocity sets.

3.6 Time and space discretization scheme

After discretizing the velocity space, the Boltzmann BGK equation governing corresponding discrete distribution function f_i is

$$\frac{d}{dt}f_i = \frac{1}{\tau} \underbrace{[f_i^{eq}(M^{\text{Slow}}(f)) - f_i]}_{\Omega(f_i)}, \quad (3.37)$$

where d/dt represents derivative along the discrete characteristics. By direct integration of this Eq. (3.37), the discrete evolution equation becomes

$$f_i(\mathbf{x} + \mathbf{c}\Delta t, t + \Delta t) - f_i(\mathbf{x}, t) = \int_{s=0}^{s=\Delta t} ds \Omega(f_i(\mathbf{x} + \mathbf{c}s, t + s)), \quad (3.38)$$

where Δt is the time increment. The R.H.S. of this equation can be approximated using the trapezoidal rule as:

$$f_i(\mathbf{x} + \mathbf{c}\Delta t, t + \Delta t) = f_i(\mathbf{x}, t) + \frac{\Delta t}{2} [\Omega(f_i(\mathbf{x}, t)) + \Omega(f_i(\mathbf{x} + \mathbf{c}\Delta t, t + \Delta t))]. \quad (3.39)$$

This relationship between populations at two different times is implicit which can be made explicit by using the following change of variables:

$$g_i = f_i - \frac{\Delta t}{2\tau} (f_i - f_i^{eq}(\rho(f), \mathbf{u}(f))). \quad (3.40)$$

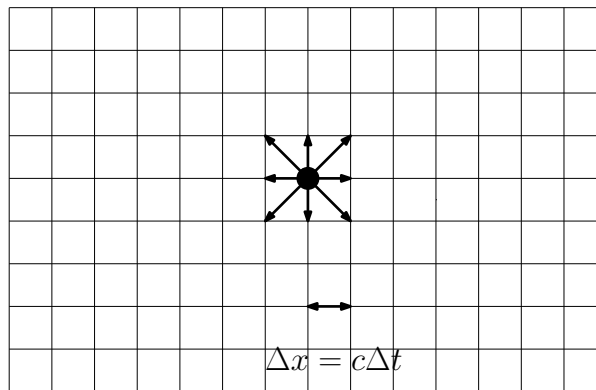


Figure 3.2: Schematic of D2Q9 velocity set on two dimensional grid.

It can be seen using Eq. (3.40), that

$$\rho(g) = \rho(f), \quad \mathbf{u}(g) = \mathbf{u}(f), \quad (3.41)$$

and thus

$$f^{\text{eq}}(\rho(f), \mathbf{u}(f)) = g^{\text{eq}}(\rho(g), \mathbf{u}(g)). \quad (3.42)$$

Using this information, Eq. (3.40) can be inverted to obtain

$$g_i^{\text{eq}}(\rho(g), \mathbf{u}(g)) - g_i = [f_i^{\text{eq}}(\rho(f), \mathbf{u}(f)) - f_i] \left(\frac{2\tau + \Delta t}{2\tau} \right). \quad (3.43)$$

Therefore, with the single relaxation (BGK) approximation, one gets

$$g_i(\mathbf{x} + \mathbf{c}\Delta t, t + \Delta t) = g_i(\mathbf{x}, t) + 2\beta [g_i^{\text{eq}}(\rho(g), \mathbf{u}(g)) - g_i(\mathbf{x}, t)], \quad (3.44)$$

where the discrete dimensionless relaxation parameter, $\beta = \Delta t / (2\tau + \Delta t)$, dictates the stability domain of the method. It should be noted that although the time marching in Eq.(3.44) looks like first order Euler discretization, it is second order accurate in time since BGK equation is approximated using second order trapezoidal scheme. It means second order accurate numerical scheme is obtained with the computational cost of first order scheme. For implementation purpose, the discrete Eq.(3.40) can be divided into two basic operations

- Collision:

$$g_i^*(\mathbf{x}, t) = g_i(\mathbf{x}, t) + 2\beta \left[g_i^{\text{eq}}(M^{\text{Slow}}) - g_i(\mathbf{x}, t) \right], \quad (3.45)$$

- Free streaming:

$$g_i(\mathbf{x}, t + \Delta t) = g_i^*(\mathbf{x} - \mathbf{c}\Delta t, t). \quad (3.46)$$

The discretization in velocity space should be mapped to the discretization in the physical space in such a manner that a lattice structure is obtained. In order to do that the discretization in the physical space is chosen as $\Delta x = c\Delta t$. An example is illustrated in Fig. 3.2 that this choice of Δx allows the streaming over the links of the D2Q9 lattice. An efficient implementation of collision and streaming manages to reach 90% of memory bandwidth (Shet *et al.* 2013a,b).

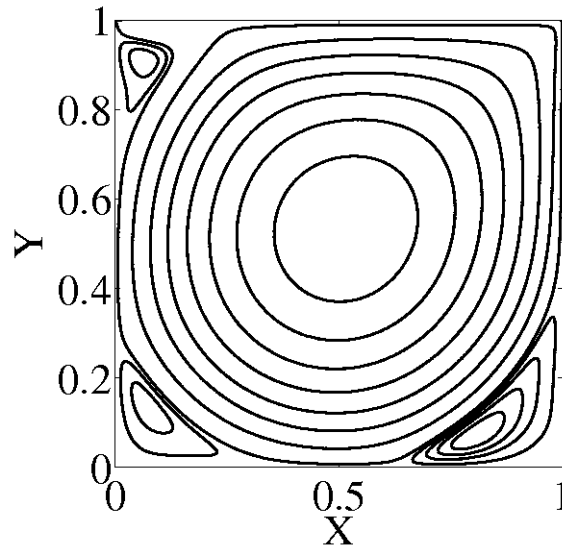


Figure 3.3: The stream-function for grid size of 312×312 for lid driven cavity.

	Central primary vortex ψ_{\max}		Lower right secondary vortex ψ_{\min}	
	(x,y)	ψ_{\max}	(x,y)	ψ_{\min}
LB	(0.48878,0.53365)	0.118169	(0.80288,0.072115)	-0.0029354
Ref. Bruneau & Saad (2006)	(0.48535,0.53516)	0.12197	(0.80566,0.073242)	-0.0030706

Table 3.1: Comparison of the primary vortex and on the lower right secondary vortex.

3.7 Benchmarking of Isothermal case

In order to show the competency of lattice Boltzmann method and its usefulness in fluid dynamics simulation methods, the examples of two-dimensional lid driven cavity is considered. The D2Q9 discrete velocity model is used in this case. In Fig. 3.3, the stream-functions are plotted for grid size of 312×312 at $Re=5000$ and $Ma= 0.1732$. The location and the value of stream-function at the center vortex and lower right secondary vortex is given in Table 3.1. This comparison of stream-function for the primary and lower right secondary vortex obtained from LB with the converged value for the same obtained in Ref. (Bruneau & Saad 2006), using finite difference method to discretize Navier-Stokes Equation shows that LB can be used as alternate for the conventional Computational Fluid Dynamics (CFD) methods.

3.8 Entropic Construction of the Equilibrium

In order to ensure the positive definiteness of distribution function, one needs to have a thermodynamically consistent description. It was pointed out in literature (Boghosian *et al.* 2001; Succi *et al.* 2002; Ansumali *et al.* 2003) that the simplest way to retain positivity of equilibrium distribution is to discretize the H -function and solve the discrete variational problem. Therefore, for isothermal case, one defines the discrete version of entropy as

$$H = \sum_{i=1}^N \left[f_i \left(\ln \left(\frac{f_i}{w_i} \right) - 1 \right) \right], \quad w_i > 0, \quad (3.47)$$

which is minimized under the constrains

$$\rho = \sum_i f_i, \quad \rho u_\alpha = \sum_{i=1}^N f_i c_{i\alpha}. \quad (3.48)$$

Here, it should be mentioned that in Ref. Karlin *et al.* (1999), it was shown for D2Q9 model that out of all possible convex entropies, only for the Boltzmann form of entropy as given by Eq.(3.47), the local equilibria are suitable to recover the Navier-Stokes equations in the framework of the lattice Boltzmann method. The formal expression for discrete equilibrium distribution, after minimizing the discrete H -function (Eq. (3.17)) reads as (Ansumali *et al.* 2003; Ansumali & Karlin 2005)

$$f_i^{\text{eq}} = w_i \exp(-(\alpha + \beta_k c_{ik})). \quad (3.49)$$

This expression is valid for an arbitrary discrete velocity set and in general for discrete lattices, it is not possible to find explicit solutions for the Lagrange multipliers. Karlin *et al.* (1999) developed a perturbation expansion to find the approximate expressions for the Lagrange multipliers. In Ref. Ansumali *et al.* (2003), it was pointed out that for the three commonly used lattices $D1Q3$, $D2Q9$ and $D3Q27$, the explicit expression of the equilibrium can be obtained by solving a quadratic equation and using factorization of the equilibrium in multi-dimensions:

$$f_i^{\text{eq}}(\rho, \mathbf{u}) = \rho w_i \prod_{j=1}^D \left[\left\{ \frac{2c - \sqrt{3u_j^2 + c^2}}{c} \right\} \left\{ \frac{2u_j + \sqrt{3u_j^2 + c^2}}{(c - u_j)} \right\}^{c_{ij}/c} \right]. \quad (3.50)$$

The equilibria given by Eq. (3.50), is positive definite particularity for $u_j < \sqrt{3\theta_0}$ with $\sqrt{\theta_0} = c/\sqrt{3}$. It is not defined for $u_j > \sqrt{3\theta_0}$. The equilibrium can be factorized into D one-dimensional solutions. Finally, like the Maxwell Boltzmann distribution function, this discrete equilibrium is symmetric, i.e., $(\mathbf{c}_i, \mathbf{u}) \rightarrow (-\mathbf{c}_i, -\mathbf{u})$. However, in practice, a polynomial approximation to the exact equilibria (Eq. (3.50)), is often used, and is same as obtained using Hermite polynomial expansion and given by Eq. (3.36).

3.8.1 Energy Conserving Discrete Equilibrium

Ansumali *et al.* (2005), pointed out that in its discrete form, the thermodynamic potential Eq. (3.15) is a natural generator for the discrete dynamics and an alternate way to formulate LBM is to directly discretize the potential using quadrature as

$$\tilde{\Xi}[f_i] = \sum_i \left[f_i \left(\log \left(\frac{f_i}{\omega_i} \right) - 1 \right) + \alpha f_i + \beta_k c_k f_i + \gamma c^2 f_i \right]. \quad (3.51)$$

Using Eq. (3.20), one can get

$$\rho = \sum_i f_i, \quad \rho \mathbf{u} = \sum_i f_i \mathbf{c}_i, \quad \frac{D}{2} \rho \frac{k_{BT}}{m} + \frac{1}{2} \rho u^2 = \sum_i f_i c_i^2. \quad (3.52)$$

In Ref. Ansumali & Karlin (2005), it was pointed out that on D2Q9 and D3Q27 lattices, the available degrees of freedom are large enough to impose the constraints related to the energy conservation. They showed that the energy conserving equilibrium on these two lattices at zero velocity is

$$f_i^{\text{eq}} \equiv \rho W_i(\theta) = \rho (3\theta_0 - \theta)^D \left(\frac{\theta}{2(3\theta_0 - \theta)} \right)^{k_i}, \quad (3.53)$$

where the set $k_i \equiv c_i^2/(3\sqrt{\theta_0}) = [0, 1, 2]$ for the nine-speed lattice. For non-zero velocity case, the equilibria is found to take the following form (Ansumali & Karlin 2005):

$$f_i^{\text{eq}} = \rho W_i(\theta) \left[1 + \frac{u_\alpha c_{i\alpha}}{\theta} + \frac{u_\alpha u_\beta}{2\theta^2} (c_{i\alpha} c_{i\beta} - \theta_i \delta_{\alpha\beta}) \right] + O(u^3). \quad (3.54)$$

It is worth noting that, formally, the above equation has the similar same form as isothermal equilibria, Eq. (3.36), with temperature defined as:

$$\theta_i \equiv \theta \frac{2\theta}{3\theta_0 - \theta} + \frac{3k_i}{D} \frac{\theta_0 - \theta}{3\theta_0 - \theta}. \quad (3.55)$$

The above relation represents a very elegant and smooth deformation/extension of the isothermal case, to which it is readily checked to reduce in the limit $\theta \rightarrow \theta_0$. The moments from the energy conserving discrete equilibrium are:

$$\sum_i^N f_i^{\text{eq}} = \rho, \quad \sum_i^N f_i^{\text{eq}} \mathbf{c}_i = \rho \mathbf{u}, \quad \sum_i^N f_i^{\text{eq}} c_i^2 = \frac{D}{2} \rho \frac{k_B T}{m} + \frac{1}{2} \rho u^2. \quad (3.56)$$

The other higher order moments like pressure tensor (say in the case of D2Q9 model) are:

$$P_{xx}^{\text{eq}} = \rho\theta + \rho u_x^2 + \frac{3\rho\Delta\theta}{2\theta} (u_y^2 - u_x^2), \quad P_{yy}^{\text{eq}} = \rho\theta + \rho u_y^2 + \frac{3\rho\Delta\theta}{2\theta} (u_x^2 - u_y^2) \quad (3.57)$$

where, $\Delta\theta = \theta - \theta_0$ Notice, that if set-up is isothermal and only source of temperature change is viscous heating, $\Delta\theta \propto u^2$. Thus, the error introduced by energy conserving models is of higher order only.

3.9 Sound Propagation in Lattice Boltzmann Method

Until now, two scenarios were discussed which are typically used in lattice Boltzmann simulation. First is the one where temperature is kept constant (isothermal) and energy conservation is lost. Second is the one in which energy conservation is introduced. In its present popular isothermal setting, sound propagation in lattice Boltzmann (Nourgaliev *et al.* 2003), takes place at constant temperature, thus following Newton's definition of sound speed,

$$c_s^2 = \left. \frac{\partial P}{\partial \rho} \right|_T = \frac{k_B T_0}{m} \equiv v_0^2, \quad (3.58)$$

where v_0 is the reference thermal speed. Thus the method is rarely used for getting the acoustic information. However, via Laplace theory, it is known that, in actual reality, sound propagation occurs via an adiabatic process, which can only be described by an energy conserving(EC) model. For an energy conserving model

$$c_s^2 = \left. \frac{\partial P}{\partial \rho} \right|_S = \gamma \frac{k_B T_0}{m}, \quad (3.59)$$

where γ is the adiabatic exponent. Traditionally, this discrepancy was largely neglected in isothermal LBM simulations, with an argument that the relevant observable is the velocity field, the sound speed being just an immaterial constant. The first implication of using the energy conserving model is that the sound speed takes on its correct, isentropic, value (Eq. 3.59). In order to show that this is indeed the case, a simulation using the D2Q9 model is performed with the following initial conditions:

$$\rho(x, y, t = 0) = 1 + \epsilon \cos(kx), \quad \theta(x, y, t = 0) = \frac{\rho}{3}, \quad u_x = u_y = 0.0. \quad (3.60)$$

Here, ϵ is a small amplitude of a periodic density perturbation which allow us to observe the acoustic mode (Dellar 2002). As the ratio of specific heat capacity $\gamma = (D + 2)/D = 2$ in the two-dimensional case, one expect the ratio of the sound speed measured from energy conserving and isothermal lattice Boltzmann to be $\sqrt{2}$. As shown in the Fig.(3.4), the ratio between the speed of sound for energy conserving with that of isothermal is indeed ≈ 1.414 . As can be seen from the figure, energy conserving model has 11 crests and 12 troughs, so the value is in between 11 and 12 (≈ 11.25), while isothermal model has 8 crests and 8 troughs. So the ratio is $11.25/8 \approx 1.406$. This shows that sound speed in an energy conserving model is the desired one as given by Eq. (3.59). This suggests that if energy conserving model can be used in place of isothermal model, LBM can be used to study the sound propagation in law Mach number limit (Singh *et al.* 2013a).

3.10 Taylor-Green vortex and convergence of Lattice Boltzmann

To investigate the difference between the energy conserving and isothermal model, as the next example, the Taylor-Green vortex is considered, for which an analytical solution for 2-D incompressible Navier-Stokes equation is given as:

$$\begin{aligned} u_x(x, y, t) &= U_0 \sin\left(\frac{2\pi}{L} kx\right) \cos\left(\frac{2\pi}{L} ky\right) \exp\left(-\frac{2k^2(2\pi)^2}{L^2} \nu t\right), \\ u_y(x, y, t) &= -U_0 \cos\left(\frac{2\pi}{L} kx\right) \sin\left(\frac{2\pi}{L} ky\right) \exp\left(-\frac{2k^2(2\pi)^2}{L^2} \nu t\right). \end{aligned} \quad (3.61)$$

where ν is the kinematic viscosity. The initial condition on density and temperature θ is

$$\rho(x, y, t = 0) = 1, \quad \theta(x, y, t = 0) = 1/3. \quad (3.62)$$

The advantage of this set-up is that the set-up can be used to contrast the numerical viscosity with that of the analytical one and the set up removes any possible error due to boundary conditions. A grid resolution study is performed using the L_1 and L_2 error norms (calculated

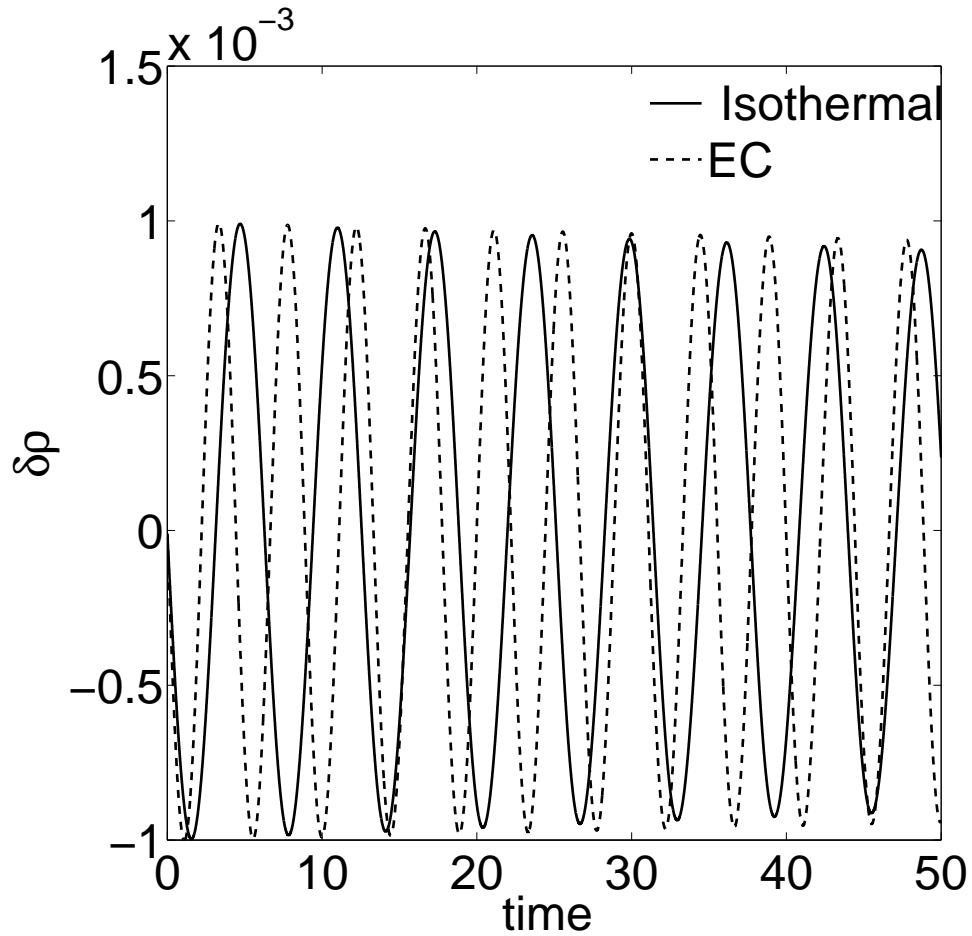


Figure 3.4: Variation of density with time in LB simulation at the center of domain for $Re=50$, $Ma=0.1$ and grid-size $=700 \times 700$

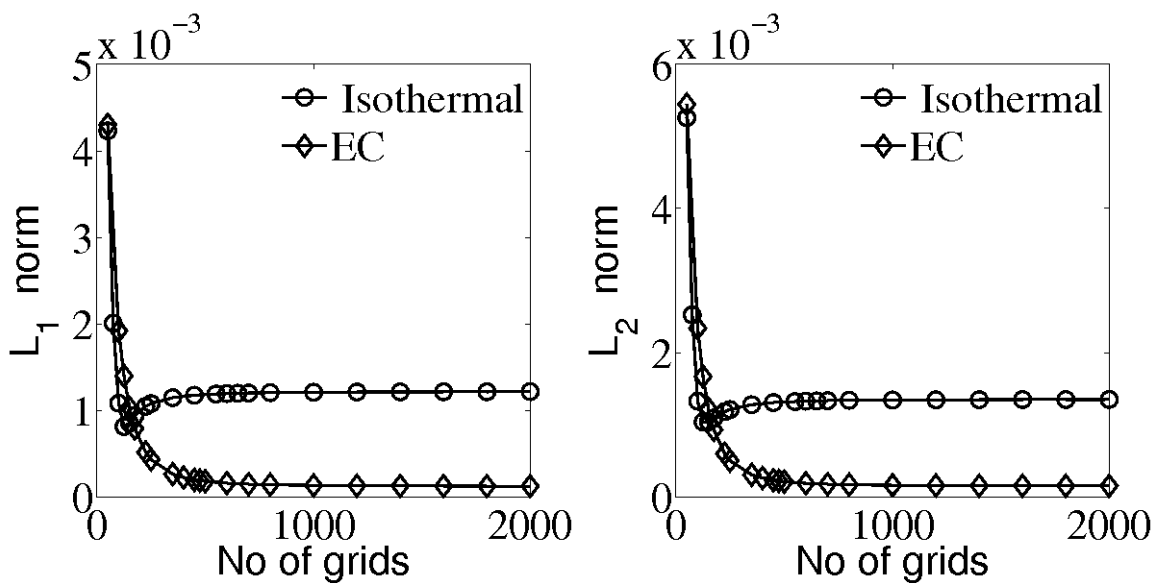


Figure 3.5: L_1 and L_2 norm for velocity in x direction at $Re=250$ and $Ma=0.05$ for Taylor-Green vortex as a function of grid size

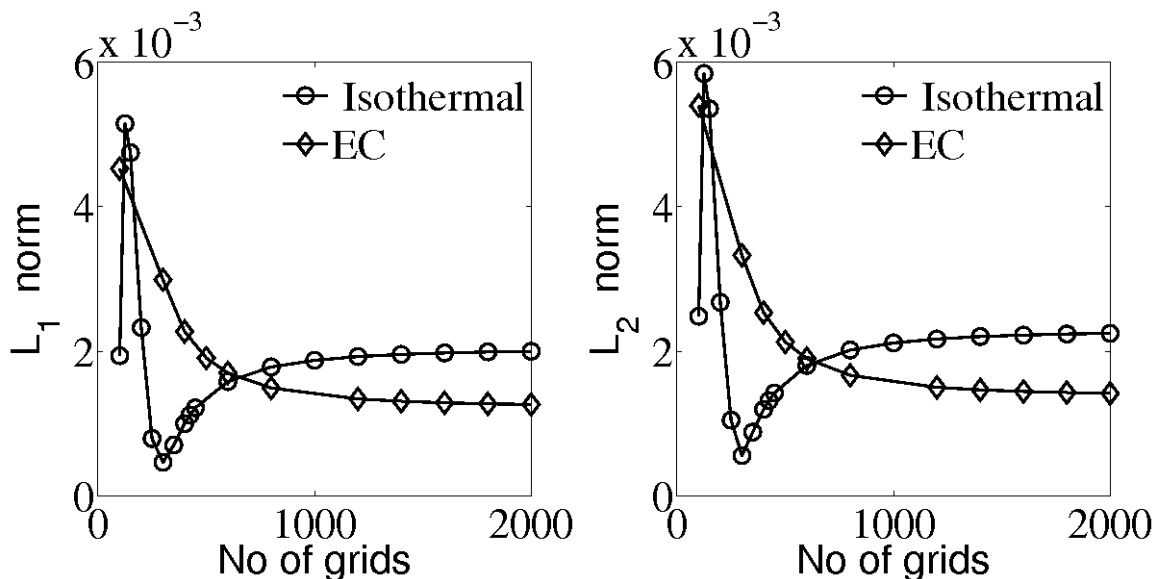


Figure 3.6: L_1 and L_2 norm for velocity in x direction at $Re = 4000$ and $Ma = 0.05$ for Taylor-Green vortex with different grid size

with respect to analytical solution) of the velocity in x direction for a given Mach (Ma) and Reynolds numbers (Re). Here, Re is based on the characteristic length of the flow-field, taken as 2π in a periodic-box of length 2π , thus $= U_0 2\pi/\nu$. Results are demonstrated in Fig.(3.5) and Fig.(3.6). The computational Mach number is defined as $Ma = U_0/\nu_0$. For the energy conserving model, the effective Mach number is lower by a factor of $\sqrt{\gamma}$ (see Eqs. (3.58) and (3.59)). This definition is chosen for comparing two methods, as this computational Mach number is the one which gives the idea about computational cost. In other words, for same computational cost, the effective Mach number is lower than in energy conserving model.

It is evident from the figures that, at $Re = 250$, the error in the energy-conserving case is an order of magnitude smaller than in the isothermal case. Even more importantly, the error does not show any sign of decay beyond $N \sim 200$. The case $Re = 4000$ conveys essentially the same message, although it is to be noted that at low resolution, the isothermal model may even lead to a smaller error than the energy-conserving one. However, as resolution is increased, the error saturates, while the energy-conserving models show a progressive, if only slow, decay. It can be seen from Fig.(3.5) and Fig.(3.6), that isothermal model shows oscillatory convergence while energy conserving model shows uniform convergence. It can also be inferred from the figures that incidentally at low resolution ($N \sim 200$), isothermal model gives smaller error than energy conserving model. However, as resolution is increased, energy conserving model becomes slightly more accurate. In Table. 3.2, error vs wavenumber for Taylor-Green flow simulation at $Ma = 0.05$ and $Re = 250$ is presented.

3.11 Cavity Flow

In actual practice, many fluid dynamic simulations take place in wall-bounded domains. Therefore, in our next example, the 2D lid driven cavity is considered, for which the polynomial-based isothermal LBM is known to produce unstable solutions at low grid resolution. The parameters

Grid	Δx	$\frac{\Delta t}{\tau}$	$\Delta k c_s \tau$	$L_{1(\text{iso})}/L_{1(\text{EC})}$
250	0.025120	11.54730	0.049998	2.49655108559788898662
450	0.0139556	6.415188	0.089997	5.94319296790443147449
600	0.01048	4.8175	0.11984	7.51231356662535934226
1000	0.0062857	2.889445	0.1998135	9.11464142525547885328
1200	0.005238	2.407833	0.2397800	9.39975804200142693178
2000	0.003142	1.44433	0.3997351	9.80366544915056078308
3000	0.0020933	0.9617607	0.60000955	9.92481386947622503649

Table 3.2: Error as a function of wavenumber

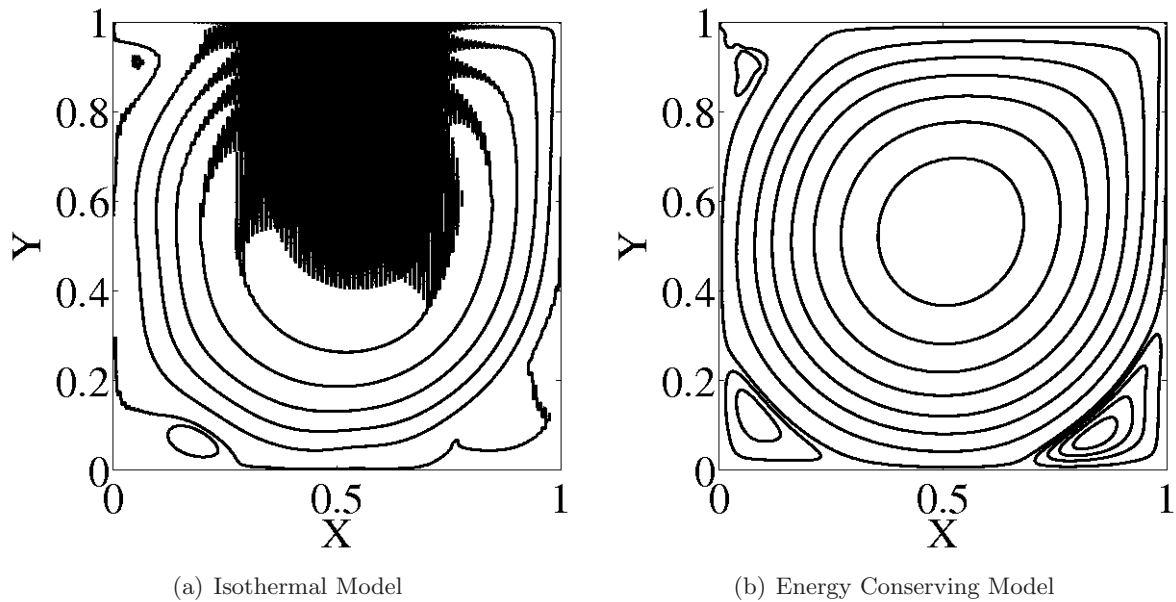


Figure 3.7: Streamline plot of cavity flow for grid-size=200×200. The isothermal model (left) is patently unstable, while the energy-conserving one (right) shows no sign of instability.

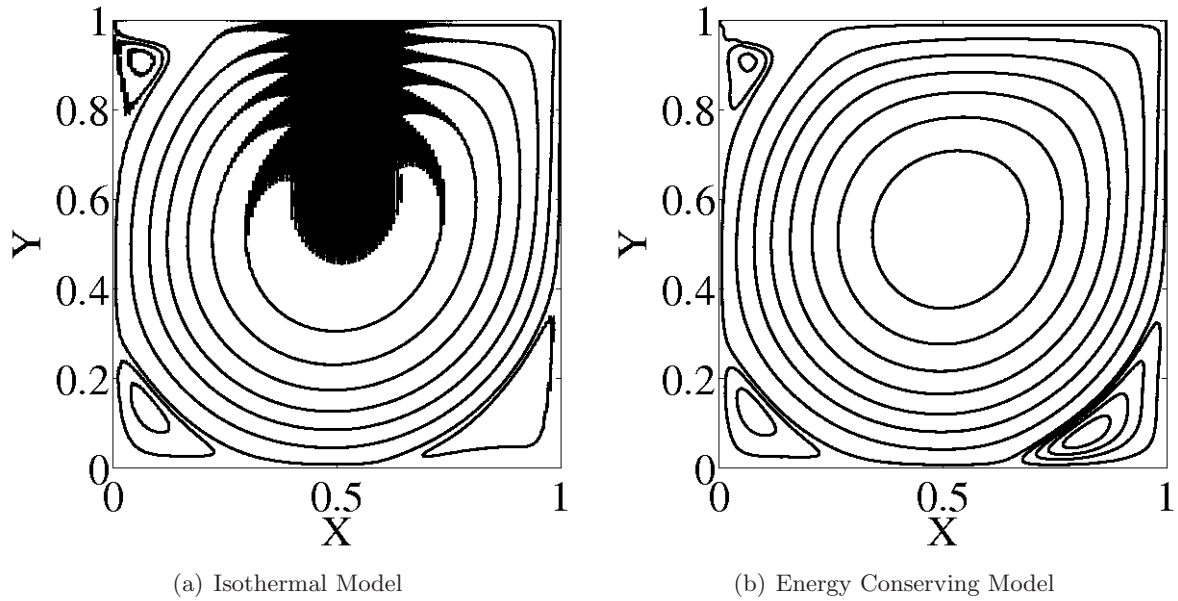


Figure 3.8: Streamline plot of cavity flow for grid-size= 256×256 . The isothermal model is still unstable, although to a less extent than for the case 200×200 . The energy-conserving one shows also a small improvement over the 200×200 , especially around the top-left corner

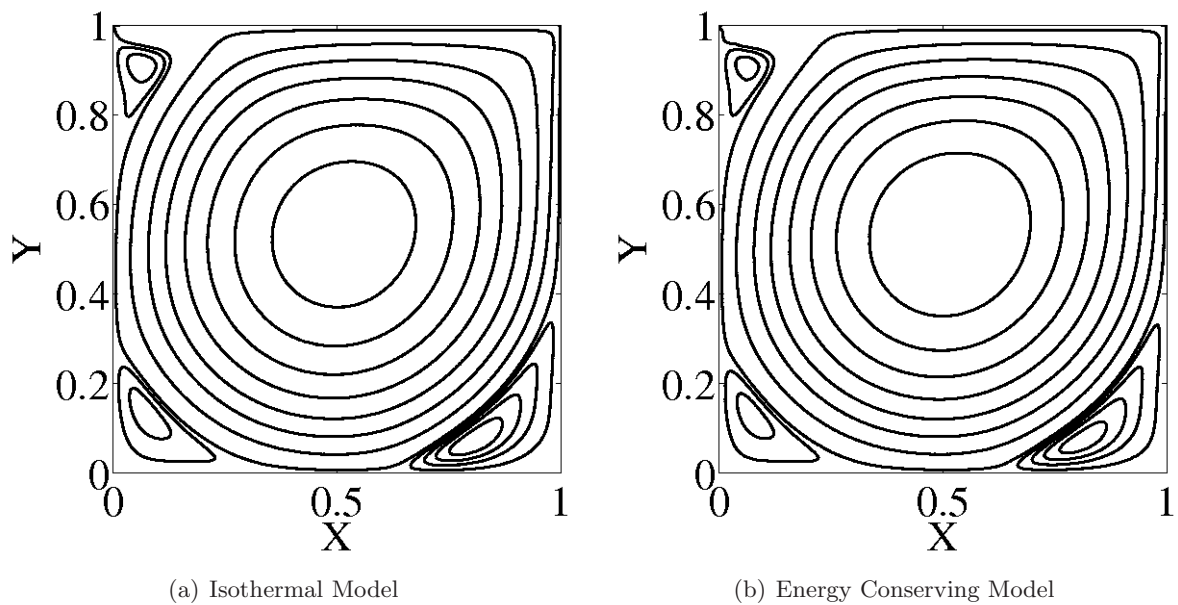


Figure 3.9: Streamline plot of cavity flow for grid-size= 312×312

Grid Points	200	256	312	375	450
Isothermal	17.92	6.067	3.616	2.328	2.148
EC	7.36	4.977	3.64	2.73	2.29

Table 3.3: Percentage error in stream function value at center vortex at $Ma = 0.05$ and $Re = 5000$.

Grid Points	200	256	312	375	450	512
Isothermal	30.88	5.067	3.1484	2.312	1.908	1.721
EC	5.223	3.903	2.837	2.017	1.509	1.369

Table 3.4: Percentage error in stream function value at center vortex at $Ma = 0.087$ and $Re = 5000$.

used in simulation are $Re = 5000$, $Ma = 0.1732$ and both isothermal (polynomial based) as well as energy-conserving simulations were performed with different grid sizes, with diffusive wall boundary conditions. From Fig. (3.7), Fig. (3.8) and Fig. (3.9), it can be seen that the energy-conserving setup converges towards a steady state value at a lower grid size than the isothermal.

In this setup, which is a prototype for bounded flows, it is observed that the differences between the two models were more pronounced. In order to show this effect, in Table. 3.3 and Table. 3.4 the percentage error in stream function value at center vortex for $Re = 5000$ and $Ma (= 0.05$ and $0.087)$ with different grid size is shown. The converged value for comparison is taken from (Bruneau & Saad 2006). It can be seen that the energy conserving model is more effective in suppressing acoustic disturbances arising near boundaries.

3.12 Quasi-equilibrium LB

In this section, another modification on lattice Boltzmann method is discussed which further improves the stability of the method. A tunable Pr number is introduced as an independent parameter in LB framework via quasi-equilibrium models (Ansumali *et al.* 2007). The multi-relaxation formulation makes use of an intermediate quasi-equilibrium f^* , (found as a minimum of H-function, under constraints on the additional fixed quasi-conserved variables).

The two-step relaxation as shown in Fig. 3.10, proceeds as follows. First, comes a fast relaxation to the quasi-equilibrium state f^* at the rate $(1/\tau_1)$, which is then followed by a slow relaxation to the equilibrium state f^{eq} with the rate $(1/\tau_2)$. The relaxation time τ_1 is related to the dynamic viscosity μ via usual relation, $\mu = \tau_1 p$, while the second relaxation time controls thermal diffusion. The Prandtl number, which is defined as the ratio of momentum diffusivity (viscosity) to thermal diffusivity, is therefore related to the ratio of time scale as τ_1/τ_2 . In order to have valid H-theorem, the relaxation time should follow the condition, $\tau_1 \leq \tau_2$ (Ansumali *et al.* 2007). Apart from the usual conserved quantities, mass, momentum and energy density, a quasi-conserved quantity, the energy flux defined as, $\mathbf{q} = \sum_{i=1}^N (f_i - f_i^{eq}) c_i^2 \mathbf{c}_i$, is also included

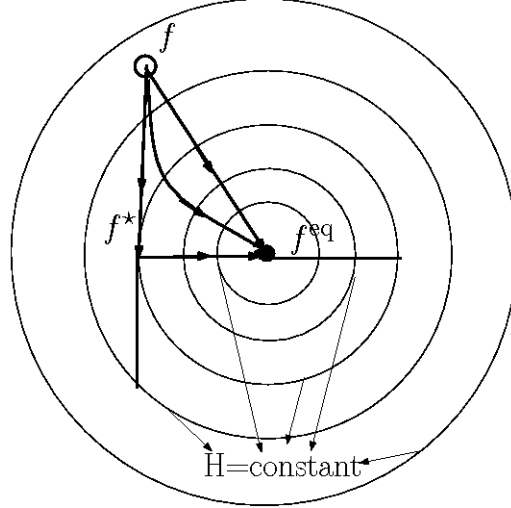


Figure 3.10: Scheme showing the relaxation of f to f^{eq} through a quasi-equilibrium state f^*

in the relaxation process, which gives quasi-equilibrium as (Ansumali *et al.* 2007):

$$f_i^* = \rho W_i(\theta) \left[1 + \frac{c_{i\alpha}}{\theta} (u_\alpha - u'_{i\alpha}) + \frac{u_\alpha u_\beta}{2\theta^2} (c_{i\alpha} c_{i\beta} - \theta_i) + \frac{q_\alpha}{(D-1)\theta^2(1-\theta)} c_{i\alpha} c_i^2 \right], \quad (3.63)$$

where

$$u'_{i\alpha} = \frac{q_\alpha(1 + (D-1)\theta)}{(D-1)\theta^2(1-\theta)}. \quad (3.64)$$

The two-time relaxation collision operator is given by

$$\Omega(f) = \frac{1}{\tau_1} [f_i^*(\rho, \mathbf{u}, \theta, \mathbf{q}) - f_i] + \frac{1}{\tau_2} [f_i^{\text{eq}}(\rho, \mathbf{u}, \theta) - f_i^*(\rho, \mathbf{u}, \theta, \mathbf{q})] \quad (3.65)$$

The kinetic equation is integrated along the characteristics, using the trapezoidal scheme to obtain the following evolution equation:

$$g_i(\mathbf{x} + \mathbf{c}\Delta t, t + \Delta t) = g_i(\mathbf{x}, t) (1 - 2\beta) + 2\beta \left[\left(1 - \frac{\tau}{\tau_1}\right) f_i^*(\rho, \mathbf{u}, \theta, \mathbf{q}) + \frac{\tau}{\tau_1} f_i^{\text{eq}}(\rho, \mathbf{u}, \theta) \right], \quad (3.66)$$

with the auxiliary population, g , defined as Eq. (3.40). The quasi conserved moment \mathbf{q} takes the following form, in terms of the auxiliary population g :

$$\mathbf{q}(g) = \mathbf{q}(f) - \frac{\Delta t}{2\tau_1} (\mathbf{q}^{\text{eq}} - \mathbf{q}). \quad (3.67)$$

3.12.1 Bench-marking via Doubly periodic Shear Layer

In this section, the set up of doubly periodic shear layer is considered to show that introducing tunable Pr number via multi-relaxation scheme indeed help in making the numerical scheme more stable. The parameters used in simulation are $\text{Re} = 30000$, $U_0 = 0.04$ for isothermal, energy conserving as well as for simulations with Pr correction. The ratio between two time scales in the latter i.e. τ_1/τ_2 , is taken to be 0.005. It can be seen from Fig (3.11), that the setup with Pr-correction converges towards a steady state value with the grid size as low as 200×200 .

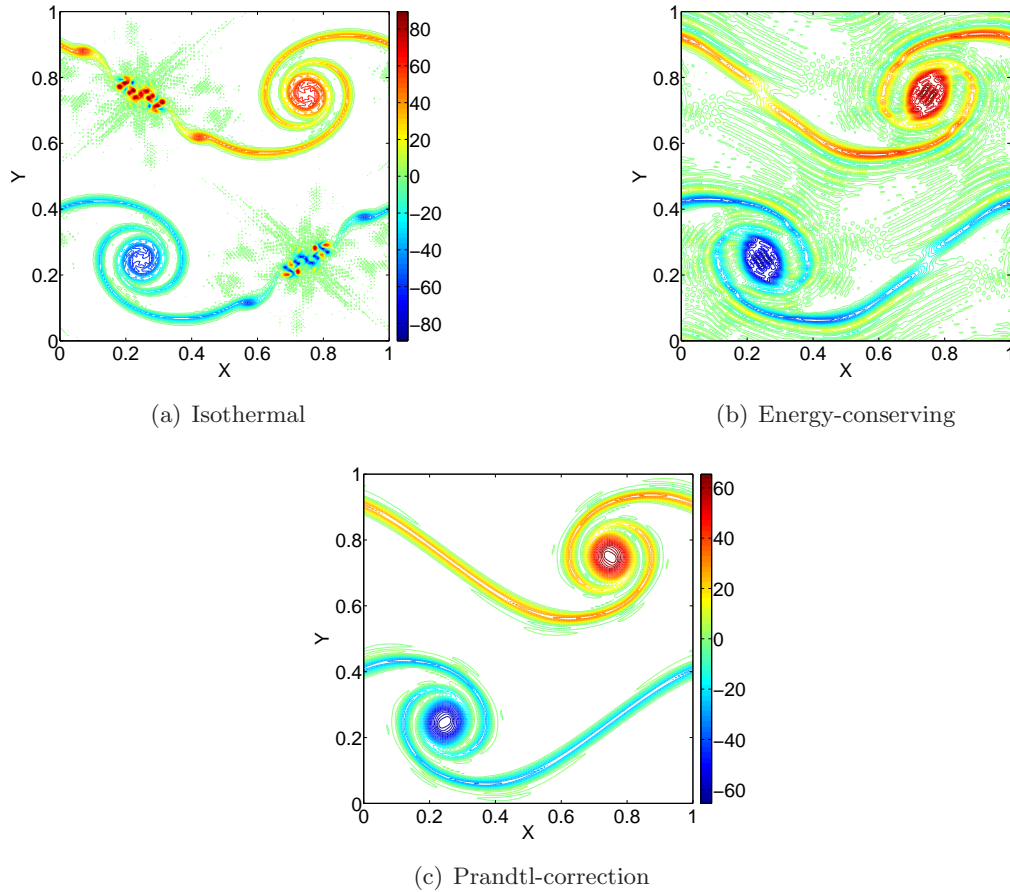


Figure 3.11: Vorticity field at convection time=1 on 200×200 grid.

At the same resolution, even though energy conserving model has stable solution, it shows some disturbance and the isothermal model blows up.

3.13 Outlook

In this chapter, the lattice Boltzmann method is reviewed. The low Mach number acoustic dynamics is recovered in terms of correct speed of sound given by Eq. (3.59). It is also shown that the thermodynamic consistency plays a major role in determining the quality of simulation results even for isothermal flows. In other words, reproducing the correct sound speed gives rise to a much more robust numerical scheme. Furthermore, on rectifying one more deficiency of LB by introducing a non-unit Prandtl (Pr) number through a multi-relaxation model makes the method even more stable. To conclude, it was shown that LBM framework and its extension via quasi-equilibrium is suitable to solve the kinetic equation in relaxation form. This kind of methodology is important for polymer solution which involves various time scales such as viscous, diffusive and elastic.

Chapter 4

Lattice Fokker Planck Method

4.1 Introduction

Direct numerical simulations of complex flows of polymer solutions (typically modeled as dumb-bell) are now regularly used in understanding of complex phenomena such as polymeric drag reduction (Virk 1975; Bird *et al.* 1987*a*). However, a substantial part of the computational resources in such simulations are spent in the polymer solver rather than the hydrodynamic solver (Somasi *et al.* 2002; Koppol *et al.* 2007). This happens for macroscopic simulations using constituting models because these models are numerically expensive to solve and often requires numerical artifacts such as addition of artificial viscosity (Sureshkumar *et al.* 1997). On the other hand, though the microscopic BD simulations of underlying Langevin equation are numerically quite simple, they require averaging over a large number of trajectories, which is quite expensive for hydrodynamic simulations. Therefore, it is desirable to devise an alternate direct approach to solve the underlying Smoluchowski equation for the configuration probability density (Risken 1996; Lozinski & Chauvière 2003; Chauvière & Lozinski 2004). One may choose to directly discretize the corresponding Fokker Planck collision operator by expanding it in a sequence of Hermite polynomials (Moroni *et al.* 2006*a,b*; Melchionna *et al.* 2006). However, the above approach would be limited to extremely weak flows, since, for strong flows, a similar expansion of the distribution function would require the inclusion of a large number of terms.

In Chapter. 2, an alternate scheme is proposed to model Fokker Planck collision operator via BGK type relaxation mechanism relying on the fact that the precise nature of the short-time momentum relaxation processes will not alter the slow dynamics of configuration distribution function governed by Smoluchowski Equation. Finally, after introducing the lattice Boltzmann method in Chapter 3 as the discrete numerical scheme for solving Boltzmann BGK equation, a similar numerical scheme for solving inertial polymer dynamics via a BGK type relaxation mechanism is described in this Chapter.

The Chapter is organized as follows: A discrete formulation based on LB for polymer phase-space dynamics is presented in Sec.4.2. In Sec.4.3, the results to validate the proposed formulation by a comparison of the bulk rheological material functions with the results of BD simulations for shear flow and the extensional flows are presented. Finally, after giving an approximate idea of simulation time required, we conclude the Chapter in Sec.4.4.

4.2 Discrete Polymer Kinetic Theory

In kinetic theory of gases, the variable of interest is the probability distribution function $f(\mathbf{x}, \mathbf{v}, t)$ which is a function of the location \mathbf{x} and the particle velocity \mathbf{v} at a given time. In this chapter,

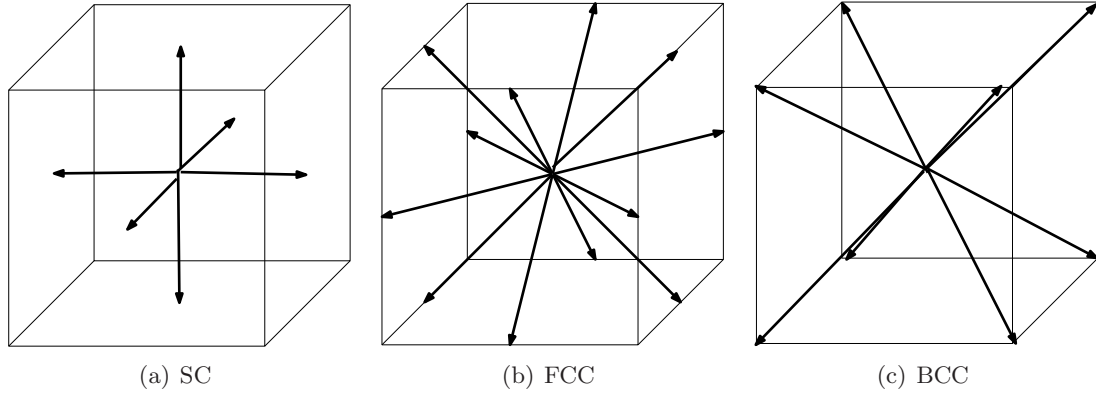


Figure 4.1: Schematic of the three elementary structures used in velocity-space models.

an LB like formulation for polymer dynamics is developed where $\dot{\mathbf{Q}}$ plays the role analogous to \mathbf{v} in discrete kinetic theory of fluids. Therefore, the quantity of interested becomes probability distribution function that depends on the the end-to-end vector \mathbf{Q} and its rate of change $\dot{\mathbf{Q}}$ at given time t . In other words,

$$f(\mathbf{x}, \mathbf{v}, t)_{\text{Hydrodynamic}} \rightarrow f(\mathbf{Q}, \dot{\mathbf{Q}}, t)_{\text{Polymer-Dumbbell}}. \quad (4.1)$$

The discrete probability distribution function in this case corresponds to discrete $\dot{\mathbf{Q}}_i$ is $f(\mathbf{Q}, \dot{\mathbf{Q}}_i, t) \equiv f_i$. The evolution equation for this discrete population f_i in non-dimensional form is

$$\frac{\partial f_i}{\partial t} + \dot{Q}_{i\alpha} \frac{\partial f_i}{\partial Q_\alpha} = \frac{1}{\epsilon} (f_i^{\text{eq}}(\psi, \bar{\mathbf{v}}^*) - f_i), \quad (4.2)$$

where the configuration probability ψ defined as $\psi = \sum_i^N f_i$ and, unlike hydrodynamics, \mathbf{v}^* is some imposed velocity field, given as:

$$\bar{v}_\alpha^* = \text{Wi} U_\alpha - \frac{F_\alpha^c}{2}. \quad (4.3)$$

As an example for the discrete velocity set $\dot{\mathbf{Q}}$, D3Q27 velocity-space model which consists of the simple cubic (SC), face-centered (FCC), body-centered (BCC) structures and a zero velocity, is chosen. The discrete velocities present in the above mentioned structures are shown in Fig.(4.1) and the weights corresponding to the different structures are:

$$w_0 = 8/27, \quad w_{\text{SC}} = \frac{2}{27}, \quad w_{\text{FCC}} = \frac{1}{54}, \quad w_{\text{BCC}} = \frac{1}{216}, \quad (4.4)$$

with the magnitude of the discrete velocities being $\dot{Q} = \sqrt{3}c_s$. We use the equilibrium distribution in the form:

$$f_i^{\text{eq}} = w_i \psi \left[1 + \frac{\bar{v}_\alpha^* \dot{Q}_{i\alpha}}{c_s^2} + \frac{\bar{v}_\alpha^* \bar{v}_\beta^*}{2 c_s^4} \left(\dot{Q}_{i\alpha} \dot{Q}_{i\beta} - c_s^2 \delta_{\alpha\beta} \right) \right]. \quad (4.5)$$

On introducing the auxiliary population g_i as done in Eq. (3.40) and after doing time and

space discretizations, the LB formulation is implemented in the following manner for obtaining polymer dynamics in \mathbf{Q} space:

$$g_i(\mathbf{Q} + \dot{\mathbf{Q}}\Delta t, t + \Delta t) = g_i(\mathbf{Q}, t) + 2\beta[g_i^{eq}(\psi(\mathbf{Q}, t), \bar{\mathbf{v}}^*(\mathbf{Q})) - g_i(\mathbf{Q}, t)], \quad (4.6)$$

where $\beta = \Delta t / (2\epsilon + \Delta t)$. As discussed in Chapter 3, the whole algorithm becomes a sequence of memory shifts and compute step on the grid in \mathbf{Q} , shown in Fig. 4.2.

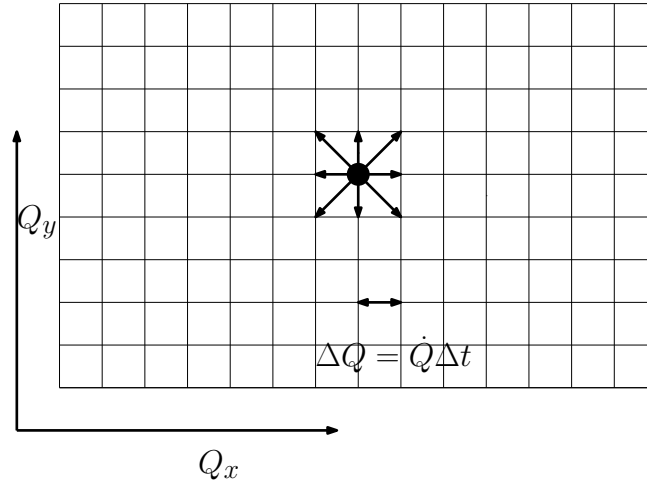


Figure 4.2: Schematic of D2Q9 velocity set on two dimensional physical grid.

The solution of the above equation gives the value of the configuration probability density ψ at a given time instant. Knowledge of the value of ψ is sufficient to predict the non-equilibrium behavior of FENE dumbbell. It should be noted that the magnitude of $\bar{\mathbf{v}}^*$ increases with Wi . Furthermore, in order to ensure the low Ma limit, we chose \dot{Q} such that $(\bar{\mathbf{v}}^*/c_s)$ is small.

4.2.1 Boundary condition

The FENE spring force $\hat{\mathbf{F}}^c = \mathbf{Q}/\{1 - Q^2/b\}$ has a singularity at $\mathbf{Q} = \sqrt{b}$. In order to avoid this singular point, the simulation domain is restricted to a sphere of radius $r \approx 0.99\sqrt{b}$ as shown in Fig. 4.3. The length of simulation box L is taken as $L = (1 + \epsilon) \times r$ where ϵ is chosen such that maximum possible volume is utilized. Typical value of ϵ chosen in the calculation is around 0.8. Finally, at the boundaries of the spherical domain, the bounce-back boundary condition for the discrete populations is applied, which in LB for hydrodynamics, is used to mimic solid boundaries (Ladd 1994; Succi 2001; Chen & Doolen 1998). The populations coming inside the sphere are corrected so that no flux condition is imposed, as

$$g_{(\dot{\mathbf{Q}} \cdot \mathbf{n} > 0)}(\mathbf{Q}, \dot{\mathbf{Q}}_i, t) = g(\mathbf{Q}, -\dot{\mathbf{Q}}_i, t) \quad |\mathbf{Q}| \leq r \quad \text{and} \quad |\mathbf{Q} + \dot{\mathbf{Q}}\Delta t| > r, \quad (4.7)$$

where \mathbf{n} is the wall normal vector. The physical idea behind using this ad-hoc boundary condition is that near boundaries $\psi \rightarrow 0$, so the precise nature of boundary condition is not important as long as it is mass conserving (Lozinski & Chauvière 2003; Chauvière & Lozinski 2004). This conjecture is verified post priori by looking at the quality of obtained results. The above mentioned condition is illustrated for the two dimensional case in the Fig.(4.4) where the incoming

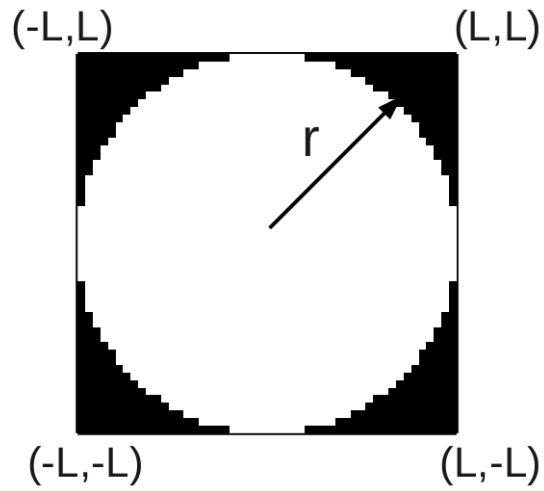


Figure 4.3: 2D cross-section of real 3D simulation domain with bounce-back boundary condition

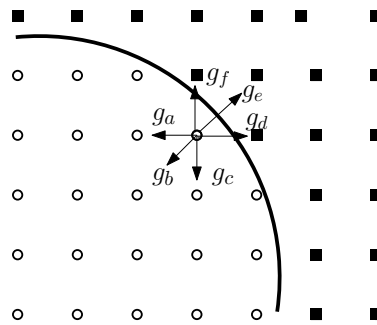


Figure 4.4: 2D implementation of the bounce-back boundary condition. Circle are nodes inside the FENE sphere and filled squares are the nodes outside the sphere

populations are corrected at a given marked point at boundary of FENE sphere as

$$g_a = g_d, \quad g_b = g_e, \quad g_c = g_f. \quad (4.8)$$

Finally, the initial value of ψ is taken as the equilibrium distribution in the absence of flow (Bird *et al.* (1987b)) which is,

$$\psi(\mathbf{Q}, 0) = \begin{cases} N_{\text{eq}}(1 - Q^2/b)^{b/2} & \text{for } |Q| \leq r \\ 0 & \text{elsewhere,} \end{cases} \quad (4.9)$$

where $N_{\text{eq}} = 2\pi b^{3/2} B\{3/2, (b+2)/2\}$ and $B\{x, y\}$ is the Beta function (Bird *et al.* 1987b).

4.3 Results

In order to validate the present scheme, the bulk rheological properties in two canonical flow situations viz. simple shear flow (section 4.3.1) and extensional flow are examined (section 4.3.2). The total stress in a polymer solution is given as $\boldsymbol{\sigma} = \boldsymbol{\sigma}_S + \boldsymbol{\sigma}_P$, where $\boldsymbol{\sigma}_S$ is the Newtonian solvent stress and $\boldsymbol{\sigma}_P$ is the extra stress due to the presence of polymer. In sections 4.3.1 and 4.3.2, the results for $\boldsymbol{\sigma}_P$ are presented for various canonical flows, with σ^P being calculated from the Kramers form of the polymer contribution to the total stress, being given by

$$\boldsymbol{\sigma}_P = n \langle \mathbf{Q}\hat{\mathbf{F}}^c \rangle - n \langle \mathbf{Q}\hat{\mathbf{F}}^c \rangle_{eq}. \quad (4.10)$$

Later in this section, it is shown that the present scheme is able to capture the important rheological properties exhibited by FENE dumbbell model which are absent in the constitutive model like FENE-p. For example, the non-zero transient value of second normal stress coefficient in shear flow and the existence of hysteresis curve between the polymeric stress and molecular extension, in the extensional flow. The simulations presented here are performed on a Sandy-bridge Intel CPU with 2×8 cores@ 2.6 GHz. The peak single core efficiency for this system is 20.8 Gflops and maximum memory bandwidth is 51.2 GB/s.

4.3.1 Shear flow

In simple shear flow, the flow is characterized by the transpose of the velocity gradient tensor:

$$\boldsymbol{\kappa} = \dot{\gamma} \begin{bmatrix} 0 & 1 & 0 \\ 0 & 0 & 0 \\ 0 & 0 & 0 \end{bmatrix}, \quad (4.11)$$

where $\dot{\gamma}$ is the shear rate which is a constant in steady shear flows. The three material functions that completely describe the behavior in simple shear flow, and more generally in any viscometric flow, are the shear viscosity, and the first and second normal stress normal stress differences,

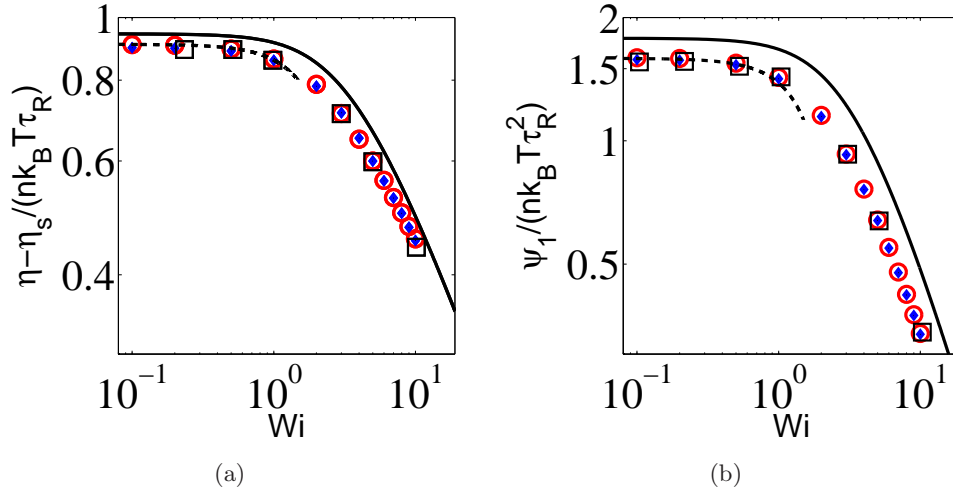


Figure 4.5: Steady state value of the shear viscosity and the first normal stress coefficient for different Wi for an extensibility parameter $b=50$. Circles, present scheme with 24^3 as the number of grid points; filled diamonds symbols, present scheme with 32^3 as the number of grid points; square, Brownian Dynamics (Herrchen & Öttinger 1997); dashed line denotes the small Wi -expansion for FENE dumbbells, while the solid line denotes the predictions of the FENE-p model.

often one works with equivalent dimensionless quantities, defined as

$$\frac{\eta(\dot{\gamma}) - \eta_s}{nk_B T \tau_R} = \frac{1}{Wi} \left(\frac{\sigma_{xy}}{nk_B T} \right), \quad \frac{\psi_1}{nk_B T \tau_R^2} = \frac{1}{Wi^2} \left(\frac{\sigma_{xx} - \sigma_{yy}}{nk_B T} \right) \quad \text{and} \quad \frac{\psi_2}{nk_B T \tau_R^2} = \frac{1}{Wi^2} \left(\frac{\sigma_{yy} - \sigma_{zz}}{nk_B T} \right), \quad (4.12)$$

where ψ_1 and ψ_2 are the first and second normal stress coefficients, and are related to the corresponding normal stress difference as $N_1 = \psi_1 \dot{\gamma}^2$ and $N_2 = \psi_2 \dot{\gamma}^2$ respectively. In Fig.(4.5), the shear viscosity and the first normal stress coefficient for steady simple shear flow are plotted with respect to Wi for an extensibility parameter $b = 50$. The numerical results are compared to a small Wi -expansion, for the FENE dumbbell (Warner 1972; Christansen & Bird 1977). As can be seen from Fig.(4.5), the present scheme is in good agreement with the analytical expansion. Further, the corresponding rheological properties for the FENE-p model (Bird *et al.* 1980) are also shown in Fig.(4.5). It is evident from Fig.(4.5) that the present scheme is capable of giving results in good agreement with BD until a reasonably high value of Wi (≈ 10) with a modest number of grid points (32^3). In contrast, the FENE-p model always over-predicts the values of the shear viscosity and the first normal stress coefficient despite the qualitative dependence on Wi being the same.

For start-up shear flow, $\dot{\gamma}$ in Eq. (4.11) is proportional to the Heaviside function, $H(t)$, that is, before the start of the flow (at time $t = 0$), the fluid is at equilibrium and the (deviatoric) stresses are zero. In Fig.(4.6) and Fig.(4.7), the growth of the time dependent shear viscosity (η^+) and the first normal stress coefficient (ψ_1^+) is presented for $Wi = 1$ and 10 , and for different values of the extensibility parameter b . The results are again in good agreement with those obtained from BD simulations. In the present case, 32 grid points in each direction for the

simulation are chosen. As seen from Fig.(4.6) and Fig.(4.7), for this choice of the number of grid points, predictions of the present scheme are already in good agreement with BD in comparison to those of FENE-p.

With increase in the shear rate, one expects an overshoot (Doyle *et al.* 1997; Hua *et al.* 1999) in the value of material functions as polymer strands stretch significantly for a small interval of time soon after the start up of shear flow before eventual retraction and alignment with the flow direction (Larson 1988). Thus, as seen from Fig.(4.7), for the increased Wi , the present scheme does predict an overshoot for both the material functions before they reach their steady state values. Note that the amplitude of the overshoot relative to the final steady value decreases with increasing values of b . This behavior is consistent with the observed absence of such a behavior in the limit of infinitely extensible Hookean dumbbells, the constitutive equation in this case being the Oldroyd-B model (Warner 1972; Bird *et al.* 1987b). The second normal

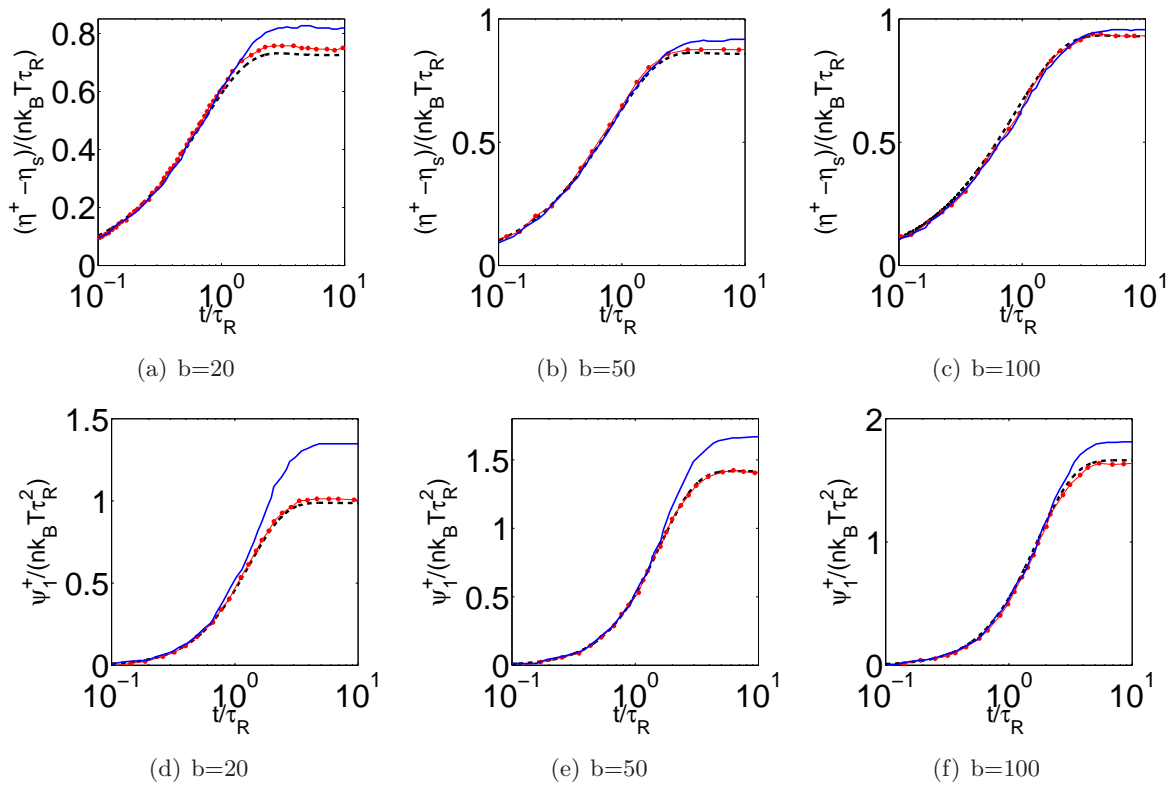


Figure 4.6: Time evolution of the shear viscosity and the first normal stress coefficient for $Wi=1.0$. Dashed lines, present scheme with 32^3 as the number of grid points; dots connected with lines, Brownian Dynamics for FENE dumbbells (Herrchen & Öttinger 1997); continuous lines, numerical solution for FENE-p (Herrchen & Öttinger 1997).

stress coefficient in start-up flow reaches a maximum value before going to zero as shown in Fig.(4.8). For the FENE-p model, ψ_2^+ is identically zero for all times. The non-zero value of ψ_2^+ for intermediate times, before vanishing at steady state, is thus a characteristic feature of the FENE model and is accurately captured by the present scheme.

It is evident from Figs (4.6)-(4.8) that the FENE-p approximation performs quite poorly with regard to predicting all rheological properties in simple shear flow. The pre-averaging

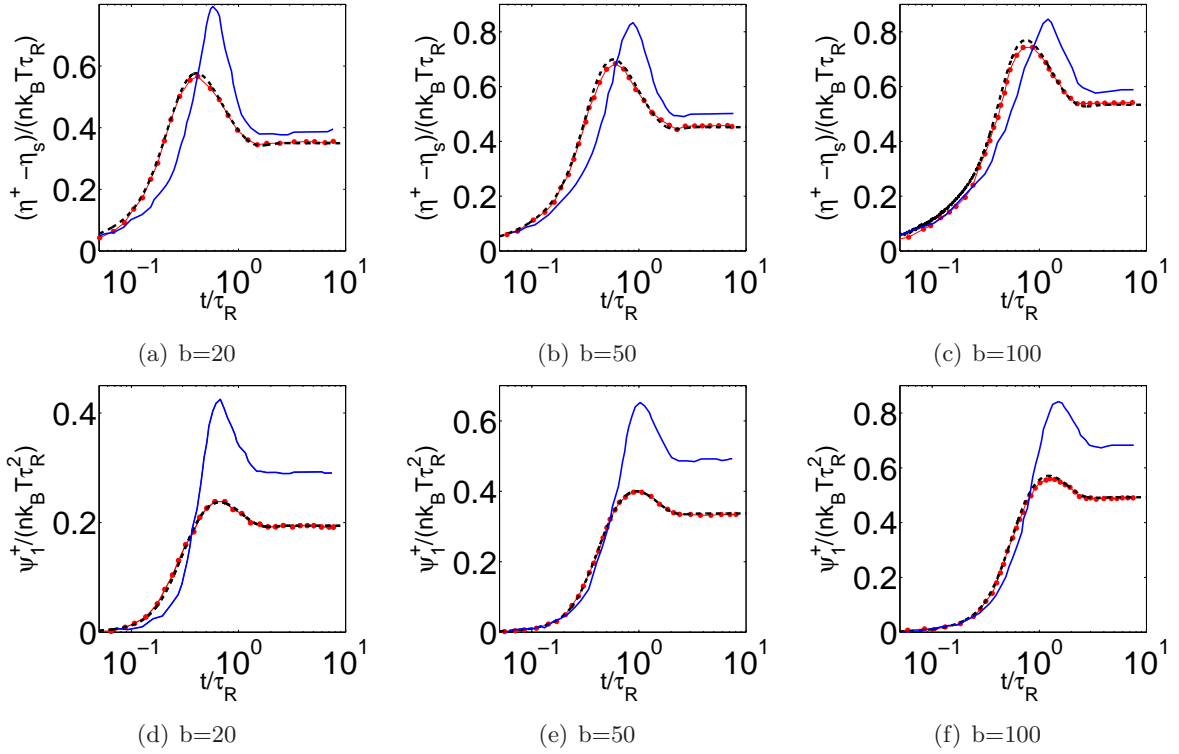


Figure 4.7: Time evolution of the shear viscosity and the first normal stress coefficient for $Wi=10.0$. Dashed lines, present scheme with 32^3 as the number of grid points; dots connected with lines, Brownian Dynamics for FENE dumbbells (Herrchen & Öttinger 1997); continuous lines, numerical solution for FENE-p (Herrchen & Öttinger 1997).

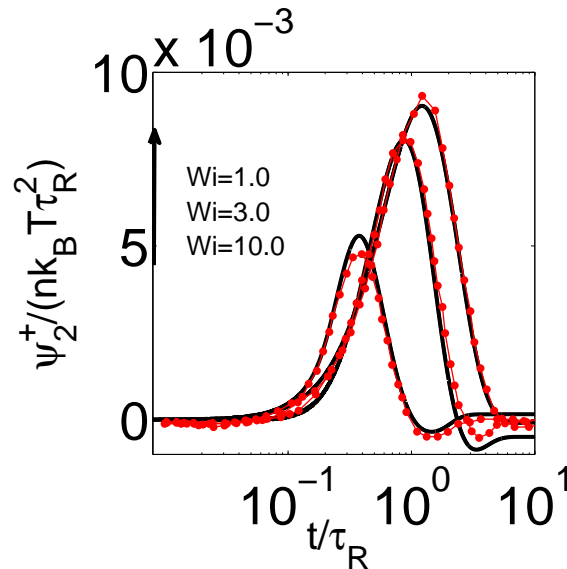


Figure 4.8: Time evolution of the second normal stress coefficient for $Wi=1,3,10$. Continuous lines, present scheme with 32^3 as the number of grid points; dots connected with lines, Brownian Dynamics for FENE (Herrchen & Öttinger 1997).

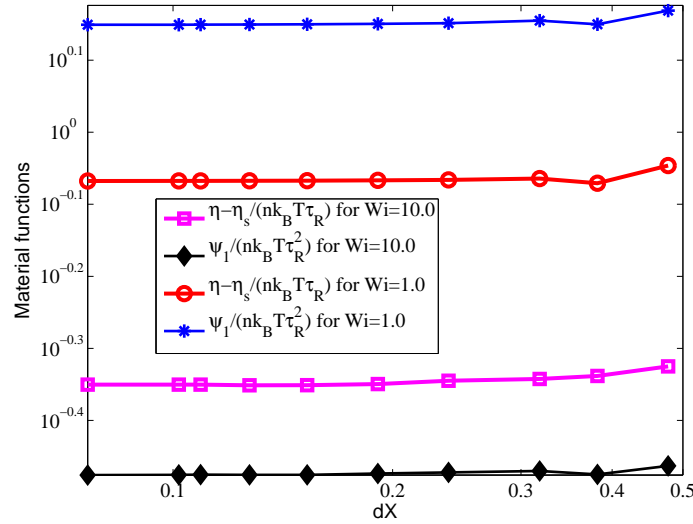


Figure 4.9: Steady state value of the shear viscosity and first normal stress coefficient at $Wi=1$ and 10 for $b=50$ with the grid spacing dX defined as $L/(\text{Number of grid points in each direction})$

approximation is known to radically change the statistical properties of the distribution of polymer configurations (Keunings 1997; Lielens *et al.* 1998; Doyle *et al.* 1998). The distribution of FENE-p dumbbells is, in fact, always Gaussian as first shown in (Öttinger 1987) and illustrated numerically in (Keunings 1997) and entirely determined by its second moment $\langle QQ \rangle$. It is only the root mean squared extension associated with this Gaussian distribution that is constrained to be less than Q_0 . The presence of polymer molecules with unphysical extensions greater than Q_0 leads to an error in the bulk properties at any Wi . The error is expected to decrease for larger values of b , and with decreasing Wi , due to the smaller fraction of unphysically extended molecules, and this trend is observed in the figures. It is worth mentioning that the assignment of a probability distribution to the FENE-p approximation is not unique, and the same constitutive equation results from assuming the distribution function to be (infinitely) localized at all times (Lielens *et al.* 1998). This interpretation is used in section (4.3.2) to rationalize the accuracy of the FENE-p predictions for values of Wi above the coil-stretch threshold.

In order to study grid convergence, the calculations with 24 and 32 grid points in each direction, are performed. In Fig. (4.9), the steady state values of the shear viscosity and first normal stress coefficient at $Wi=1$ and 10 for $b=50$, for different grid sizes, is plotted. From Table 4.1, one may conclude that the converged values for the bulk rheological properties may be taken to be that of a simulation with 75^3 ($dX \approx 0.1$) grid points. In Fig.(4.10), the percentage errors in the shear the viscosity and the first normal stress coefficient for different Wi are presented. The main objective of Fig.(4.10) is to show that that the percentage error is reasonably low (around 1.0-1.5%) even for small resolutions(24^3 and 32^3 grid points) and high Wi (≈ 10). Although, the simulation with 20^3 and 16^3 as the number of grid points, the results have a more than 5% error which is also evident from Fig. (4.9).

The two possible sources of error in the present scheme are poor space discretization and the artificiality of the bounce-back boundary condition. The error due to the boundary condition is expected to be prominent for the case when the the probability density function of polymer

Table 4.1: Steady state value of shear viscosity and first normal stress-coefficient at $Wi=1.0$ and 10.0 for $b=50$ with different grid sizes

N		16	20	32	50	75	100
$\frac{\eta-\eta_s}{nk_B T \tau_R}$	Wi=1.0	0.8988	0.8495	0.8586	0.8565	0.8558	0.85570
	Wi=10.0	0.4730	0.4588	0.4518	0.4455	0.4463	0.4463
$\frac{\psi_1}{nk_B T \tau_R}$	Wi=1.0	1.4750	1.4119	1.4168	1.4118	1.4100	1.4097
	Wi=10.0	0.34423	0.33495	0.33708	0.33455	0.33452	0.33433

configurations, $(\psi(\mathbf{Q}))$, touches the boundaries (which is typically the case for large Wi) and violates the condition of $\psi(\mathbf{Q}) \rightarrow 0$ near boundaries. The discretization error is expected to be significant when probability density function is concentrated around the center of the domain (usually the case for small Wi). As a result, one expects the error to be minimum at an intermediate value of the Weissenberg number, a fact that is confirmed for both shear and extensional flows (see Figs.(4.10) and (4.19)). In Fig.(4.11) the probability density $\psi(\mathbf{Q})$ is plotted with respect to $|\mathbf{Q}|$ which, expectedly, shows that at low Wi (≈ 1) the distribution is more or less concentrated at the equilibrium extension, while at high Wi (≈ 10) it tends to spread over the whole domain. Thus, as shown in Fig.(4.10), for small Wi (≈ 1), the discretization error is very high for low resolutions (24^3 grids). But, at the higher Wi ($Wi = 10$), the difference between the errors with the two grid resolutions becomes small which implies that, as the probability distribution function tends to spread throughout the complete configurational domain, the discretization error may not matter and coarser discretization can be used to get accurate results.

It is important to note that the uniform spread of the probability density function over the entire configuration domain is due to the inability of shear flow, a weak flow, to stretch polymer chains. As a result, the error due to the bounce-back boundary condition does not affect the results to a great extent, and the error for a given discretization rises only weakly with increasing Wi beyond that corresponding to the minimum error. The general feature of the configuration distribution being uniformly spread across the entire domain, at high Wi and for simple shear flow, has been observed earlier by (Hur *et al.* 2000), and this led to the average extension (defined by the reference (Hur *et al.* 2000) as the projection onto the flow-vorticity plane) asymptoting to only approximately half the value at full extension even as Wi approached infinity. Hur *et al.* (2000) obtained qualitatively similar results for $\psi(Q)$ for both a fine-scale Kramers bead-rod model and a FENE dumbbell, although the latter over predicted the averaged extension due to the absence of additional internal degrees of freedom. A direct comparison of Fig.(4.11) with these results is, however, not possible since the ratio of the fully extended to the equilibrium lengths, used in the above calculation ($b=447$), is much larger than that used here ($b = 50$). It should also be noted that although decreasing the number of grid points does not affect value of η and ψ_1 to a great extent, it has a drastic effect on the time dependent behavior of the second normal stress coefficient (ψ_2^+). As can be seen from Fig.(4.12), at $Wi=1.0$, a small number of

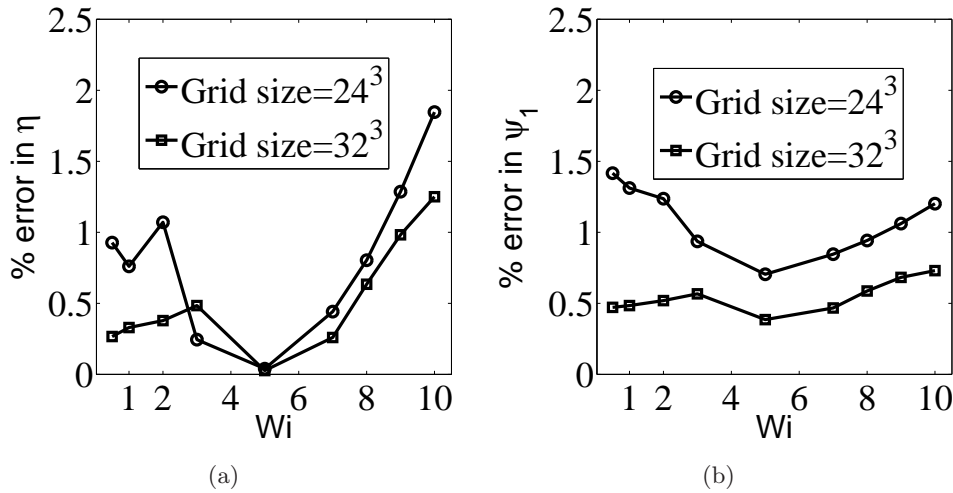


Figure 4.10: Percentage error in shear viscosity and first normal stress coefficient for different Wi with two different grid sizes ($b=50$).

grid points results in a different time dependent behavior of ψ_2 , while for $Wi=10.0$ simulations, both grid sizes give almost the same behavior; consistent with the aforementioned arguments.

As discussed in Sec 2.4, the correct dynamics in Q -space emerges in the Chapman-Enskog expansion as the first correction from equilibrium. The corresponding order in the traditional kinetic theory framework for dilute gases (Chapman & Cowling 1991) would lead to the Navier-Stokes equation. However, the absence of momentum conservation implies that the symmetry requirements are less stringent compared to hydrodynamics. Thus, the number of discrete velocities in phase space can be reduced, further contributing to the economy of computation. It should be noted that in isothermal Navier-Stokes hydrodynamics, the fourth-order moment of the zero velocity discrete equilibrium distribution is required to be isotropic. As a result, the number of discrete velocities typically chosen for isothermal hydrodynamic computations are 27 (D3Q27), 19 (D3Q19) and 15 (D3Q15) where the D3Q15 model is not as accurate and less stable compared to the others (Chikatamarla *et al.* 2006). In contrast, even the D3Q13 model yields reasonable results for the present problem. In order to examine the efficiency, in terms of accuracy, of models with fewer discrete velocities, D3Q13, D3Q15 and D3Q19 velocity models with 13, 15 and 19 discrete velocities respectively are chosen. The D3Q13 model contains only an FCC structure which has 12 discrete velocities with an additional zero velocity. The D3Q15 model contains 15 discrete velocities- a zero, 6 corresponding to an SC structure and 8 corresponding to an BCC structure. Finally, the D3Q19 model contains 19 discrete velocities- a zero, 6 corresponding to an SC structure and 12 corresponding to an FCC structure. The weights corresponding to these velocity-space models are given in Table 4.2. All the velocity-space models above predict almost the same values for the shear viscosity and the first normal stress coefficient at reasonably good resolution (32^3 grid points). As can be seen from Fig.(4.13), on further decreasing the resolution (to 24^3), the percentage error in the steady state value of the shear viscosity and first normal stress coefficient remains small (around 2 to 2.5) for all the four velocity-space models. The converged value is again taken to be that of the simulation with 75^3 grid points. In Fig.(4.14) and (4.15), the temporal dynamics of the second normal stress

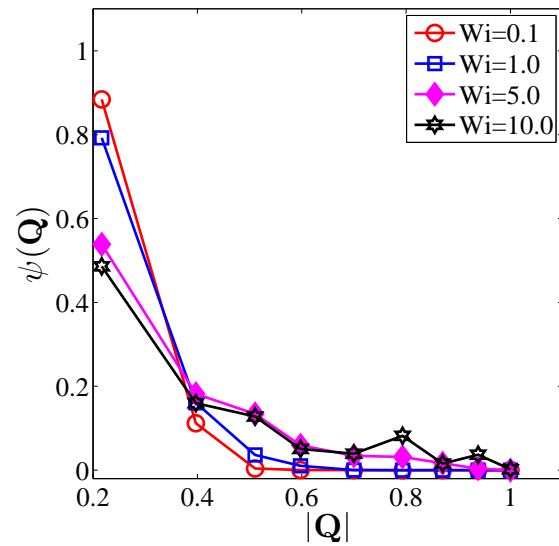


Figure 4.11: Probability density $\psi(\mathbf{Q})$, as a function of $|\mathbf{Q}|$, at steady state for simple shear flow for different Wi ($b=50$).

Velocity-space model	w_0	w_{SC}	w_{FCC}	w_{BCC}
D3Q13	1/2	-	1/24	-
D3Q15	2/9	1/9	-	1/72
D3Q19	1/3	1/18	1/36	-

Table 4.2: Weights for different velocity-space models

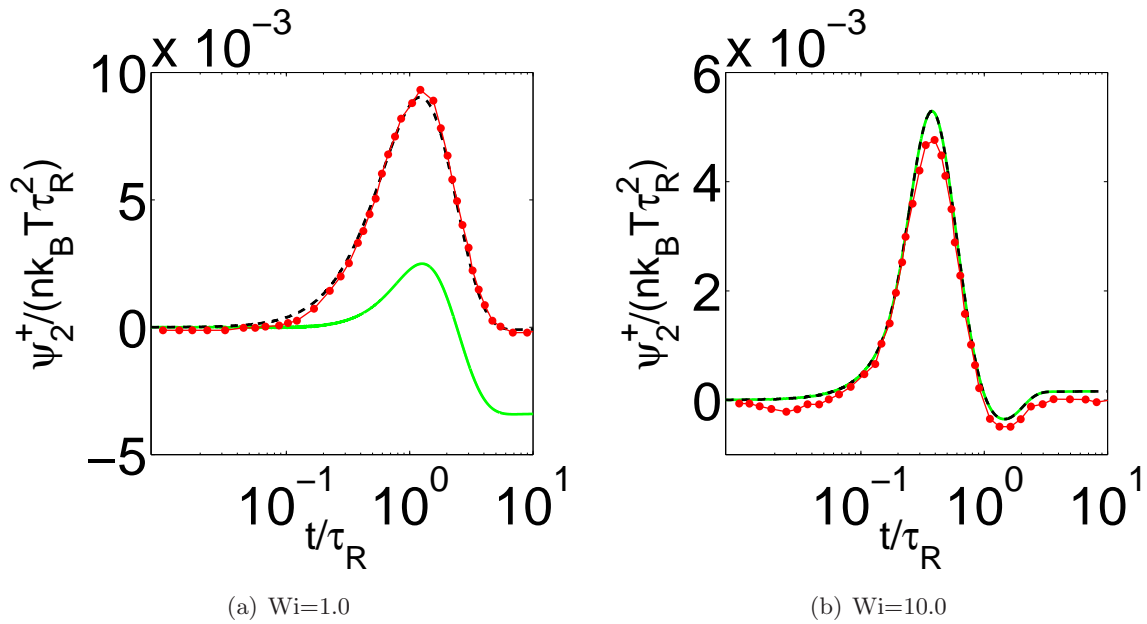


Figure 4.12: Time evolution of the second normal stress coefficient for $Wi=1.0$ and $Wi=10.0$ for different grid sizes. Dashed lines, present scheme with 32^3 as the number of grid points; continuous lines, present scheme with 24^3 as the number of grid points; dots connected with lines, Brownian Dynamics for FENE (Herrchen & Öttinger 1997).

coefficient for $Wi=1$ and $Wi=10$, is plotted for the different velocity-space models, and with 24^3 and 32^3 as the total number grid points. While the resolution of 32^3 grid points is sufficient to capture the variation in time of the second normal stress coefficient accurately for all the four velocity-space models, the simulation with 24^3 grid points predicts different time dynamics of the second normal stress coefficient for the different velocity-space models. As discussed earlier, there may be two sources of error: one due to boundary condition and the other due to poor discretization. It is suggested by Figs.(4.14) and (4.15) that the difference in the prediction of the time dependence of the second normal stress coefficient by the different velocity-space models might be the result of competition between these two errors which requires further investigation.

4.3.2 Extensional Flow

In this section, a canonical non-viscometric flow namely an axisymmetric extensional flow is considered. This provides a more stringent test for the proposed scheme since it is well known that polymer molecules, above a critical extensional rate, undergo a coil-stretch transition (De Gennes 1974; Hinch 1977; Larson 1988). This transition is accompanied by a dramatic change in the underlying distribution of polymer configurations, and therefore, in $\psi(\mathbf{Q})$. The velocity gradient tensor for axisymmetric extensional flow is defined as:

$$\boldsymbol{\kappa} = \dot{\epsilon} \begin{bmatrix} 1 & 0 & 0 \\ 0 & -1/2 & 0 \\ 0 & 0 & -1/2 \end{bmatrix}, \quad (4.13)$$

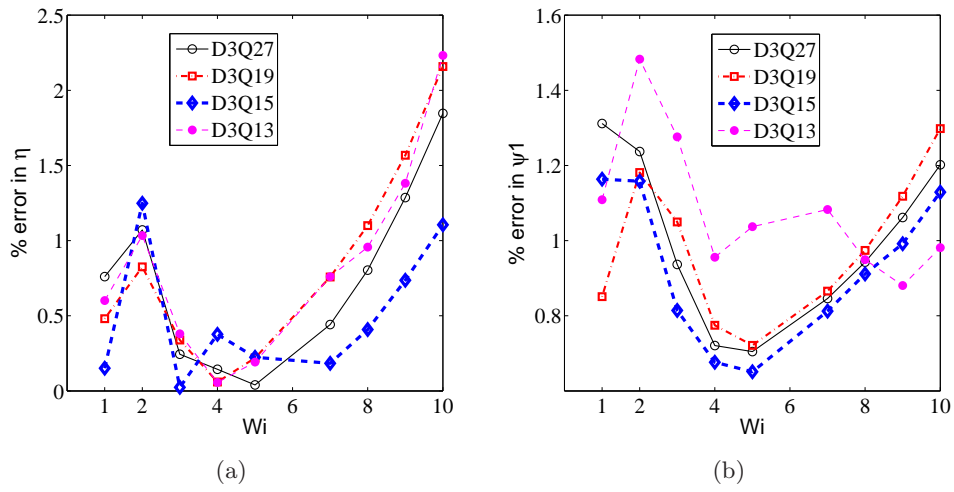


Figure 4.13: Percentage error in the steady state value of shear viscosity and first normal stress coefficient for different LB models for 24^3 grid points for $b=50$.

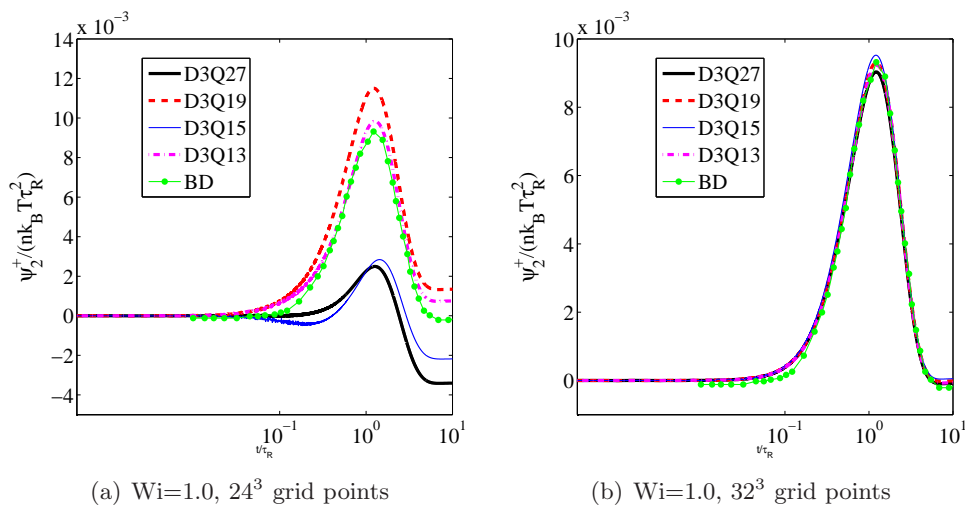


Figure 4.14: Time evolution of the second normal stress coefficient for $Wi=1.0$ for three different LB models with 24^3 and 32^3 grid points for $b=50$

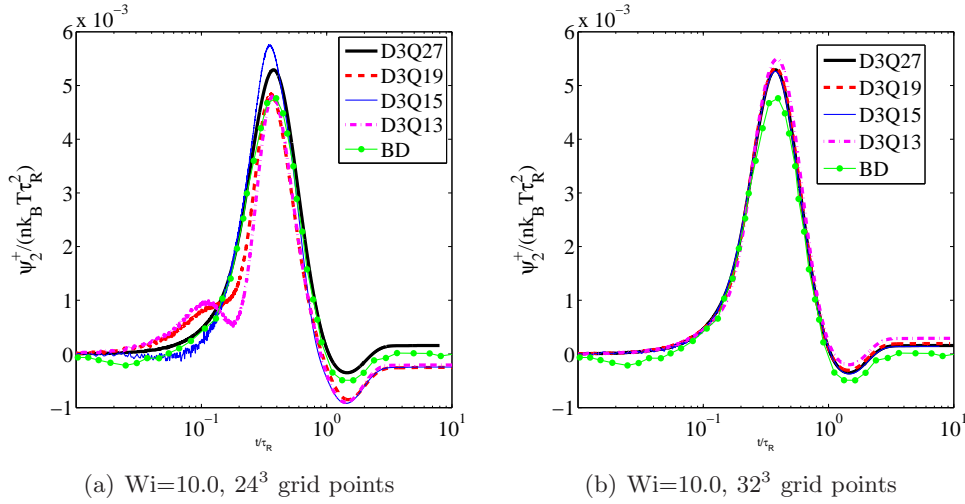


Figure 4.15: Time evolution of the second normal stress coefficient for $Wi=10.0$ for three different LB models with 24^3 and 32^3 grid points for $b=50$

where $\dot{\epsilon}$ is the extensional rate. The material function that characterizes the fluid response in this flow is the extensional viscosity

$$\frac{\eta(\dot{\epsilon}) - 3\eta_s}{nk_B T \tau_R} = \frac{1}{Wi} \left(\frac{\sigma_{xx} - \sigma_{yy}}{nk_B T} \right). \quad (4.14)$$

In Fig.(4.16), the steady state value of the extensional viscosity is presented for an extensibility parameter $b=50$. Around $Wi=0.5$, there is a drastic increase in the extensional viscosity and then, again a plateau, corresponding to a much higher value, at higher Wi . The results are in good agreement with BD; although, with increasing Wi , the number of grid points to capture the high Wi plateau has to be increased. As mentioned earlier, this sudden increase of the extensional viscosity is known as coil-stretch transition (De Gennes 1974; Hinch 1977; Schroeder *et al.* 2003). The small- Wi plateau corresponds to weakly stretch dumbbells with lengths of order the equilibrium extension ($\sqrt{k_B T / H}$), while the high- Wi plateau corresponds to the stress levels arising from nearly fully stretched dumbbells with lengths of $O(\sqrt{b})$.

Asymptotic expressions for the extensional viscosity, for both small and large Wi , have been obtained in Bird *et al.* (1987b), and are shown as dashed lines in Fig.(4.16). The prediction of the FENE-p (continuous lines) model has been obtained in Bird *et al.* (1980) and is also shown.

In order to characterize the coil-stretch transition from the microscopic point of view, the probability density $\psi(\mathbf{Q})$ with respect to \mathbf{Q} , at steady state is examined, for various value of Wi in Fig.(4.17). Knowing $\psi(\mathbf{Q})$, the root mean square extension can be found as $\sqrt{\langle Q^2 \rangle} = \sqrt{(\sum_{\mathbf{Q}} \psi(\mathbf{Q}) Q^2) / (\sum_{\mathbf{Q}} \psi(\mathbf{Q}))}$, and, in Fig.(4.17), this root mean square extension is plotted with respect to Wi . The plot confirms the coil-stretch transition inferred in Fig.(4.16) from the bulk rheological property (extensional viscosity). The probability density, $\psi(\mathbf{Q})$, is very sensitive to the value of Wi in extensional flow, and rapidly transitions, over a narrow range of Wi , from being centered around the equilibrium extension, to being localized near the edge of the near the edge of configurational space ($Q \sim b^{1/2}$). Capturing the coil-stretch transition in strong flows is a demonstration of the competency of the present scheme. At high enough Wi , in sharp

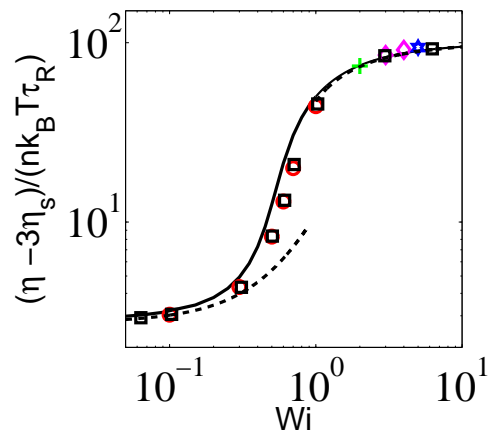


Figure 4.16: Steady state value of extensional viscosity with different Wi for extensibility parameter $b=50$. Circle, present scheme with 24^3 as the number of grid points; plus symbol, present scheme with 32^3 as the number of grid points; diamond symbols, present scheme with 50^3 as the number of grid points; hexagon symbol, present scheme with 75^3 as the number of grid points; square, Brownian Dynamics (Herrchen & Öttinger 1997); dashed lines asymptotic expansion for FENE and continuous line expansion for FENE-p.

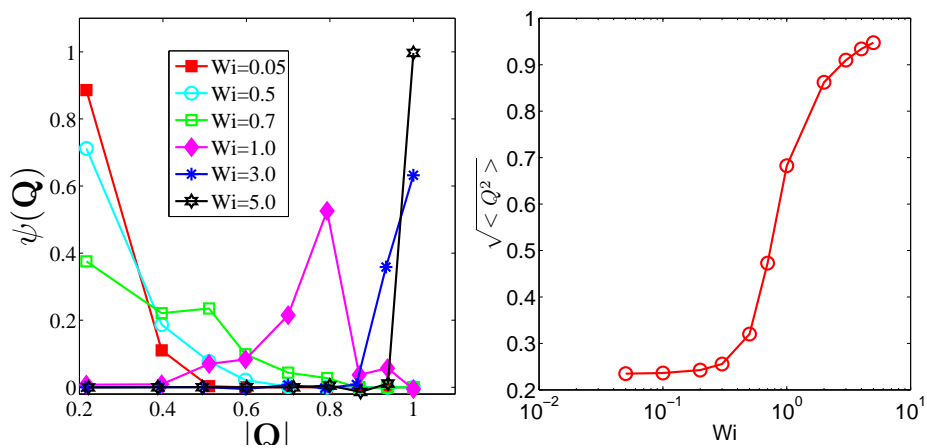


Figure 4.17: Probability density $\psi(\mathbf{Q})$ at steady state with different $|\mathbf{Q}|$, and the root mean square extension as a function of Wi , showing the coil-stretch transition. ($b=50$)

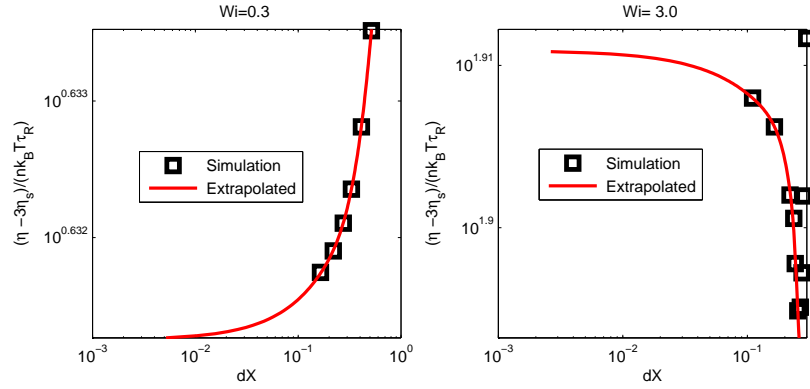


Figure 4.18: Steady state value of the extensional viscosity with respect to dX at $Wi = 0.3$ and 3.0 and $b=50$.

contrast to shear flow, $\psi(\mathbf{Q})$ is concentrated in a very small region at the edge of the domain.

In Fig. (4.18), the steady state value of the extensional viscosity for $Wi = 0.3$ and 3.0 and $b=50$, for different grid sizes, is plotted. The grid requirement increases with increasing Wi and therefore the steady state elongational viscosity value corresponding to the limit $dX \rightarrow 0$, dX being the grid spacing, is taken as the converged value. It is of interest to note that the convergence of the calculated value towards the correct estimate is non-monotonic for Wi above the coil-stretch transition. This arises due to a minimum number of points being required to resolve the peak in the configurational probability density near full extension. Beyond this minimum, the extensional viscosity increases monotonically towards the converged value. In Fig.(4.19), the percentage error in the value of extensional viscosity at steady state is plotted as a function of Wi at two different grid resolutions corresponding to 32^3 ($dX \approx 0.24$) and 50^3 ($dX \approx 0.15$) grid points; the grid requirement increases with increasing Wi , and a 24^3 simulation does not converge at very high Wi . As may be seen from the figure, the percentage error again exhibits a minimum at an intermediate Wi when the distribution is not very localized (either at the equilibrium or at the full extension). However, unlike simple shear flow, both types of error (artificiality of the bounce-back boundary condition and poor spatial discretization) become important, and in particular, the importance of the bounce-back error at high Wi implies that the percentage error rises rapidly with Wi increasing beyond the minimum.

Furthermore, a start-up extensional flow is considered in which case $\dot{\epsilon}$ in Eq. (4.13) is proportional to the Heaviside function, $H_\alpha(t)$ where $H_\alpha(t) = 0$ for $t < \alpha$; $= 1$ for $t > \alpha$. Here, $\alpha = 0$ is taken. In Fig.(4.20) and (4.21), the growth of the extensional viscosity is shown with different values of the extensibility parameter b and for two different Wi . Below the coil-stretch transition threshold, the time dependent behavior of the extensional viscosity is similar for FENE and FENE-p models, although the latter model over-predicts the steady state value as shown in Fig.(4.20). The time-dependent behavior is similar to that seen earlier for the bulk rheological properties in the start-up shear flow (see Fig.(4.6)), indicating the flow-independent nature of the small Wi -regime. It is worth noting that, for the start-up shear flow, the FENE-p model exhibited a discrepancy, at steady state for both $Wi=1.0$ and $Wi=10$ (see Fig.(4.6) and Fig.(4.7)). In contrast, the FENE-p model provides an accurate estimate of the extensional

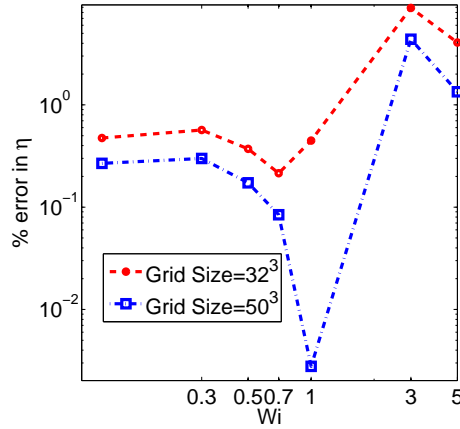


Figure 4.19: Percentage error in the steady state value of extensional viscosity for two different grid sizes. ($b=50$)

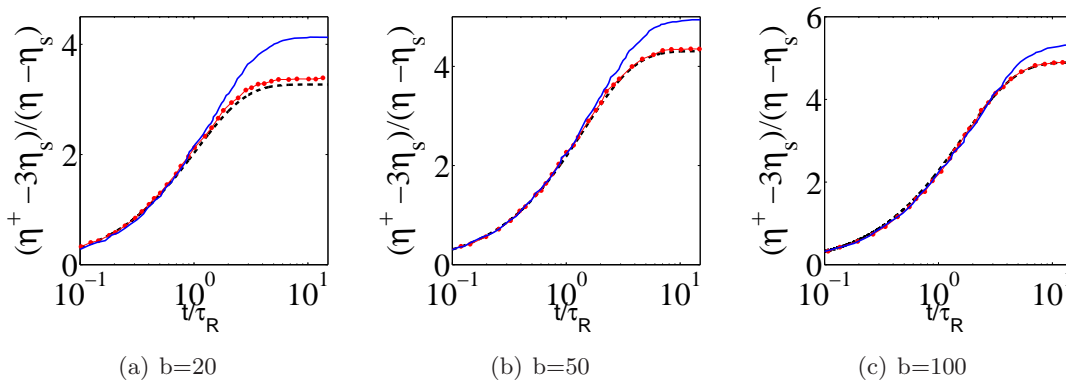


Figure 4.20: Time evolution of the extensional viscosity for $Wi=0.3$. Dashed lines, present scheme with 32^3 as the number of grid points; dots connected with lines, Brownian Dynamics for FENE (Herrchen & Öttinger 1997); continuous lines, numerical solution for FENE-p (Herrchen & Öttinger 1997).

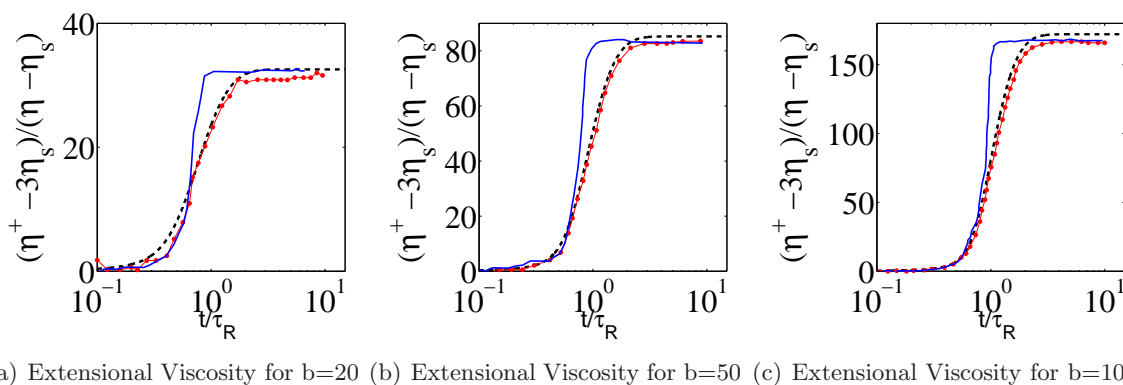


Figure 4.21: Time evolution of the extensional viscosity for $Wi=3.0$. Dashed lines, present scheme with 50^3 as the number of grid points; dots connected with lines, Brownian Dynamics for FENE (Herrchen & Öttinger 1997); continuous lines, numerical solution for FENE-p (Herrchen & Öttinger 1997).

viscosity at the higher value of Wi ($Wi=3.0$; see Fig.(4.21)). This is because the pre-averaging approximation, $Q^2 = \langle Q^2 \rangle$, works best for the case of a sharply peaked distribution (and is exact for the limiting case of a delta function) which is the case for extensional flow above the coil-stretch threshold. Above the threshold, although the steady values are close for both FENE and FENE-p models, the time dependent values are not, as shown in Fig.(4.21). The FENE-p model exhibits a much sharper transition at higher Wi . The present scheme is again in quite good agreement with BD for the same flow.

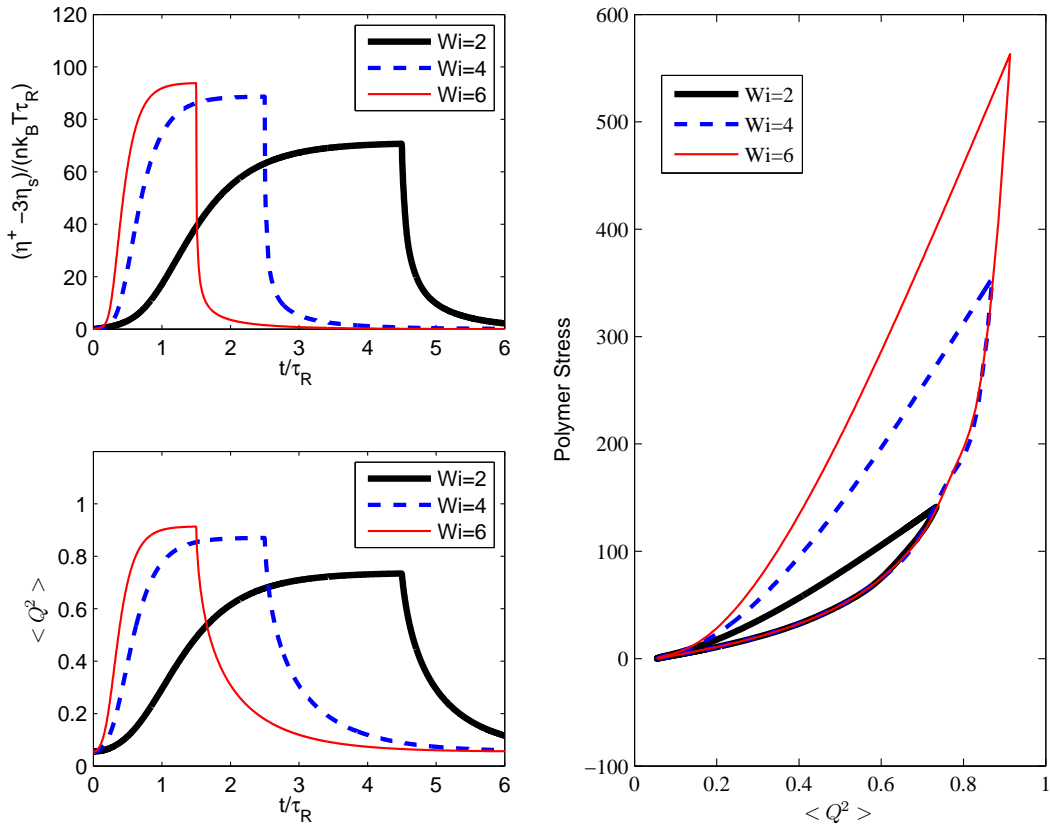


Figure 4.22: Time evolution of the extensional viscosity and mean square extension, as well as polymer stress, with respect to mean square extension at $Wi=2,4,6$ for $b=50$.

Finally, following (Lielens *et al.* 1999), the present scheme is subjected to a more stringent test consisting of a start-up extensional flow followed by relaxation. In this case,

$$\dot{\epsilon} = Wi\{H_0(t) - H_{9/Wi}(t)\}, \quad (4.15)$$

which implies that the extensional flow continues up until $t = 9/Wi$ and the maximum strain applied before relaxation is 9 for each Wi (Lielens *et al.* 1999). In Fig.(4.22), the extensional viscosity and the mean square extension, $\langle Q^2 \rangle$, are plotted for different values of Wi . A hysteretic behavior in the plot of polymer stress against molecular extension, for Wi in excess of the threshold for coil-stretch transition, is characteristic of the FENE model. (Bird *et al.* 1987b; Keunings 1997; Lielens *et al.* 1998, 1999). Below the coil-stretch transition, the hysteretic behavior is absent, and the dynamics in stress- $\langle Q^2 \rangle$ space collapses to a point. As can

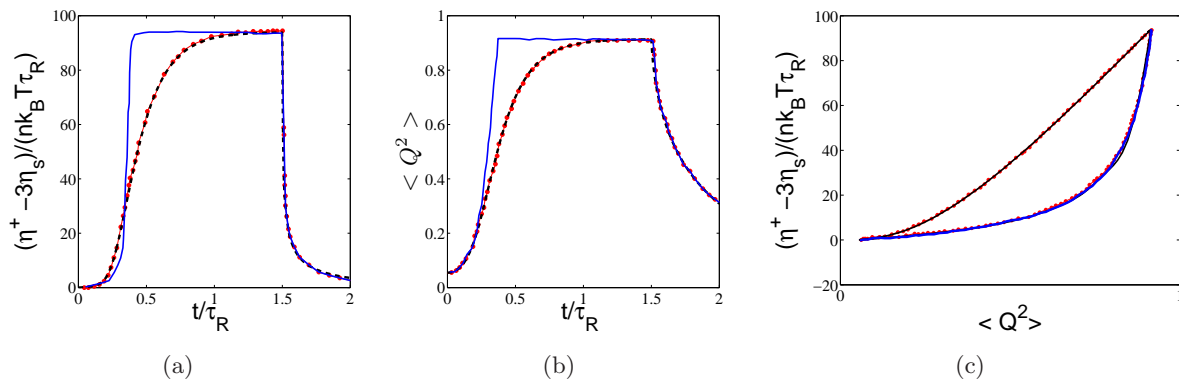


Figure 4.23: Time evolution of the (a) extensional viscosity and (b) mean square extension and (c) extensional viscosity with respect to mean square extension for $Wi=6.0$ and $b=50$. Dashed lines, present scheme; dots connected with lines, predictor corrector stochastic simulation for FENE (Lielens *et al.* 1999); continuous lines, numerical solution for FENE-p (Lielens *et al.* 1999).

be seen from the figure, the present scheme is capable of predicting the hysteretic behavior properly. Furthermore, in order to do a quantitative comparison, in Figs.(4.23(a) and 4.23(b)), the growth of extensional viscosity and mean square extension is compared with earlier results obtained from a predictor-corrector stochastic simulation for FENE and a numerical solution for the FENE-p model (Lielens *et al.* 1999), at $Wi=6.0$ for $b=50$. In Fig.(4.23(c)), the growth in extensional viscosity is plotted with respect to mean square extension and it is evident from the figure that although the FENE-p model fails to show a hysteretic loop, the present scheme is capable of capturing the hysteretic behavior and is in good agreement with the stochastic simulation. Note that the presence of a hysteretic loop indicates the absence of a one-to-one correspondence between the stress and the mean molecular extension, and is referred to as a distribution hysteresis (Ghosh *et al.* 2001). Such a correspondence is, however, enforced by the FENE-p closure. With the aim of capturing the hysteresis phenomena, there have been attempts to incorporate the higher (than second) order moments in the closure, and this leads to the so called FENE-L and FENE-LS models (Lielens *et al.* 1998, 1999). As the current approach is directly solving for the distribution function, it does not require any ad-hoc assumption to capture the effect. It should be noted that the present hysteresis is unrelated to the original coil-stretch hysteresis (De Gennes 1974; Hinch 1977) which requires the surface area (for traction) to change as a function of the extension (that is, a configuration-dependent drag). The latter hysteresis is crucially linked to an underlying bi-modal distribution of polymer configuration (during the relaxation phase) which is absent in the present case.

4.4 Outlook

A discrete kinetic approach based on lattice Boltzmann method is validated for steady and unsteady shear and extensional flows. The present approach complements the existing methodology of BD. Since Wi is the ratio of the amplitudes of the imposed deterministic motion to the random diffusive motion (in \mathbf{Q} -space), the central limit theorem implies that the number of

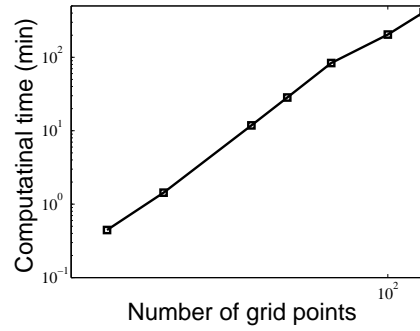


Figure 4.24: Simulation time required to reach $t/\tau_R = 1$ with respect to the number of grid points in each direction.

sample space trajectories, needed to obtain bulk properties to a given degree of accuracy, diverges as Wi^{-2} for $Wi \rightarrow 0$. Thus, stochastic simulation techniques become increasingly inefficient for small Wi (Melchior & Öttinger 1996). In order to give an approximate idea of simulation time requirement for the present scheme, the computation time to reach $t = \tau_R$ with the number of grid points in each direction is plotted in the Fig.(4.24). Present simulation results indicate that in order to obtain good quality results, 32^2 number of grid points are required and the simulation time needed to reach $t = \tau_R$ at this resolution is only 1 min 26 sec (see Fig. 4.24). The runtime of this serial code can be further optimized upto a factor of 2 on using vectorization scheme.

Although the present numerical scheme is quite fast for a dumbbell model, the RAM requirement grows dramatically as number of beads increases. Similar to any other grid based method the memory requirement for N-dimensions system is M^N where M is the number of grid points in each direction. Hence, memory required for the present scheme even when $M=16$ for 6 dimensions (that is the case of trumbell) is around 8 GB. Thus, results in this chapter indicate that though the method is expected to be good tool for dumbbell model, the efficiency of the scheme cannot be extended to large chain molecules.

Chapter 5

Lattice Fokker Planck Method with hydrodynamic interaction

5.1 Introduction

Traditionally, the hydrodynamics of dilute polymeric solutions is modeled in terms of constitutive relations for the stress tensor coupled with a Navier-Stokes description for the solvent. However, the validity of these models is questionable in the case of strong flows and often fails to take into account change in rheological properties due to hydrodynamic interaction between the beads. The hydrodynamic interaction between the beads is due to the velocity disturbance induced by the other beads and are known to significantly influence the relaxation spectra of dilute polymer solutions (Kirkwood & Riseman 1948). These interactions are crucial in capturing the correct molecular weight dependence of the polymer diffusivity and the contribution to the polymer shear viscosity. They also influence the bulk rheological properties (for instance, they lead to a nonzero second normal stress difference in the FENE model). Moreover, the constitutive modeling is cumbersome to solve numerically and require self-consistence averaging (Öttinger 1985, 1987).

Thus, a multi-scale procedure, where stresses are directly computed from an appropriate microscopic solver, is increasingly being used in numerical simulations of polymer solutions (Laso & Öttinger 1993; Feigl *et al.* 1995; Jendrejack *et al.* 2004). In most of these approaches, the macroscopic flow solver is coupled with microscopic BD simulations where one solves the system of Langevin equations for the polymer molecules to obtain ensemble-averaged configuration statistics. In a typical multi-scale polymer dynamics simulations, the substantial part of the computational resources are spent in the polymer solver. The inclusion of conformation-dependent hydrodynamic interaction in stochastic solvers, like BD simulations, is numerically expensive. The BD algorithms with hydrodynamic interaction requires long computational time which increases drastically with the increase in the number of beads in bead-chain model. The reason for stochastic simulations requiring long simulation time can be explained by the fact that one needs to calculate the square-root of diffusion tensor at every time step (Zylka & Öttinger 1989; Öttinger 1996), which is the most time-consuming operation in the simulation. Thus, good amount of algorithmic efforts have been made to optimize this step. Indeed, the state of art Brownian dynamics scheme scales as $O(N \log N)$ where N is the number of beads (Jendrejack *et al.* 2000).

In this chapter, we eliminate the need to calculate square-root of diffusion tensor by doing a direct discretization of underlying Smoluchowski equation. Therefore, it becomes instructive to

contrast the the stochastic differential equation

$$d\mathbf{X}_t + \mathbf{A}(t, \mathbf{X}_t) + \mathbf{B}(t, \mathbf{X}_t) \cdot d\mathbf{W}_t, \quad (5.1)$$

with the corresponding Fokker Planck Equation

$$\frac{\partial}{\partial t}\psi(\mathbf{x}, t) + \frac{\partial}{\partial \mathbf{x}} \cdot [\mathbf{A}(\mathbf{x}, t)\psi] + \frac{1}{2} \frac{\partial}{\partial \mathbf{x}} \frac{\partial}{\partial \mathbf{x}} : [\mathbf{D}(\mathbf{x}, t)\psi], \quad (5.2)$$

where $d\mathbf{W}_t$ is the standard Wiener process and

$$\mathbf{D}(\mathbf{x}, t) = \mathbf{B}^T \cdot \mathbf{B} \quad (5.3)$$

As one could see that in stochastic differential equation one needs to compute the square root of diffusion tensor whereas if one could develop an efficient scheme for solving the underlying Smoluchowski equation, the step of calculating the square root of diffusion tensor can be eliminated. Therefore, a direct discretization scheme for solving the underlying Smoluchowski equation is quite useful.

In Chapter 2, it has been proposed that on replacing the the actual diffusive dynamics in momentum space of polymer dumbbell by relaxation dynamics of the BGK type, the slow dynamics of probability density remains unaltered (Singh *et al.* 2011, 2013b). Based on this assumption, an LB based direct discretization approach for the phase-space description of inertial polymer dynamics is presented in Chapter 4. In this Chapter, an LB based scheme is presented that accounts for the hydrodynamic interaction between the beads.

The Chapter is organized as follows: In Sec.5.2, the concept of hydrodynamic interaction is introduced which is followed by a BGK type kinetic description in Sec.5.3 which results in an appropriate Smoluchowski equation containing the contribution due to hydrodynamic interaction. With the purpose of introducing hydrodynamic interaction effect, the modification on the previous discrete formulation (see Chapter 4) is presented in Sec.5.4. In Sec.5.5, simple shear flow is considered to obtain various rheological functions that are shown to reproduce the desired effect due to the presence of hydrodynamic interaction. The results are also compared with the corresponding BD simulations. Finally, the work is concluded in Sec.5.6 by showing that the present scheme is indeed efficient in term of CPU time required as compared to BD simulations.

5.2 Hydrodynamic interaction

In the Chapter 2, a BGK-type kinetic scheme for polymer dumbbell model without hydrodynamic interaction was developed. However, hydrodynamic interactions between the beads due to the disturbance velocity induced by the individual beads are also present in general (Kirkwood & Riseman 1948). Before modeling it in inertial FP equation for polymer dumbbell, the notion of hydrodynamic interaction is reviewed by revisiting the i^{th} bead equation of motion:

$$m_B \frac{d}{dt} \dot{\mathbf{R}}_i(t) = \mathbf{F}_i^c(t) + \mathbf{F}_i^D(t) + \mathbf{F}_i^B(t), \quad (5.4)$$

where, the total hydrodynamic drag force exerted by the solvent on the i^{th} bead is assumed to be of the form

$$\mathbf{F}_i^{\text{D}} = -\zeta(\dot{\mathbf{R}}_i - (\mathbf{u}_i + \Delta\mathbf{u}_i)), \quad (5.5)$$

where the friction constant, ζ , for a spherical bead is given as $\zeta = 6\pi\eta_s a$ with a as the radius of the bead and η_s as the solvent viscosity. The velocity field $(\mathbf{u}_i + \Delta\mathbf{u}_i)$ is the total velocity of the solvent at the i^{th} bead position. The total solvent velocity consists of the imposed velocity $\mathbf{u}_i = \mathbf{u}_0 + \boldsymbol{\kappa} \cdot \mathbf{R}_j$ and $\Delta\mathbf{u}_i$, which is the total perturbation in the velocity field at \mathbf{R}_i caused by the hydrodynamic forces exerted on the solvent by the other beads in the dumbbell. The velocity perturbation at the location i due to the bead present at location j is

$$\Delta\mathbf{u}_i = \boldsymbol{\Omega}(\mathbf{R}_i - \mathbf{R}_j) \cdot (-\mathbf{F}_j^{\text{D}}), \quad (5.6)$$

where hydrodynamic interaction tensor $\boldsymbol{\Omega}$ is a tensorial function of $(\mathbf{R}_i - \mathbf{R}_j)$ and \mathbf{F}_j^{D} . Further, using the inertia-less limit of Eq. (5.4), one can say that:

$$\Delta\mathbf{u}_i = \boldsymbol{\Omega}(\mathbf{R}_i - \mathbf{R}_j) \cdot (\mathbf{F}_i^{\text{c}} + \mathbf{F}_i^{\text{B}}). \quad (5.7)$$

A common choice of hydrodynamic interaction is the Oseen-Burgers tensor, which is the first approximation to the hydrodynamic-interaction tensor (Bird *et al.* 1987b):

$$\boldsymbol{\Omega}_{\text{Oseen}} = \frac{3}{4}h^* \frac{\sqrt{\pi k_{\text{B}}T/H}}{\zeta} \frac{1}{Q} \left(\boldsymbol{\delta} + \frac{\mathbf{Q}\mathbf{Q}}{Q^2} \right), \quad (5.8)$$

where the parameter $h^* = a/\sqrt{\pi k_{\text{B}}T_0/H}$, represents the strength of the hydrodynamic interaction. In the case of homogeneous flow, the dynamics of center of mass is irrelevant and can be ignored. The dynamics of interest is that of configuration space. The stochastic differential equation governing this dynamics of \mathbf{Q} is (Öttinger 1996; Zylka & Öttinger 1989)

$$d\mathbf{Q} = \left[\boldsymbol{\kappa} \cdot \mathbf{Q} - \frac{2H}{\zeta} [\boldsymbol{\delta} - \zeta\boldsymbol{\Omega}(\mathbf{Q})] \cdot \frac{\mathbf{Q}}{1 - \frac{Q^2}{Q_0^2}} \right] dt + \sqrt{dt} \mathbf{B} \cdot \boldsymbol{\lambda}(t), \quad (5.9)$$

where $\boldsymbol{\lambda}(t)$ is the Gaussian random variables which is completely characterized by the first two correlation functions as

$$\langle \boldsymbol{\lambda}(t) \rangle = \mathbf{0}, \quad \langle \boldsymbol{\lambda}(t) \boldsymbol{\lambda}(t') \rangle = \boldsymbol{\delta} \delta(t - t'), \quad (5.10)$$

and the configuration-dependent tensor \mathbf{B} has to satisfy the following condition:

$$\mathbf{B} \cdot \mathbf{B}^{\text{T}} = \frac{4k_{\text{B}}T}{\zeta} (\boldsymbol{\delta} - \zeta\boldsymbol{\Omega}), \quad (5.11)$$

where \mathbf{B}^{T} is the transpose of \mathbf{B} . For a given $\boldsymbol{\Omega}$, i.e., for a given conformation of the system, \mathbf{B} is not unique but any \mathbf{B} satisfying Eq. (5.11) can be used in Eq. (5.9). The tensor \mathbf{B} can be obtained by Cholesky decomposition of $\frac{4k_{\text{B}}T}{\zeta} (\boldsymbol{\delta} - \zeta\boldsymbol{\Omega})$.

It should be reminded here that the Oseen-Burgers tensor, $\boldsymbol{\Omega}_{\text{Oseen}}$, suffers from a drawback that it leads to a non-positive-definite diffusion tensor for small distances. The BD simulations

for the Oseen-Burgers tensor are possible only for positive-definite diffusion tensors. Therefore, hydrodynamic interaction tensor is chosen such that the diffusion tensor ($\delta - \Omega$) is always positive-definite for all configurations. In order to remove this problem, the Rotne-Prager-Yamakawa (RPY) tensor was introduced which modifies the small separation disturbance in such a manner that the diffusion tensor is always positive-definite (Rotne & Prager 1969; Yamakawa 1970). The RPY tensor has two parts depending on the extension of the dumbbell as:

$$\Omega_{\text{RPY}}(\mathbf{Q}) = \frac{3}{4} h^* \frac{\sqrt{\pi k_B T_0 / H}}{\zeta} \frac{1}{Q} \begin{cases} \left(1 + \frac{2a^2}{3Q^2}\right) \delta + \left(1 - \frac{2a^2}{Q^2}\right) \frac{\mathbf{Q}\mathbf{Q}}{Q^2} & \text{for } Q \geq 2a \\ \frac{Q}{2a} \left(\frac{8}{3} - \frac{3Q}{4a}\right) \delta + \frac{Q}{4a} \frac{\mathbf{Q}\mathbf{Q}}{Q^2} & \text{for } Q < 2a. \end{cases} \quad (5.12)$$

Throughout our study, Ω_{RPY} is used to model hydrodynamic interaction. Instead of working in terms of the dynamics of the random variable \mathbf{Q} , one could choose to work in terms of probability of finding \mathbf{Q} at an instance of time ($\psi(\mathbf{Q}, t)$). The Smoluchowski equation governing the dynamics of the configuration distribution function $\psi(\mathbf{Q}, t)$ in the presence of the hydrodynamic interaction is (Bird *et al.* 1987b)

$$\frac{\partial \psi}{\partial t} + \frac{\partial}{\partial Q_\alpha} \left\{ \kappa \cdot \mathbf{Q} \psi - \frac{2H}{\zeta} (\delta - \zeta \Omega_{\text{RPY}}) \cdot \frac{\mathbf{Q}}{1 - \frac{Q^2}{Q_0^2}} \psi \right\} = \frac{2k_B T_0}{\zeta} \frac{\partial}{\partial \mathbf{Q}} \cdot (\delta - \zeta \Omega) \cdot \frac{\partial \psi}{\partial \mathbf{Q}}. \quad (5.13)$$

5.3 Boltzmann BGK formulation for inclusion of hydrodynamic interaction

In this section, similar to Sec. 2.4, it is shown that the correct slow dynamics of configuration distribution function $\psi(\mathbf{Q}, t)$ with the inclusion of hydrodynamic interaction is recovered, if one chooses to work with a kinetic equation of the BGK form and appropriate imposed velocity. As discussed in Sec. 2.4, the phase-space model differs from usual Boltzmann BGK equation because the momentum is not a conserved variable rather an imposed variable. Using τ_R and $\sqrt{(2k_B T)/m_B}$ for time and velocity scale respectively, the non-dimensional form Boltzmann BGK equation is

$$\frac{\partial}{\partial t} f(\mathbf{Q}, \dot{\mathbf{Q}}, t) + \dot{Q}_\alpha \frac{\partial}{\partial Q_\alpha} f(\mathbf{Q}, \dot{\mathbf{Q}}, t) = \frac{1}{\epsilon} [f^{\text{eq}}(\psi(\mathbf{Q}, t), \bar{\mathbf{v}}, T) - f(\mathbf{Q}, \dot{\mathbf{Q}}, t)]. \quad (5.14)$$

The imposed velocity $\bar{\mathbf{v}}$, in the absence of hydrodynamic interaction (see Sec. 2.4) is

$$\bar{\mathbf{v}}(\mathbf{Q}, t) = \left(\text{Wi} \kappa \cdot \mathbf{Q} - \frac{1}{2} \mathbf{F}^c \right). \quad (5.15)$$

Since the velocity is an imposed quantity and is not given by the first moment of f , doing a Chapman-Enskog expansion around equilibrium of the form $\mathbf{u} = \bar{\mathbf{v}} + \epsilon \mathbf{u}^{(1)} + \dots$ results in a diffusion term in the evolution equation configuration probability density ψ .

The effect of hydrodynamic interaction can be introduced in the slow dynamics if one

chooses the imposed velocity \mathbf{v}_{HI} to be

$$\bar{\mathbf{v}}_{\text{HI}}(\mathbf{Q}, t) = \left(\text{Wi} \boldsymbol{\kappa} \cdot \mathbf{Q} - \frac{1}{2} \{ \mathbf{I} - \zeta \boldsymbol{\Omega}_{\text{RPY}}(\mathbf{Q}) \cdot \mathbf{F}^c \} \right) + \frac{1}{2\psi} \boldsymbol{\Omega}_{\text{RPY}}(\mathbf{Q}) \frac{\partial \psi}{\partial \mathbf{Q}}. \quad (5.16)$$

It should be noted that the moment equations remain the same, the only difference as compared to the case where hydrodynamic interaction is not considered, is the form of imposed velocity. On doing a simple Chapman-Enskog expansion in terms of parameter ϵ , we find that the dynamics at $O(1)$ is governed by Smoluchowski equation (5.13). The non-dimensional form of Smoluchowski equation, after choosing the relevant length scale as the equilibrium extension, is given as:

$$\frac{\partial \psi}{\partial t} + \frac{\partial}{\partial \mathbf{Q}} \cdot \left\{ \psi \text{Wi} \boldsymbol{\kappa} \cdot \mathbf{Q} - \frac{1}{2} \frac{\mathbf{Q}}{1 - \frac{Q^2}{b}} \cdot (\boldsymbol{\delta} - \zeta \boldsymbol{\Omega}_{\text{RPY}}(\mathbf{Q})) \psi \right\} = \frac{1}{2} \frac{\partial}{\partial \mathbf{Q}} \cdot (\boldsymbol{\delta} - \zeta \boldsymbol{\Omega}_{\text{RPY}}(\mathbf{Q})) \cdot \frac{\partial \psi}{\partial \mathbf{Q}}. \quad (5.17)$$

Hence, on choosing the appropriate form of imposed velocity that contains the hydrodynamic effects, the relaxation mechanism at kinetic level resulted in the correct slow dynamics.

5.4 Discrete formulation

The discrete formulation based on LB method is similar as discussed in Sec 4.2 with the exception that the imposed velocity is

$$\bar{\mathbf{v}}_{\text{HI}}(\mathbf{Q}, t) = \left(\text{Wi} \boldsymbol{\kappa} \cdot \mathbf{Q} - \frac{1}{2} \{ \mathbf{I} - \zeta \boldsymbol{\Omega}_{\text{RPY}}(\mathbf{Q}) \cdot \mathbf{F}^c \} \right) + \frac{1}{2\psi} \boldsymbol{\Omega}_{\text{RPY}}(\mathbf{Q}) \frac{\partial \psi}{\partial \mathbf{Q}}, \quad (5.18)$$

where the central-difference scheme is used in order to calculate the gradient of configuration probability density ($\nabla \psi$) that is being used to calculate the imposed velocity $\bar{\mathbf{v}}_{\text{HI}}$. At the boundaries, either forward or backward difference (depending on the boundary) is used to calculate the same. The D3Q19 model is used throughout the study and bounce-back boundary condition is used as discussed in Sec.4.2.1.

5.5 Results

In this section, the effect of hydrodynamic interaction on material functions is examined under simple shear flow. The rheological quantities of interest are the polymer contribution to viscosity η , first normal stress coefficient ψ_1 and the second normal stress coefficient ψ_2 (see Eq. (4.12)). The values of material functions obtained by direct FP solver are contrasted with the BD results. In Fig. (5.1), the shear viscosity and the first normal stress coefficient for steady simple shear flow are plotted with respect to Wi for an extensibility parameter $b = 50$ and hydrodynamic interaction parameter $h^* = 0.15$. As can be seen from the figure, the steady state material function matches well with BD results. All the BD simulations are performed with 10^7 number of trajectory and $dt = 0.001$.

The steady state value of second normal stress coefficient vanishes in the absence of hydrodynamic interaction for FENE dumbbell. However, in the presence of hydrodynamic interaction, the steady state value of second normal stress coefficient starts from negative value for small Wi

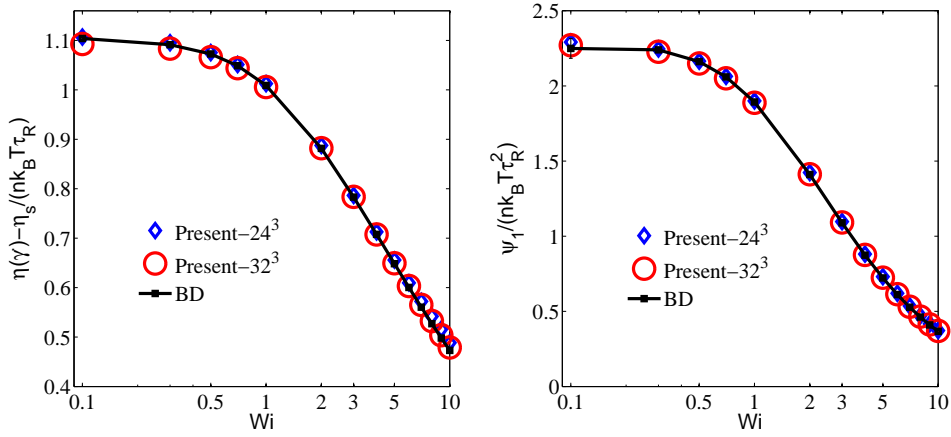


Figure 5.1: (Color online) Steady state value of the shear viscosity and the first normal stress coefficient with different Wi for an extensibility parameter $b = 50$ and $h^* = 0.15$.

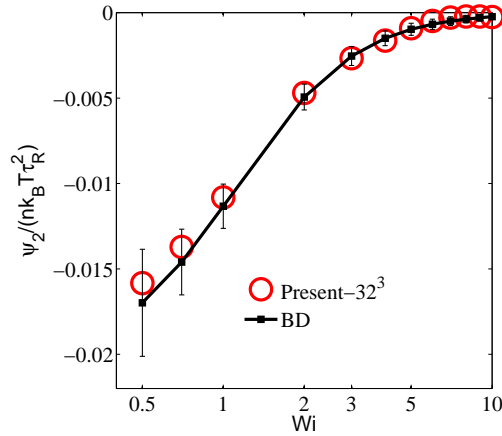


Figure 5.2: Steady state value of the second normal stress coefficient with different Wi for an extensibility parameter $b = 50$ and $h^* = 0.15$.

and reaches a saturated value of zero for high Wi number. As can be seen from Fig. 5.2, the present scheme is capable of accurately predicting this behavior. At very low Wi , the statistical errors are very large which is also evident by large error bars for BD simulations.

As a second test, a startup shear flow where $\dot{\gamma}$ is proportional to the Heaviside function $H(t)$, is considered. In Fig. 5.3, the time-dependent shear viscosity η^+ and the first normal stress coefficient ψ_1^+ is presented for $Wi = 1$ and 10 , and compared with those obtained from BD simulations. Finally, the time dynamics of second normal stress coefficient ψ_2^+ is presented in Fig. 5.4. In order to analyze the effect of hydrodynamic interaction on the shear thinning behavior, the steady state value of the shear viscosity and the first normal stress coefficient as a function of Wi for different h^* is plotted in Fig. 5.5. It can be seen from this figure that the material functions associated with small Wi number are pushed towards higher value as the strength of hydrodynamic interaction increases. It is also evident from the figure that the shear-thinning behavior becomes more stronger with increasing h^* (Bird *et al.* 1987b; Rudisill & Cummings 1992). It has been suggested in Ref. Wedgewood & Öttinger (1988) that the onset of

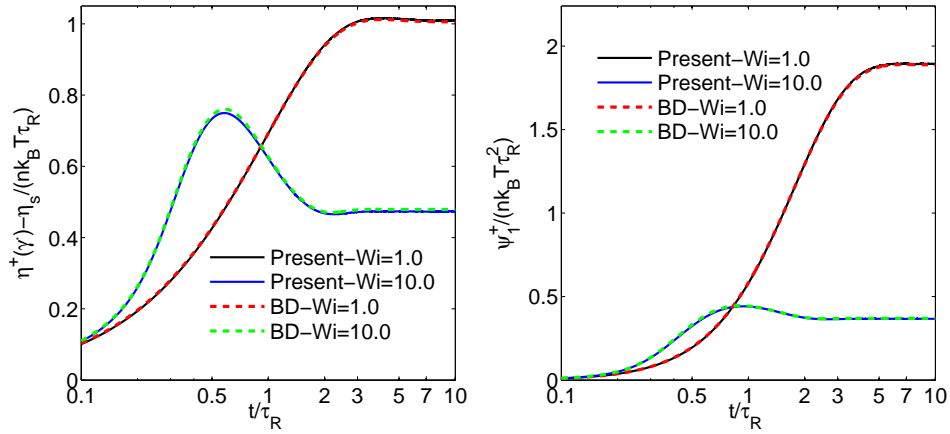


Figure 5.3: Time evolution of the shear viscosity and the first normal stress coefficient for $Wi = 1.0$ and 10 ($b = 50, h^* = 0.15$).

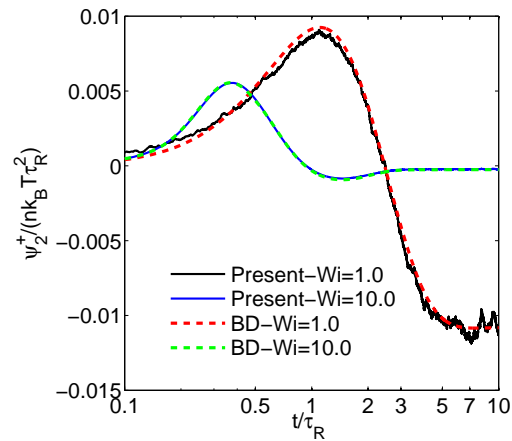


Figure 5.4: Time evolution of the second normal stress coefficient for $Wi = 1.0$ and 10 ($b = 50, h^* = 0.15$).

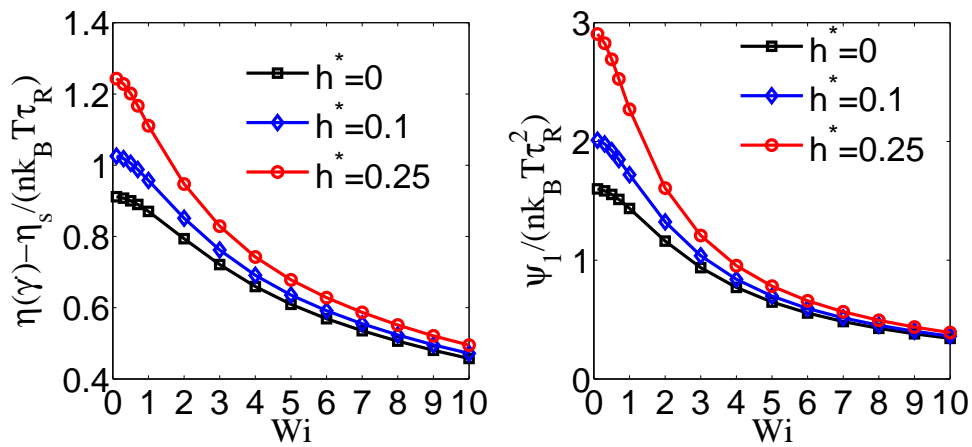


Figure 5.5: (Color online) Steady state value of the shear viscosity and the first normal stress coefficient with respect to different h^* as function of Wi for extensibility parameter $b = 50$. These calculations have been performed with 32 grid points in each direction.

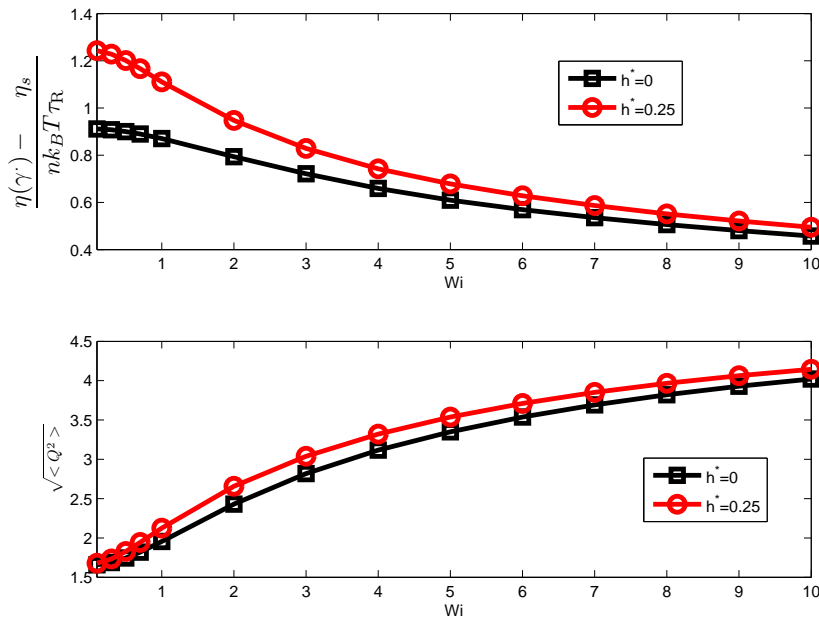


Figure 5.6: Steady state value of the root mean square extension and shear viscosity as function of Wi for two values of $h^* = 0$ and 0.25 with extensibility parameter $b = 50$.

shear thinning at small shear rates should be attributed to hydrodynamic interaction and finite extensibility becomes particularly significant to the shear thinning properties of dilute polymer solutions at high shear rates. In order to support this argument, the shear viscosity as well as the root mean square extension at steady state is plotted as a function of Wi in Fig. 5.6 for two values of hydrodynamic interaction parameter, $h^* = 0$ and 0.25 , with extensibility parameter $b = 50$. It can be seen from the Fig. 5.6, that in the case of small Wi , where hydrodynamic interaction is important, the root mean square extension is small. Fig. 5.6 also reveals that the onset of shear thinning takes place before there is any noticeable deviation in the root mean square extension. At high Wi , as the root mean square extension increases (the hydrodynamic interaction becomes less effective), the shear viscosity becomes closer to the values that are obtained without considering hydrodynamic interaction. This suggests that at high shear finite extensibility is responsible for shear thinning effect in dilute polymer solution.

5.6 Outlook

To conclude, the present scheme gives qualitatively correct description of hydrodynamic interaction. As we have direct access to the distribution function in current methodology, it can be used to get an insight about the behavior of higher moments in presence of hydrodynamic interaction. This method has a unique feature that the ensemble average is not required as we have direct access to the distribution itself. Thus, macroscopic quantities can be obtained as an appropriate moment of the distribution function. As current method does not require square root calculation and ensemble averaging, it takes very less computational time as compared to its stochastic counterpart (BD). In order to provide an estimate for the gain in computational time, CPU time required in simulations for reaching $t = 10\tau_R$ is presented in Table 5.1. The

simulations are performed on the Intel(R) Xeon(R) CPU E5645 @ 2.40GHz.

BD (dt=0.001)		lattice FP	
No. of trajectories	CPU-time	No. of grid points	CPU-time
10^4	1 min 29 sec	16^3	1 min 12 sec
10^5	14 min 25 sec	20^3	2 min 57 sec
10^6	2hr 24 min 16 sec	24^3	6 min 7 sec
10^7	23 hr 36m 35 sec	32^3	19 min 55 sec

Table 5.1: CPU time required to reach $t = \tau_R$ at different resolution of present scheme as well as different number of trajectories for BD at fixed dt=0.001 ($Wi=0.1$, $b=50$ and $h^* = 0.15$).

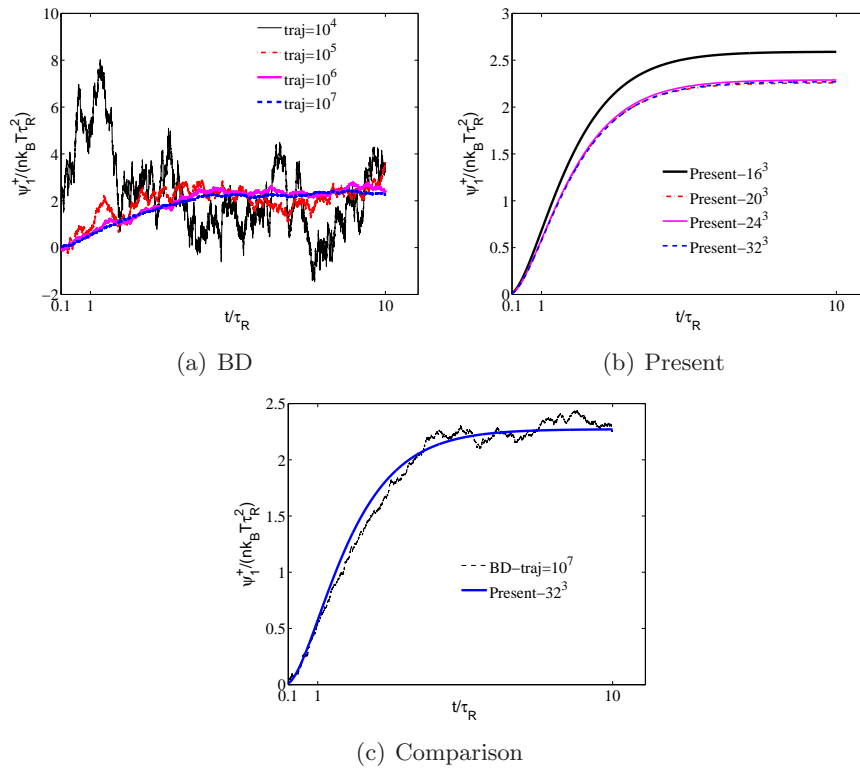


Figure 5.7: Time evolution of first normal stress coefficient at $Wi=0.1$ and $h^* = 0.15$ at different resolution of present scheme as well as different number of trajectories for BD.

It is worth pointing out here that the BD code was using an explicit Euler time integration scheme which can be optimized either by using variance reduced scheme introduced by Öttinger (Öttinger 1996) or by using the semi-implicit scheme by Ref. Jendrejack *et al.* (2000, 2002). On the other hand, the present scheme can also be optimized by using proper vectorization schemes (Shet *et al.* 2013*a,b*). Thus, we do not claim that our efficiency comparison is very rigorous. However, Table 5.1, provides a fair estimate of simplicity and efficiency of the present scheme over BD.

Finally, we wish to comment on the choice of number of trajectories used in BD simulations. It can be seen from the Fig. 5.7(a) that, for $Wi = 0.1$, 10^7 trajectories are required to get the time dynamics of first normal stress coefficient with less statistical error. On the other hand present scheme converges very fast towards correct value with reasonably low number of grid

points. Finally, it can be seen from the Fig 5.7 that, even with 10^7 number of trajectories, BD value for first normal stress coefficient contains some statistical fluctuation for $Wi=0.1$. While in the present scheme, number of grid points as low as 20^3 are sufficient to get the converged value (see Fig. 5.7(b)).

Chapter 6

Mixture hydrodynamics and kinetic models

6.1 Introduction

A phase space kinetic theory in terms of BGK model was developed in chapter 2 for the homogeneous polymer solutions. In subsequent chapters, a discrete LB like framework was developed to numerically solve this phase space kinetic theory and the resulting numerical method was contrasted with existing BD solvers. The high accuracy and efficiency of discrete FP solver suggests that it might be quite advantageous to extend this approach to inhomogeneous systems where phase space kinetic theory is not so well developed (Öttinger & Petrillo 1996).

In last two decades, continuum two fluid models of fluid mixtures were extended for polymer solutions. These models are found to be quite useful in describing hydrodynamics of inhomogeneous polymer solutions. However, these efforts are limited to continuum modeling so far to the best of our knowledge. Boltzmann kinetic theory of gaseous mixture is not extended so far to polymer solutions. In this chapter, the kinetic theory of binary gas mixture is reviewed with the aim of extending these approaches towards the polymer solutions. The emphasis of this review is towards phenomenological modeling of polymer solvent mixture. Here, it should be reminded that a straightforward extension of BGK model to the gas mixture is not adequate due to the fact Schmidt number is not an independent parameter in such a model. Thus, one needs a multi-relaxation time approach to describe the gas mixtures. Many attempts have been made in order to formulate kinetic model for mixture (Gross & Krook 1956; Hamel 1965; Garzó *et al.* 1989; Goldman & Sirovich 2004; Arcidiacono *et al.* 2006; Levermore *et al.* 1988) which overcome this limitation. Before describing some of these models, Boltzmann kinetic theory is used to formulate restrictions on kinetic models of gas mixtures. For example, a good kinetic model for binary mixture should be able to reproduce mass, momentum and energy conservation at the continuum level as well as should follow in-differentiability principle at the kinetic level. Another expected quality is that the kinetic model should obey the H -theorem. After giving a brief review of the kinetic model for binary gas mixture in this chapter, a kinetic formulation for polymer solution is proposed in the 7.

This Chapter describes the binary gas mixture at continuum level in Sec.6.2. After giving a brief description of the kinetic models which reproduce the correct mixture hydrodynamics in Sec.6.3, a BGK type collision model for mixture is reviewed in Sec.6.3.1 and the limitation of BGK model for mixture in terms of fixed Schmidt number is presented. Finally, the quasi-equilibrium based models which have tunable viscosity as well as diffusivity, are explained in detail in Sec.6.3.2.

6.2 Two fluid continuum model for binary mixture

For two components mixture, the hydrodynamics is typically formulated in terms of the component mass density ρ_j ($j = A, B$). As the mass of the individual component are conserved, the continuity equation for the individual component are:

$$\frac{\partial \rho_j}{\partial t} + \frac{\partial}{\partial \mathbf{r}} \cdot \rho_j \mathbf{u}_j = 0, \quad (6.1)$$

where \mathbf{u}_j is the individual component velocity. For the solution total density $\rho = \rho_A + \rho_B$, we recover the continuity equation for the mixture as:

$$\frac{\partial \rho}{\partial t} + \frac{\partial}{\partial \mathbf{r}} \cdot \mathbf{J} = 0, \quad (6.2)$$

which is similar to the single component case with mass average velocity $\mathbf{J} = \rho \mathbf{U} \equiv (\mathbf{J}_A + \mathbf{J}_B)$ appearing in place of component velocity. The velocity for individual component can be written in terms of mass average velocity as:

$$\mathbf{u}_A = \mathbf{U} + \frac{\mathbf{V}_D}{\rho_A}, \quad \mathbf{u}_B = \mathbf{U} - \frac{\mathbf{V}_D}{\rho_B}, \quad (6.3)$$

where the mass diffusion flux, \mathbf{V}_D , by definition is

$$\mathbf{V}_D = \frac{\rho_A \rho_B}{\rho} (\mathbf{u}_A - \mathbf{u}_B). \quad (6.4)$$

In the term of mass diffusion flux, \mathbf{V}_D , the continuity equations for the component are:

$$\frac{\partial}{\partial t} \rho_A + \frac{\partial}{\partial \mathbf{r}} \cdot (\rho_A \mathbf{U} + \mathbf{V}_D) = 0, \quad \frac{\partial}{\partial t} \rho_B + \frac{\partial}{\partial \mathbf{r}} \cdot (\rho_B \mathbf{U} - \mathbf{V}_D) = 0, \quad (6.5)$$

which shows that the individual component get convected with the mixture velocity and the diffusion velocity is representing the role of relative velocity. The role of diffusion velocity becomes apparent, if we write the evolution of the mass fraction of one of the component. For example, the evolution equation for mass fraction of component A, defined as $\phi_A = \rho_A/\rho$, is

$$\frac{\partial \phi_A}{\partial t} + \mathbf{U} \cdot \frac{\partial \phi_A}{\partial \mathbf{r}} = -\frac{1}{\rho} \frac{\partial}{\partial \mathbf{r}} \cdot \mathbf{V}_D. \quad (6.6)$$

According to the Fick's law of diffusion (Bird *et al.* 2007), the constitutive model for the diffusion velocity is:

$$\mathbf{V}_D = -\rho D_{AB} \frac{\partial \phi_A}{\partial \mathbf{r}} \quad (6.7)$$

where, D_{AB} is the mass diffusivity. Thus, the concentration of component A obeys advection diffusion equation:

$$\frac{\partial \phi_A}{\partial t} + \mathbf{U} \cdot \frac{\partial \phi_A}{\partial \mathbf{r}} = \frac{1}{\rho} \frac{\partial}{\partial \mathbf{r}} \cdot \rho D_{AB} \frac{\partial \phi_A}{\partial \mathbf{r}}. \quad (6.8)$$

Similarly, $\phi_B = \rho_B/\rho$, obeys the following advection diffusion equation:

$$\frac{\partial \phi_B}{\partial t} + \mathbf{U} \cdot \frac{\partial \phi_B}{\partial \mathbf{r}} = \frac{1}{\rho} \frac{\partial}{\partial \mathbf{r}} \cdot \rho D_{AB} \frac{\partial \phi_B}{\partial \mathbf{r}}. \quad (6.9)$$

Only one of the equations between Eq. (6.8) and Eq. (6.9) is independent because $\phi_A + \phi_B = 1$. This can also be seen from by adding Eq. (6.8) and Eq. (6.9), which gives

$$\frac{\partial}{\partial t}(\phi_A + \phi_B) = 0. \quad (6.10)$$

Along with total mass density (see Eq.(6.2)), the total momentum \mathbf{J} and total energy E of the mixture, are also conserved:

$$\begin{aligned} \frac{\partial}{\partial t} \mathbf{J} + \frac{\partial}{\partial \mathbf{r}} p + \frac{\partial}{\partial \mathbf{r}} \cdot (\rho \mathbf{U} \mathbf{U} + \mathbf{\Pi}) &= 0, \\ \frac{\partial}{\partial t} E + \frac{\partial}{\partial \mathbf{r}} \cdot [E \mathbf{U} + \mathbf{q} + p \mathbf{U} + \mathbf{\Pi} \cdot \mathbf{U}] &= 0. \end{aligned} \quad (6.11)$$

where p is the total pressure and the total stress of the mixture, $\mathbf{\Pi}$ and total energy flux \mathbf{q} are defined as:

$$\begin{aligned} \mathbf{\Pi} &= -\mu \left[\left(\frac{\partial \mathbf{U}}{\partial \mathbf{r}} \right) + \left(\frac{\partial \mathbf{U}}{\partial \mathbf{r}} \right)^T - \frac{2\delta}{D} \frac{\partial}{\partial \mathbf{r}} \cdot \mathbf{U} \right], \\ \mathbf{q} &= -\kappa \frac{\partial T}{\partial \mathbf{r}} + \sum_j^{A,B} F_j \mathbf{J}_j, \end{aligned} \quad (6.12)$$

where T is the total temperature of the mixture, μ is the shear viscosity, κ is the thermal conductivity and the function F_j depends on the enthalpy of component j (Bird *et al.* 2007). It should be noted that the total stress of the mixture depends on the mass average velocity of the mixture. Thus we see that in mixture hydrodynamics, the central variable are the total density, mass average velocity and the concentration of the components. Furthermore, the mass average velocity satisfy the Navier-Stokes Equation.

6.3 Kinetic Theory for gas mixture

In this section, kinetic models of gas mixture is reviewed. For the simplicity of description, we will consider the case of binary mixture. The basic quantity of interest is the one particle distribution function $f_j(\mathbf{r}, \mathbf{v}_j, t)$ for each of the component $j = A, B$ which defines the probability of finding the particle of component j at position \mathbf{r} with velocity \mathbf{v}_j at time t . The mass density ρ_j , the momentum density \mathbf{J}_j and and the energy density E_j of each component is

$$\rho_j = \langle m_j, f_j \rangle, \quad \mathbf{J}_j = \rho_j \mathbf{u}_j = \langle m_j \mathbf{v}_j, f_j \rangle, \quad E_j = \frac{1}{2} \langle m_j v_j^2, f_j \rangle, \quad (6.13)$$

where m_j is the mass of one molecule of j th component and the angular brackets are defined as

$$\langle \phi_j, f_j \rangle = \int f_j \phi_j d\mathbf{v}_j \quad (6.14)$$

We know that apart from the individual masses, the microscopic collision for mixture conserves total momentum $\mathbf{J} = \mathbf{J}_A + \mathbf{J}_B$ and total energy $E = E_A + E_B$ of the mixture. This implies that the relevant macroscopic slow variables are

$$M^{\text{Slow}} = \{\rho_A, \rho_B, \mathbf{J}, E\} = \{\langle m_A, f_A \rangle, \langle m_B, f_B \rangle, \sum_j^{A,B} (\langle m_j \mathbf{v}_j, f_j \rangle, \langle m_j v_j^2, f_j \rangle)\}. \quad (6.15)$$

The temperature of the mixture is defined as

$$T = \frac{2E - \rho U^2}{nk_B} \quad (6.16)$$

where the total number density $n = n_A + n_B$ with $n_j = \rho_j/m_j$. The evolution equation for the distribution function of both the component is of Boltzmann form:

$$\begin{aligned} \frac{\partial}{\partial t} f_A(\mathbf{r}, \mathbf{v}_A, t) + v_{A\alpha} \frac{\partial}{\partial r_\alpha} f_A(\mathbf{r}, \mathbf{v}_A, t) &= \Omega_{AA}(f_A, f_A) + \Omega_{AB}(f_A, f_B). \\ \frac{\partial}{\partial t} f_B(\mathbf{r}, \mathbf{v}_B, t) + v_{B\alpha} \frac{\partial}{\partial r_\alpha} f_B(\mathbf{r}, \mathbf{v}_B, t) &= \Omega_{BB}(f_B, f_B) + \Omega_{BA}(f_B, f_A). \end{aligned} \quad (6.17)$$

where Ω_{jj} represents the self-collision between the particle of same component and Ω_{jk} with $j \neq k$ represents the cross-collision between the molecule of component j and component k . The collision term has the following properties:

- The self-collision does not affect the mass momentum and energy conservation. In other words,

$$\left\langle m_j \Omega_{jj}, \begin{Bmatrix} 1 \\ \mathbf{v}_j \\ \frac{v_j^2}{2} \end{Bmatrix} \right\rangle = 0. \quad (6.18)$$

- The cross-collision as well does not affect mass conservation, that is $\langle m_j \Omega_{jk} \rangle = 0$ with $j \neq k$. However, the momentum is exchanged between the components via cross-collision in such a manner that the total momentum is conserved:

$$\langle m_A \Omega_{AB}, \mathbf{v}_A \rangle + \langle m_B \Omega_{BA}, \mathbf{v}_B \rangle = 0. \quad (6.19)$$

- Similarly, the energy is exchanged between the component so that total energy is conserved.

$$\left\langle m_A \Omega_{AB}, \frac{\mathbf{v}_A^2}{2} \right\rangle + \left\langle m_B \Omega_{BA}, \frac{\mathbf{v}_B^2}{2} \right\rangle = 0. \quad (6.20)$$

It should be noted that the cross collisions do not preserve momentum and energy of individual component.

- In-differentiability: the mixture description reduces to the single component description when the component become mechanically equivalent which means when $m_A = m_B$, the total distribution $f = f_A + f_B$, obeys the single specie Boltzmann equation (Andries *et al.* 2002; Goldman & Sirovich 2004).

- Similar to Boltzmann collision term, the model should have H - theorem of the form

$$\frac{\partial H}{\partial t} + \frac{\partial}{\partial \mathbf{r}} \cdot \mathbf{J}_H = -\sigma, \quad (6.21)$$

with $\sigma \geq 0$. Here, the H function is defined as

$$H = \sum_j^{A,B} \int m_j f_j (\log f_j - 1) d\mathbf{v}, \quad (6.22)$$

the flux of H -function

$$\mathbf{J}_H = \sum_j^{A,B} \int m_j f_j (\log f_j - 1) \mathbf{v}_j d\mathbf{v}_j, \quad (6.23)$$

the entropy production

$$\sigma = \sum_j^{A,B} \langle m_j \log f_j, \Omega_j \rangle. \quad (6.24)$$

Furthermore, the entropic production $\sigma = 0$ if and only if $f_j = f_j^{\text{MB}}(M^{\text{Slow}})$ which implies

$$\Omega_j = 0 \iff f_j = f_j^{\text{MB}}(M^{\text{Slow}}). \quad (6.25)$$

Before the discussing the exact form of collision operator Ω_j , it would be instructive to analyze the moments of individual component. As mentioned in previous section that it is often convenient to break component momentum into two parts: the total or average momentum density \mathbf{J} and the mass diffusion flux \mathbf{V}_D . The evolution of individual mass density is given by Eq. (6.5) and the evolution of total momentum density and second order stress tensor is

$$\begin{aligned} \frac{\partial}{\partial t} \mathbf{J}_j + \frac{\partial}{\partial \mathbf{r}} \cdot \mathbf{P}_j &= \underbrace{\langle \Omega_{jk}, m_j \mathbf{v}_j \rangle}_{A_j}, \\ \frac{\partial}{\partial t} \mathbf{P}_j + \frac{\partial}{\partial \mathbf{r}} \cdot \mathbf{Q}_j &= \langle \Omega_{jj}, m_j \mathbf{v}_j \mathbf{v}_j \rangle + \langle \Omega_{jk}, m_j \mathbf{v}_j \mathbf{v}_j \rangle, \end{aligned} \quad (6.26)$$

where $j \neq k$ and the momentum flux \mathbf{P}_j and the energy flux \mathbf{Q}_j can be represented in terms of the distribution function as

$$\mathbf{P}_j = \langle m_j \mathbf{v}_j \mathbf{v}_j, f_j \rangle, \quad \mathbf{Q}_j = \langle m_j \mathbf{v}_j v_j^2, f_j \rangle \quad (6.27)$$

In order to have correct continuum description, the term A_j appearing in Eq. (6.26) should be related to to the mass diffusion flux, \mathbf{V}_D (Eq. (6.4)), (Goldman & Sirovich 2004) as

$$A_j = \frac{\mathbf{V}_D}{\tau}, \quad (6.28)$$

where τ is the time associated with the drag force. Using Eq. (6.19), it can be seen that the

total momentum is conserved

$$\frac{\partial}{\partial t} \mathbf{J} + \frac{\partial}{\partial \mathbf{r}} p + \frac{\partial}{\partial \mathbf{r}} \cdot (\rho \mathbf{U} \mathbf{U} + \mathbf{\Pi}) = 0. \quad (6.29)$$

The total pressure tensor \mathbf{P} can further be divided into equilibrium and non-equilibrium as $\mathbf{P} = \mathbf{P}^{\text{eq}} + \mathbf{P}^{\text{neq}}$ and the evolution for \mathbf{P}^{neq} is

$$\begin{aligned} \frac{\partial \mathbf{P}^{\text{neq}}}{\partial t} + \frac{\partial}{\partial \mathbf{r}} \cdot \mathbf{Q}^{\text{neq}} + nk_{\text{B}} T \left[\left(\frac{\partial \mathbf{U}}{\partial \mathbf{r}} \right) + \left(\frac{\partial \mathbf{U}}{\partial \mathbf{r}} \right)^{\text{T}} - \frac{2\delta}{D} \frac{\partial}{\partial \mathbf{r}} \cdot \mathbf{U} \right] + \Gamma(\rho_j, \mathbf{P}_j^{\text{neq}}) \\ = \sum_j^{A,B} [\langle \Omega_{jj}, \mathbf{v}_j \mathbf{v}_j \rangle + \langle \Omega_{jk}, \mathbf{v}_j \mathbf{v}_j \rangle]. \end{aligned} \quad (6.30)$$

Similarly, the evolution of the mass-diffusion flux is

$$\frac{\partial \mathbf{V}_{\text{D}}}{\partial t} - \frac{\mathbf{J}}{\rho} \frac{\partial}{\partial \mathbf{r}} \cdot \mathbf{V}_{\text{D}} + \frac{k_{\text{B}}}{\rho} \left(\rho_B \frac{\partial (n_A T)}{\partial \mathbf{r}} - \rho_A \frac{\partial (n_B T)}{\partial \mathbf{r}} \right) + \Xi(\rho_j, \mathbf{P}_j^{\text{neq}}) = \frac{1}{2} \langle \Omega_{AB}, \mathbf{v}_A \rangle - \langle \Omega_{BA}, \mathbf{v}_B \rangle. \quad (6.31)$$

The equilibrium mass diffusion flux $\mathbf{V}_{\text{D}}^{\text{eq}}$ is zero, since both the components have the same velocity at equilibrium. In order to obtain the exact form of the functions Ξ and Γ , please refer (Bird *et al.* 2007).

6.3.1 BGK collision term

In this section, the BGK (Bhatnagar *et al.* 1954) type models for binary gas mixtures is briefly described. After considering the aforementioned criteria on collision operator, a single-relaxation time approximation, known as a Bhatnagar-Gross-Krook (BGK) approximation (Bhatnagar *et al.* 1954), is used to model $\Omega_j = \Omega_{jj} + \Omega_{jk}$ as (Andries *et al.* 2002)

$$\Omega_j = \frac{1}{\tau} (f_j^{\text{MB}}(\rho_j, \mathbf{U}, T) - f_j), \quad (6.32)$$

which gives

$$\frac{1}{2} (\langle \mathbf{v}_A, \Omega_A \rangle - \langle \mathbf{v}_B, \Omega_B \rangle) = -\frac{1}{\tau} (\mathbf{V}_{\text{D}}^{\text{neq}}), \quad \sum_j^{A,B} \langle \mathbf{v}_j \mathbf{v}_j, \Omega_j \rangle = -\frac{1}{\tau} (\mathbf{P}^{\text{neq}}). \quad (6.33)$$

On using the fact that at equilibrium $\mathbf{V}_{\text{D}}^{\text{eq}} = 0$. The Eq. (6.33) shows that for BGK model, mass diffusion flux and the pressure tensor are relaxing at the same rate which results in fixed Schmidt number, Sc (the ratio of the momentum diffusivity and mass diffusivity), for a given viscosity. However, one need at-least two different relaxation rate each associated with the relaxation of mass diffusion flux and total momentum flux separately. This suggests BGK collision kernel is not an appropriate model for binary mixture.

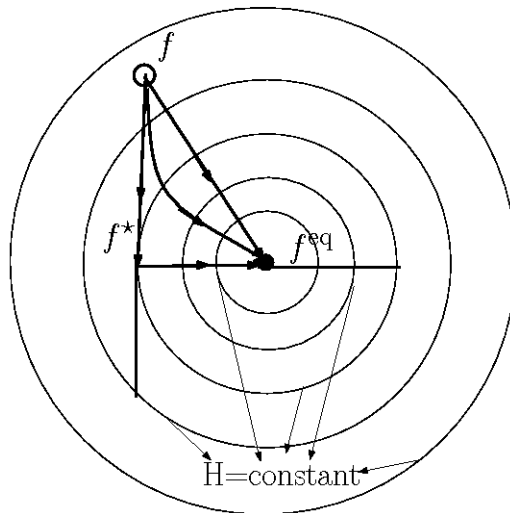


Figure 6.1: Scheme showing the relaxation of f to f^{eq} through a quasi-equilibrium state f^* .

6.3.2 Quasi-equilibrium Model

In the Refs. Arcidiacono *et al.* (2006); Ansumali *et al.* (2007), a collision model with an intermediate quasi-equilibrium state has been proposed in order to have a tunable Sc. The concept of quasi-equilibrium state can be explained by the Fig. 6.1. As can be seen from the Fig. 6.1, there is fast relaxation of the distribution function f towards the the quasi-equilibrium state f^* , followed by a slow relaxation towards the equilibrium state f^{eq} . Both the stages of relaxation can be modeled as BGK type terms with τ_1 and τ_2 as the rates of respective relaxation. The equilibrium distribution function f^{eq} is evaluate by minimizing H - function under the constraints of fixed slow variables M^{Slow} . Similarly, the quasi-equilibrium, f^* , is found by the minimizing of H -function under the constraints of fixed fast or quasi-slow variables which in the present case are the individual momentum and energy density. The simplest generalization of the BGK model using f^* can be written as:

$$\Omega_j = \frac{1}{\tau_1}[f_j^*(\rho_j, \mathbf{u}_j, T_j) - f_j] + \frac{1}{\tau_2}[f_j^{\text{eq}}(\rho_j, \mathbf{U}, T) - f_j^*(\rho_j, \mathbf{u}_j, T_j)]. \quad (6.34)$$

It is worth noting that in order to satisfy H - theorem, proper ordering of the relaxation is required which is present case is $\tau_1 \leq \tau_2$ (Gorban & Karlin 1994; Ansumali *et al.* 2007). Using the fact $\mathbf{P}^* = \mathbf{P}^{\text{eq}}$, it can be seen that that

$$\sum_j^{\text{A,B}} \langle \mathbf{v}_j \mathbf{v}_j, \Omega_j \rangle = -\frac{1}{\tau_1} \mathbf{P}^{\text{neq}}, \quad \frac{1}{2} (\langle \mathbf{v}_A, \Omega_A \rangle - \langle \mathbf{v}_B, \Omega_B \rangle) = -\frac{1}{\tau_2} \mathbf{V}_D^{\text{neq}}. \quad (6.35)$$

The Chapman-Enskog expansion reveals that the first order non-equilibrium contribution to the pressure tensor \mathbf{P} and the mass diffusion flux \mathbf{V}_D is (Arcidiacono *et al.* 2006)

$$\begin{aligned}\mathbf{P}^{\text{neq}} &= -\tau_1 n k_B T \left[\left(\frac{\partial \mathbf{U}}{\partial \mathbf{r}} \right) + \left(\frac{\partial \mathbf{U}}{\partial \mathbf{r}} \right)^T - \frac{2\delta}{D} \frac{\partial}{\partial \mathbf{r}} \cdot \mathbf{U} \right], \\ \mathbf{V}_D^{\text{neq}} &= \tau_2 k_B \left[\frac{\rho_A}{\rho} \frac{\partial(n_B T)}{\partial \mathbf{r}} - \frac{\rho_B}{\rho} \frac{\partial(n_A T)}{\partial \mathbf{r}} \right].\end{aligned}\quad (6.36)$$

It is evident from the Eq. (6.36) that the shear viscosity μ is related to relaxation time τ_1 as $\mu = n k_B T \tau_1$ and (after some rearrangement) the diffusion coefficient D_{AB} can be related to the relaxation time τ_2 giving tunable Sc where $\text{Sc} = \mu / (\rho D_{AB})$. The choice of the quasi-equilibrium defined by Eq. (6.34), leads to a limitation on the Sc: $\text{Sc} \leq \text{Sc}^*$. The reference Schmidt number Sc^* depends on the mass fraction, $Y_j(\rho_j/\rho)$, and the mole fractions, $X_j(n_j/n)$, of the two components as: $\text{Sc}^* = (Y_A Y_B) / (X_A X_B)$. The detailed of the calculation can be found in the Ref. Arcidiacono *et al.* (2006). If the molecular mass, m_j , of the two component is of same order, the Sc^* comes out to be the ratio of masses in the dilute limit case. In other words, attainable Sc in this case is of order one. In order to avoid this limitation, the stress tensor \mathbf{P}_j of component j can be chosen as quasi-conserved variable along with the slow variables as the individual mass density ρ_j and total momentum density $\rho \mathbf{U}$, for the purpose of to minimizing H -function to obtain the quasi-equilibrium $f^{**}(\rho_j, \mathbf{U}, \mathbf{P}_j)$. The collision integral will then take the following form:

$$\Omega_j = \frac{1}{\tau_1} [f_j^{**}(\rho_j, \mathbf{U}, \mathbf{P}_j) - f_j] + \frac{1}{\tau_2} [f_j^{\text{eq}}(\rho_j, \mathbf{U}, T) - f_j^{**}(\rho_j, \mathbf{U}, \mathbf{P}_j)], \quad (6.37)$$

and therefore,

$$\sum_j^{\text{A,B}} \langle \mathbf{v}_j \mathbf{v}_j, \Omega_j \rangle = -\frac{1}{\tau_2} \mathbf{P}^{\text{neq}}, \quad \frac{1}{2} (\langle \mathbf{v}_A, \Omega_A \rangle - \langle \mathbf{v}_B, \Omega_B \rangle) = -\frac{1}{\tau_1} \mathbf{V}_D^{\text{neq}}. \quad (6.38)$$

The first order non-equilibrium contribution to the pressure tensor \mathbf{P} and the mass diffusion flux \mathbf{V}_D then becomes (Arcidiacono *et al.* 2006)

$$\begin{aligned}\mathbf{P}^{\text{neq}} &= -\tau_2 n k_B T \left[\left(\frac{\partial \mathbf{U}}{\partial \mathbf{r}} \right) + \left(\frac{\partial \mathbf{U}}{\partial \mathbf{r}} \right)^T - \frac{2\delta}{D} \frac{\partial}{\partial \mathbf{r}} \cdot \mathbf{U} \right], \\ \mathbf{V}_D^{\text{neq}} &= \tau_1 k_B \left[\frac{\rho_A}{\rho} \frac{\partial(n_B T)}{\partial \mathbf{r}} - \frac{\rho_B}{\rho} \frac{\partial(n_A T)}{\partial \mathbf{r}} \right],\end{aligned}\quad (6.39)$$

which relates the viscosity μ to τ_2 and the diffusion coefficient D_{AB} can be related to the relaxation time τ_1 . The limitation on Sc will reverse and become $\text{Sc} \geq \text{Sc}^*$.

Chapter 7

Two fluid kinetic theory for polymer solution

7.1 Introduction

Boltzmann kinetic theory is quite successful in predicting the macroscopic transport phenomena and associated modeling in terms of microscopic particle picture. Indeed, one of the early success of the kinetic theory was to predict Soret and Dufour effects from Boltzmann collision dynamics of gaseous mixture (Mazur & de Groot 1963; Bird *et al.* 2007). In recent years, it has been realized that the polymeric mixture shows much richer behavior than gas mixture of structure-less particles. Few typical examples are the stress-gradient induced migration and concentration fluctuation which are analyzed in the Refs. Helfand & Fredrickson (1989); Apostolakis *et al.* (2002). Typically, such non-trivial behavior of polymer solutions is modeled via macroscopic two fluid models (Doi & Onuki 1992; Mavrantzas & Beris 1992; Apostolakis *et al.* 2002). Though Curtiss & Bird (1996) has made an initial attempt to create a rigorous kinetic theory for polymer solution, the development of full phase space kinetic theory of polymer solution is still in elementary stage.

If one wants to model both the polymer and solvent at the kinetic level, due to non-locality of polymer dumbbell, asymmetry in the description comes into play. This happens because the polymer dumbbell is governed by a two particle distribution function whereas the solvent phase molecule is governed by a single particle distribution function. Due to this non-local behavior and asymmetric description, various technical difficulties arise. For example, what are the collisional invariants? What is the preferred location of collision with polymer (bead-center or center-of-mass)? How does polymeric stress arise in this kinetic description? What are the set of slow moments, and starting from two-particle distribution for polymer, what is the best way to define moments at a given location? In this chapter, these issues are discussed by writing a Boltzmann type collision integral. The qualitative properties of this collision model are used to write a quasi-equilibrium based relaxation type collision model. Finally, an extension of lattice Fokker Planck method is created to address an inhomogeneous flow scenario with one way coupling of polymer dumbbell to the imposed Poiseuille flow where there is no feedback to the solvent.

The Chapter is organized as follows: In Sec.7.2, the traditional polymer solution description in terms of two fluid theory is discussed. In Sec.7.3, the kinetic description of the system where polymer is modeled as a dumbbell and solvent as a structure-less particle, is presented. A brief description of collision mechanism of binary gas mixture is given in Sec.7.3.1. In Sec.7.4, a Boltzmann type kinetic description for polymer-solvent collision is presented which is followed by

the discussion of local conservation laws in Sec.7.4.1. The Sec.7.5 deals with a quasi equilibrium based collision model for polymer-solvent mixture, which is shown to reproduce the desired continuum description. In order to numerically validate the model, an example of one way coupling is considered in Sec. 7.6 where polymer is subjected to an imposed Poiseuille flow. After briefly describing the discrete numerical scheme in Sec. 7.6.1, the result, in terms of polymer migration towards the center of channel, is presented in Sec. 7.6.2. Finally, the outlook is given in Sec. 7.7.

7.2 Polymer solution as a two component mixture

The traditional description of polymer solution is often in terms of a homogeneous solution where polymer concentration is taken to be constant. In last two decades, the role of concentration fluctuation is well understood and models which represent the polymer solution as two component fluid mixture are often used (Helfand & Fredrickson 1989; Milner 1991; Doi & Onuki 1992; Milner 1993; Beris & Mavrantzas 1994; Jou *et al.* 1996; Fredrickson 2002). In these models, the independent variables of interest are the mass density of polymer dumbbell ρ_P , the mass density of solvent ρ_S , the momentum density of polymer $\mathbf{J}_P = \rho_P \mathbf{u}_P$ and the momentum density of solvent $\mathbf{J}_S = \rho_S \mathbf{u}_S$. The total mass density of the solution is $\rho = \rho_S + \rho_P$ and the total mass average velocity is $\mathbf{U} = (\mathbf{J}_P + \mathbf{J}_S)/\rho$. As the mass density of both polymer and solvent are conserved, the evolution equations for component densities are given by continuity equations:

$$\frac{\partial \rho_S}{\partial t} + \frac{\partial}{\partial \mathbf{r}} \cdot \rho_S \mathbf{u}_S = 0, \quad \frac{\partial \rho_P}{\partial t} + \frac{\partial}{\partial \mathbf{r}} \cdot \rho_P \mathbf{u}_P = 0. \quad (7.1)$$

Similarly, the total momentum conservation equation, in the limit of low Reynolds number, is

$$\frac{\partial \mathbf{J}}{\partial t} = \frac{\partial}{\partial \mathbf{r}} \cdot (\mathbf{\Pi}_S + \mathbf{P}_P^{\text{osmotic}} + \mathbf{\Theta}) + \frac{\partial}{\partial \mathbf{r}} p^{\text{Ideal}}, \quad (7.2)$$

where p^{Ideal} is the hydrodynamic pressure, $\mathbf{\Theta}$ is the polymeric elastic stress which is communicated down the backbone of the chain (Milner 1991), $\mathbf{P}_P^{\text{osmotic}}$ is the osmotic stress term originating due to non-ideality and viscous stress is $\mathbf{\Pi}_S = \eta_s (\nabla \mathbf{u}_S + (\nabla \mathbf{u}_S)^T)$ with η_s as the solvent viscosity. In general, viscous dissipation should be given in terms of mixture velocity. However, the viscous dissipation of polymer is neglected when one is interested in the dilute and semi-dilute polymer solutions. The three types of stress terms in the total momentum balance are well understood. However, writing the individual component momentum balance equation requires modeling. Typically, two fluid polymer solution models write component momentum balance as (Milner 1991, 1993)

$$\begin{aligned} \frac{\partial \mathbf{J}_P}{\partial t} &= \frac{\partial}{\partial \mathbf{r}} \cdot (\mathbf{P}_P^{\text{osmotic}} + \mathbf{\Theta}) + \zeta (\mathbf{u}_S - \mathbf{u}_P), \\ \frac{\partial \mathbf{J}_S}{\partial t} &= \frac{\partial}{\partial \mathbf{r}} \cdot \mathbf{\Pi}_S + \frac{\partial p^{\text{Ideal}}}{\partial \mathbf{r}} - \zeta (\mathbf{u}_S - \mathbf{u}_P), \end{aligned} \quad (7.3)$$

where it is assumed that the role of relative motion of the two components is to introduce a drag force between the two components with ζ as the drag coefficient per unit volume of solution. The solvent momentum balance contains viscous stress, pressure and the drag force terms. The

polymer momentum balance contains the elastic stress, drag force, the osmotic stress terms. In the case of dilute limit, $\rho_P/(\rho_S + \rho_P) \ll 1$, the polymer and solvent velocities are approximately given as:

$$\mathbf{u}_S = \mathbf{U}, \quad \mathbf{u}_P = \mathbf{U} + (\mathbf{u}_P - \mathbf{u}_S). \quad (7.4)$$

Similarly, in the dilute limit, the drag coefficient per unit volume of solution, ζ , can be written as $\zeta = \zeta_0 \rho_P$ with ζ_0 as the friction coefficient of each polymer molecule. Further, if the inertial terms are neglected in Eq. (7.3), one gets

$$\mathbf{u}_P - \mathbf{u}_S = (\zeta_0 \rho_P)^{-1} \frac{\partial}{\partial \mathbf{r}} \cdot (\mathbf{P}_P^{\text{osmotic}} + \boldsymbol{\Theta}). \quad (7.5)$$

The evolution equation of mass density for the polymer phase, in the dilute limit, is

$$\frac{\partial \rho_P}{\partial t} + \frac{\partial}{\partial \mathbf{r}} \cdot \left[\rho_P \mathbf{U} - \frac{1}{\zeta_0} \frac{\partial}{\partial \mathbf{r}} \cdot (\mathbf{P}_P^{\text{osmotic}} + \boldsymbol{\Theta}) \right] = 0. \quad (7.6)$$

If the polymer molecule is modeled as Hookean dumbbell, the elastic contribution to the stress tensor $\boldsymbol{\Pi}_P^{(e)}$ is given as

$$\boldsymbol{\Theta} = H n_P \mathbf{c} - n_P k_B T \boldsymbol{\delta}, \quad (7.7)$$

where n_P is the polymer number density, H is the spring constant of spring force, $\boldsymbol{\delta}$ is the unit tensor and \mathbf{c} is referred as conformation or structure tensor.

7.3 Kinetic Description

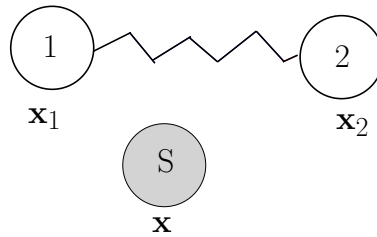


Figure 7.1: Schematic showing the polymer modeled as a dumbbell and solvent as a structure-less particle.

Typically, the polymer solution is modeled as a two component mixture with one of the components being structure-less solvent particle of mass m_S and the other component being the polymer dumbbell of two point masses m_B connected by a massless spring. The spring force $\mathbf{F}_\nu(\mathbf{x}_\xi - \mathbf{x}_\nu)$ (for $\nu, \xi = 1, 2$) is such that $\mathbf{F}_1 = -\mathbf{F}_2$. The schematic of the model is shown in Fig. 7.1. The solvent phase component is governed by the dynamics of single-particle distribution function $f_S^I(\mathbf{x}, \mathbf{v}_S, t)$ which dictates the probability of finding the solvent molecule at position \mathbf{x} with velocity \mathbf{v}_S at an instant of time t . The solvent mass density ρ_S , momentum density $\rho_S \mathbf{u}_S$ and temperature T_S is

$$\rho_S = \langle m_S, f_S^I \rangle, \quad \mathbf{J}_S = \rho_S \mathbf{u}_S = \langle m_S \mathbf{v}_S, f_S^I \rangle, \quad \rho_S T_S = \langle m_S (v_S - u_S)^2, f_S^I \rangle. \quad (7.8)$$

Similarly, the dynamics of solute (polymer) is governed by two particle distribution function

$f_{\text{P}}^{\text{II}}(\mathbf{x}_1, \mathbf{x}_2, \mathbf{v}_1, \mathbf{v}_2, t)$ which defines the probability of finding the dumbbell such that the bead 1 is at \mathbf{x}_1 with velocity \mathbf{v}_1 and bead 2 is located at \mathbf{x}_2 with velocity \mathbf{v}_2 at any instant of time t . The mass density of the polymer dumbbell is then defined as:

$$\begin{aligned} \rho_{\text{P}}(\mathbf{x}, t) &= m_{\text{B}} \int f_{\text{P}}^{\text{II}}(\mathbf{x}_1, \mathbf{x}_2, \mathbf{v}_1, \mathbf{v}_2, t) \delta(\mathbf{x} - \mathbf{x}_1) d\mathbf{v}_1 d\mathbf{v}_2 d\mathbf{x}_2 \\ &+ m_{\text{B}} \int f_{\text{P}}^{\text{II}}(\mathbf{x}_1, \mathbf{x}_2, \mathbf{v}_1, \mathbf{v}_2, t) \delta(\mathbf{x} - \mathbf{x}_2) d\mathbf{v}_1 d\mathbf{v}_2 d\mathbf{x}_1, \end{aligned} \quad (7.9)$$

With this definition of polymer mass density, it is natural to define the momentum density as (Öttinger & Petrillo 1996):

$$\begin{aligned} \mathbf{J}_{\text{P}}(\mathbf{x}, t) &= m_{\text{B}} \int \mathbf{v}_1 f_{\text{P}}^{\text{II}}(\mathbf{x}_1, \mathbf{x}_2, \mathbf{v}_1, \mathbf{v}_2, t) \delta(\mathbf{x} - \mathbf{x}_1) d\mathbf{v}_1 d\mathbf{v}_2 d\mathbf{x}_2 \\ &+ m_{\text{B}} \int \mathbf{v}_2 f_{\text{P}}^{\text{II}}(\mathbf{x}_1, \mathbf{x}_2, \mathbf{v}_1, \mathbf{v}_2, t) \delta(\mathbf{x} - \mathbf{x}_2) d\mathbf{v}_1 d\mathbf{v}_2 d\mathbf{x}_1. \end{aligned} \quad (7.10)$$

Similarly, the stress can be generalized as:

$$\begin{aligned} \mathbf{P}_{\text{P}\alpha\beta}(\mathbf{x}, t) &= m_{\text{B}} \int v_{1\alpha} v_{1\beta} f_{\text{P}}^{\text{II}}(\mathbf{x}_1, \mathbf{x}_2, \mathbf{v}_1, \mathbf{v}_2, t) \delta(\mathbf{x} - \mathbf{x}_1) d\mathbf{v}_1 d\mathbf{v}_2 d\mathbf{x}_2 \\ &+ m_{\text{B}} \int v_{2\alpha} v_{2\beta} f_{\text{P}}^{\text{II}}(\mathbf{x}_1, \mathbf{x}_2, \mathbf{v}_1, \mathbf{v}_2, t) \delta(\mathbf{x} - \mathbf{x}_2) d\mathbf{v}_1 d\mathbf{v}_2 d\mathbf{x}_1. \end{aligned} \quad (7.11)$$

The trace of the stress tensor $\mathbf{P}_{\text{P}\alpha\beta}$ is associated with the energy density of the polymer. Here onwards, we introduce the convention that post-collisional velocities will be denoted by prime, and subscripts S, P denote solvent and polymer respectively. In this notation, if the solvent-bead collision happens at location \mathbf{x}_1 with initial velocity of polymer and solvent being $\mathbf{v}_{\text{P}1}$ and \mathbf{v}_{S} respectively, the momentum balance is

$$m_{\text{S}}\mathbf{v}_{\text{S}} + m_{\text{B}}\mathbf{v}_{\text{P}1} = m_{\text{S}}\mathbf{v}'_{\text{S}1} + m_{\text{B}}\mathbf{v}'_{\text{P}1}. \quad (7.12)$$

Similarly, for a collision at location \mathbf{x}_2 with initial velocity of polymer and solvent being $\mathbf{v}_{\text{P}2}$ and \mathbf{v}_{S} respectively, the momentum balance is

$$m_{\text{S}}\mathbf{v}_{\text{S}} + m_{\text{B}}\mathbf{v}_{\text{P}2} = m_{\text{S}}\mathbf{v}'_{\text{S}2} + m_{\text{B}}\mathbf{v}'_{\text{P}2}. \quad (7.13)$$

Here, it should be pointed out that the kinetic description of the polymer solution simplifies in terms of a one particle probability distribution

$$f_{\text{P}}^{\text{I}}(\mathbf{x}, \mathbf{v}_{\text{P}}, t) = \int d\mathbf{x}_2 d\mathbf{v}_{\text{P}2} f_{\text{P}}^{\text{II}}(\mathbf{x}, \mathbf{x}_2, \mathbf{v}_{\text{P}}, \mathbf{v}_{\text{P}2}, t) + \int d\mathbf{x}_1 d\mathbf{v}_{\text{P}1} f_{\text{P}}^{\text{II}}(\mathbf{x}_1, \mathbf{x}, \mathbf{v}_{\text{P}1}, \mathbf{v}_{\text{P}}, t), \quad (7.14)$$

which corresponds to the probability of finding any of the beads of the dumbbell at location \mathbf{x} with velocity \mathbf{v}_{P} . As shown in the Fig. 7.2, the physical meaning of this distribution can also be seen in alternate coordinate system where the configuration of polymer dumbbell is defined in terms of \mathbf{r} and \mathbf{Q} with $\mathbf{Q} = \mathbf{x}_2 - \mathbf{x}_1$. This convention corresponds to either bead 1 or bead 2 being at location \mathbf{r} with velocity \mathbf{v}_{P} and the end-to-end distance with the other bead is \mathbf{Q} with velocity $\dot{\mathbf{Q}}$. It should be noted that in Fig. 7.2 the center of mass is located at $\mathbf{r} - \mathbf{R}_{\text{c}}$,

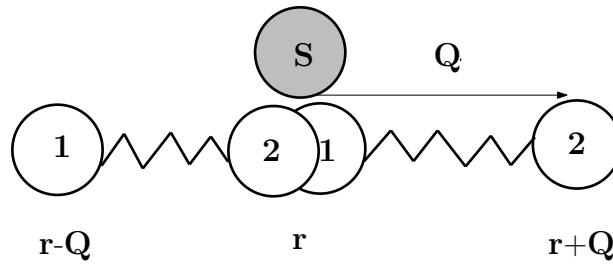


Figure 7.2: Schematic of polymer configuration

where $\mathbf{R}_\nu = (-1)^\nu \mathbf{Q}/2$ is the vector from the center of mass of the dumbbell to the ν^{th} bead. The displaced position argument for the center of mass is a result of the finite extension of the dumbbell in space. Similarly, the velocity associated with center of mass for both configurations can be defined as $\mathbf{v}_P - \dot{\mathbf{R}}_\nu$. In this convention, the one particle distribution function for polymer as defined by Eq. (7.14), takes the following form:

$$f_P^I(\mathbf{r}, \mathbf{v}_P, t) = \sum_\nu \int f_P^{II}(\mathbf{r} - \mathbf{R}_\nu, \mathbf{Q}, \mathbf{v}_P - \dot{\mathbf{R}}_\nu, \dot{\mathbf{Q}}, t) d\mathbf{Q} d\dot{\mathbf{Q}}. \quad (7.15)$$

Before going into the details of the kinetic model of polymer-solvent mixture, the collision mechanism in binary gas mixture is contrasted with that of polymer-solvent mixture in Sec.7.3.1.

7.3.1 Collision in binary gas mixture

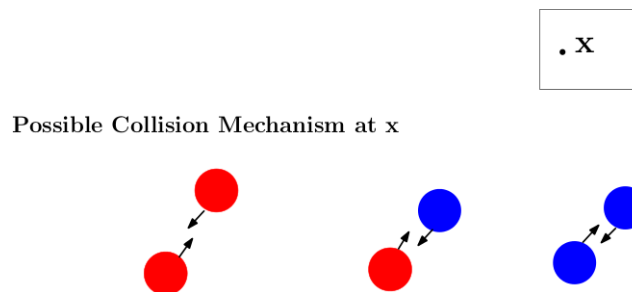


Figure 7.3: Schematic showing different types of collision in binary gas mixture

In a binary gas mixture consisting of two components $j = A, B$ having mass m_j , three kinds of collisions can occur at a given location \mathbf{x} in space at any instant of time. As shown in the Fig. 7.3, the three possible type of collisions are: self collision between two particle of type A, self collision between two particle of type B and cross collision between A and B. In this case, the kinetic equation governing the dynamics of probability distribution function of individual components are

$$\begin{aligned} \frac{\partial}{\partial t} f_A(\mathbf{x}, t) + \mathbf{v}_A \cdot \frac{\partial f_A}{\partial \mathbf{x}} &= \underbrace{\Omega_{AA}(f_A, f_A) + \Omega_{AB}(f_A, f_B)}_{\Omega_A}, \\ \frac{\partial}{\partial t} f_B(\mathbf{x}, t) + \mathbf{v}_B \cdot \frac{\partial f_B}{\partial \mathbf{x}} &= \underbrace{\Omega_{BA}(f_B, f_A) + \Omega_{BB}(f_B, f_B)}_{\Omega_B}, \end{aligned} \quad (7.16)$$

where Ω_{AA}, Ω_{BB} are self-collision contributions and Ω_{AB}, Ω_{BA} are cross-collision contributions. The self-collision between the particles of same component does not affect the mass, momentum and the energy conservation. The cross-collision does not affect the mass conservation, however the momentum and energy are exchanged between the components via cross-collision in such a manner that the total momentum and energy is conserved. Using the kinetic equation for the mixture Eq.(7.16), the evolution equations for individual component momentum are

$$\begin{aligned} \frac{\partial \mathbf{J}_A}{\partial t} + \frac{\partial \mathbf{P}_A}{\partial \mathbf{x}} &= \langle m_A \Omega_{AB}, \mathbf{v}_A \rangle, \\ \frac{\partial \mathbf{J}_B}{\partial t} + \frac{\partial \mathbf{P}_B}{\partial \mathbf{x}} &= \langle m_B \Omega_{BA}, \mathbf{v}_B \rangle. \end{aligned} \quad (7.17)$$

The term on the right hand side of Eq. (7.17), is related to mass diffusion flux, \mathbf{V}_D , as (Goldman & Sirovich 2004)

$$\langle m_A \Omega_{AB}, \mathbf{v}_A \rangle = - \langle m_B \Omega_{BA}, \mathbf{v}_B \rangle = \frac{\mathbf{V}_D}{\tau}, \quad (7.18)$$

where τ is the time scale associated with diffusion coefficient and $\mathbf{V}_D = [(\rho_A \rho_B) / \rho] (\mathbf{u}_A - \mathbf{u}_B)$ in the hydrodynamic limit. Based on quasi-equilibrium approach, a collision model for binary gas mixture which reproduce the accurate continuum level description has been given in Refs. Arcidiacono *et al.* (2006); Ansumali *et al.* (2007) and explained in detail in Chapter 6.

7.4 Collision in polymer-solvent mixture

As compared to the collision dynamics of binary gas mixture, the cross-collision between the solvent and polymer particles adds an extra degree of complication. Unlike binary gas mixture, by definition, collisions in polymer solutions are non-local due to the fact that the polymer dumbbell will collide with the solvent molecule located at \mathbf{x} if either of the beads of dumbbell is located at \mathbf{x} (see Fig.7.4). Thus, in order to extend the kinetic models of binary mixture model

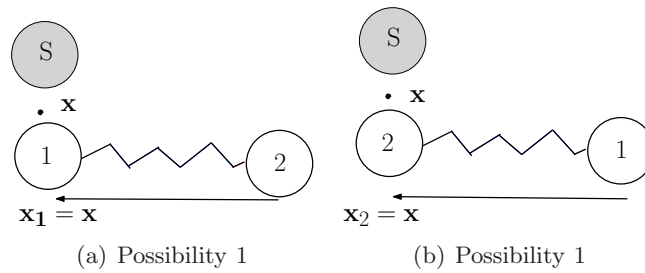


Figure 7.4: Possible cross collision between solvent molecule and polymer dumbbell at location \mathbf{x} .

to polymer solutions, one needs to describe the dynamics of solvent molecule by one particle distribution function $f_S^I(\mathbf{x}, \mathbf{v}_S, t)$ and that of polymer dumbbell by two particle distribution function $f_P^{II}(\mathbf{x}_1, \mathbf{x}_2, \mathbf{v}_{P1}, \mathbf{v}_{P2}, t)$.

These collision terms can be written explicitly in terms of the transition probability distribution for the collision $\omega(\mathbf{v}'_{S1}, \mathbf{v}'_{P1} | \mathbf{v}_S, \mathbf{v}_{P1}) = \omega(\mathbf{v}_S, \mathbf{v}_{P1} | \mathbf{v}'_{S1}, \mathbf{v}'_{P1})$, which denotes the probability of obtaining post collisional velocities to be given by pre-collisional velocities and the symmetry of

pre and post-collision are used in the equality. In the dilute limit (Cercignani 1988), assuming molecular chaos, the evolution equation for the solvent probability densities can be written as

$$\left(\frac{\partial}{\partial t} + \mathbf{v}_S \frac{\partial}{\partial \mathbf{x}} \right) f_S^I(\mathbf{x}, \mathbf{v}_S, t) = \Omega_{SS}(f_S^I, f_S^I) + \Omega_{SP}, \quad (7.19)$$

where Ω_{SS} accounts for the collision between the solvent molecules and Ω_{SP} accounts for the cross-collision between solvent molecule and polymer dumbbell and in explicit form is

$$\begin{aligned} \Omega_{SP}(\mathbf{x}, \mathbf{v}_S, t) &= \int d\mathbf{v}'_{S1} d\mathbf{v}_{P1} d\mathbf{v}'_{P1} d\mathbf{v}'_{P2} d\mathbf{x}_2 [f_S(\mathbf{x}, \mathbf{v}'_{S1}, t) f_P^{II}(\mathbf{x}, \mathbf{x}_2, \mathbf{v}'_{P1}, \mathbf{v}'_{P2}, t) - f_S(\mathbf{x}, \mathbf{v}_S, t) f_P^{II}(\mathbf{x}, \mathbf{x}_2, \mathbf{v}_{P1}, \mathbf{v}_{P2}, t)] \omega_1 \\ &+ \int d\mathbf{v}'_{S2} d\mathbf{v}_{P2} d\mathbf{v}'_{P2} d\mathbf{v}'_{P1} d\mathbf{x}_1 [f_S(\mathbf{x}, \mathbf{v}'_{S2}, t) f_P^{II}(\mathbf{x}_1, \mathbf{x}, \mathbf{v}'_{P1}, \mathbf{v}'_{P2}, t) - f_S(\mathbf{x}, \mathbf{v}_S, t) f_P^{II}(\mathbf{x}_1, \mathbf{x}, \mathbf{v}_{P1}, \mathbf{v}_{P2}, t)] \omega_2 \end{aligned} \quad (7.20)$$

where, short hand notations

$$\omega_1 \equiv \omega(\mathbf{v}'_{S1}, \mathbf{v}'_{P1} | \mathbf{v}_S, \mathbf{v}_{P1}), \quad \omega_2 \equiv \omega(\mathbf{v}'_{S2}, \mathbf{v}'_{P2} | \mathbf{v}_S, \mathbf{v}_{P2}), \quad (7.21)$$

are used for the transition probability and the collision between solvent and bead located at \mathbf{x}_1 is accounted by first term and similarly that with bead at location \mathbf{x}_2 is accounted by the second term. In terms of the reduced distribution f_P^I (see Eq. (7.14)), cross-collision term Ω_{SP} is re-written as

$$\Omega_{SP}(f_S^I, f_P^I) = \int d\mathbf{v}'_{S1} d\mathbf{v}_{P1} d\mathbf{v}'_{P1} [f_S(\mathbf{x}, \mathbf{v}'_{S1}, t) f_P^I(\mathbf{x}, \mathbf{v}'_{P1}, t) - f_S(\mathbf{x}, \mathbf{v}_S, t) f_P^I(\mathbf{x}, \mathbf{v}_{P1}, t)] \omega_1, \quad (7.22)$$

which is analogous to the cross-collision term in the Boltzmann equation for gas mixture (Andries *et al.* 2002). Similarly, the formal evolution equation for the solute is

$$\left(\frac{\partial}{\partial t} + \mathbf{v}_1 \frac{\partial}{\partial \mathbf{x}_1} + \mathbf{v}_2 \frac{\partial}{\partial \mathbf{x}_2} + \frac{\mathbf{F}_1}{m_B} \frac{\partial}{\partial \mathbf{v}_1} + \frac{\mathbf{F}_2}{m_B} \frac{\partial}{\partial \mathbf{v}_2} \right) f_P^{II}(\mathbf{x}_1, \mathbf{x}_2, \mathbf{v}_1, \mathbf{v}_2, t) = \Omega_{PS}, \quad (7.23)$$

where \mathbf{F}_1 and \mathbf{F}_2 are the spring forces. The self-collision between the polymer molecule can be neglected at the moment because in the dilute or semi-dilute limit one is not interested in this contribution. The cross-collision term Ω_{PS} is given as:

$$\begin{aligned} \Omega_{PS}(\mathbf{x}_1, \mathbf{x}_2, \mathbf{v}_{P1}, \mathbf{v}_{P2}, t) &= \int d\mathbf{v}_S d\mathbf{v}'_{S1} d\mathbf{v}'_{P1} [f_S(\mathbf{x}_1, \mathbf{v}'_{S1}, t) f_P^{II}(\mathbf{x}_1, \mathbf{x}_2, \mathbf{v}'_{P1}, \mathbf{v}_{P2}, t) - f_S(\mathbf{x}_1, \mathbf{v}_S, t) f_P^{II}(\mathbf{x}_1, \mathbf{x}_2, \mathbf{v}_{P1}, \mathbf{v}_{P2}, t)] \omega_1 \\ &+ \int d\mathbf{v}_S d\mathbf{v}'_{S2} d\mathbf{v}'_{P2} [f_S(\mathbf{x}_2, \mathbf{v}'_{S2}, t) f_P^{II}(\mathbf{x}_1, \mathbf{x}_2, \mathbf{v}_{P1}, \mathbf{v}'_{P2}, t) - f_S(\mathbf{x}_2, \mathbf{v}_S, t) f_P^{II}(\mathbf{x}_1, \mathbf{x}_2, \mathbf{v}_{P1}, \mathbf{v}_{P2}, t)] \omega_2, \end{aligned} \quad (7.24)$$

where, the first term on right hand side accounts for collision between solvent and bead 1 located at \mathbf{x}_1 and the second term accounts for collision between solvent and bead 2 located at \mathbf{x}_2 .

7.4.1 Mass and Momentum Conservation Laws

A priori, it is not obvious that the local conservation laws exist in this system. In this section, collision mechanism is carefully analyzed to understand the appropriate choice of moments for which local conservation holds. Similar to the Boltzmann equation for the gaseous mixture, cross-collisions conserve the mass in present model too. Furthermore, as expected, the total momentum is conserved, while individual momentum is not. However, unlike binary gas mixture, the natural way to define solute momentum density is by Eq. (7.10). In this section, the set of conservation laws for present kinetic description (Eq. (7.19) and Eq. (7.23)) is discussed.

On integrating Eq. (7.19) over all possible values of \mathbf{v}_S and using Eq. (7.22) for cross-collision terms, one gets

$$\begin{aligned} \partial_t \rho^S + \partial_{\mathbf{x}} \cdot \mathbf{J}_S &= m_S \int d\mathbf{v}_S d\mathbf{v}'_{S1} d\mathbf{v}_{P1} d\mathbf{v}'_{P1} f_S(\mathbf{x}, \mathbf{v}'_{S1}) f_P^I(\mathbf{x}, \mathbf{v}'_{P1}) \omega(\mathbf{v}'_{S1}, \mathbf{v}'_{P1} | \mathbf{v}_S, \mathbf{v}_{P1}) \\ &\quad - m_S \int d\mathbf{v}_S d\mathbf{v}'_{S1} d\mathbf{v}_{P1} d\mathbf{v}'_{P1} f_S(\mathbf{x}, \mathbf{v}'_{S1}) f_P^I(\mathbf{x}, \mathbf{v}'_{P1}) \omega(\mathbf{v}_S, \mathbf{v}_{P1} | \mathbf{v}'_{S1}, \mathbf{v}'_{P1}), \\ &= 0, \end{aligned} \quad (7.25)$$

which implies the existence of mass conservation for solvent. Here, symmetry of transition probability with respect to pre and post collisional velocity is utilized in the loss term to show that the contribution to the mass density of solvent due to cross collision is zero. Similarly, the evolution of momentum density for solvent is

$$\begin{aligned} \partial_t \mathbf{J}_S + \partial_{\mathbf{x}} \cdot \mathbf{P}_S &= m_S \int d\mathbf{v}_S d\mathbf{v}'_{S1} d\mathbf{v}_{P1} d\mathbf{v}'_{P1} \mathbf{v}_S [f_S(\mathbf{x}, \mathbf{v}'_{S1}, t) f_P^I(\mathbf{x}, \mathbf{v}'_{P1}, t) - f_S(\mathbf{x}, \mathbf{v}_S, t) f_P^I(\mathbf{x}, \mathbf{v}_{P1}, t)] \omega_1 \\ &= m_S \int d\mathbf{v}_S d\mathbf{v}'_{S1} d\mathbf{v}_{P1} d\mathbf{v}'_{P1} [\mathbf{v}_S - \mathbf{v}'_{S1}] f_S(\mathbf{x}, \mathbf{v}'_{S1}, t) f_P^I(\mathbf{x}, \mathbf{v}'_{P1}, t) \omega_1, \end{aligned} \quad (7.26)$$

where similar to binary gas mixture, the term on the right hand side of the equation should account for the momentum exchange between the two components.

Unlike solvent, showing the existence of mass conservation for the polymer phase is more subtle due to non-locality of the dumbbell. The evolution equation for the polymer density, defined via Eq.(7.9), shows existence of such a conservation law. This evolution equation for the polymer density is written using Eq.(7.40) as

$$\begin{aligned} \partial_t \rho_P + \partial_{\mathbf{x}} \cdot \mathbf{J}_P &= m_B \int d\mathbf{x}_2 d\mathbf{v}_{P1} d\mathbf{v}_{P2} \Omega_{PS}(\mathbf{x}_1, \mathbf{x}_2, \mathbf{v}_{P1}, \mathbf{v}_{P2}, t) \delta(\mathbf{x} - \mathbf{x}_1) \\ &\quad + m_B \int d\mathbf{x}_1 d\mathbf{v}_{P1} d\mathbf{v}_{P2} \Omega_{PS}(\mathbf{x}_1, \mathbf{x}_2, \mathbf{v}_{P1}, \mathbf{v}_{P2}, t) \delta(\mathbf{x} - \mathbf{x}_2), \end{aligned} \quad (7.27)$$

which on using symmetry of the transition probability reduces to the usual continuity equation for the component density as

$$\partial_t \rho_P + \partial_{\mathbf{x}} \cdot \mathbf{J}_P = 0, \quad (7.28)$$

where the effective momentum of the polymer, defined via Eq. (7.10), appears as the momentum

density. Thus, the polymer solution kinetic equation is analogous to the binary gas mixture with the mass density and the momentum density defined via Eq.(7.9) and Eq.(7.10). The evolution equation for this effective momentum is

$$\begin{aligned}
& \partial_t \mathbf{J}_P + \partial_{\mathbf{x}} \cdot \mathbf{P}_P - \mathbf{I} \\
& = m_B \int d\mathbf{v}_S d\mathbf{v}'_{S1} d\mathbf{v}'_{P1} d\mathbf{v}_{P1} d\mathbf{v}_{P2} d\mathbf{x}_2 \mathbf{v}_{P1} [f_S(\mathbf{x}, \mathbf{v}'_{S1}) f_P^{\text{II}}(\mathbf{x}, \mathbf{x}_2, \mathbf{v}'_{P1}, \mathbf{v}_{P2}) - f_S(\mathbf{x}, \mathbf{v}_S) f_P^{\text{II}}(\mathbf{x}, \mathbf{x}_2, \mathbf{v}_{P1}, \mathbf{v}_{P2})] \omega_1 \\
& + m_B \int d\mathbf{v}_S d\mathbf{v}'_{S2} d\mathbf{v}'_{P2} d\mathbf{v}_{P1} d\mathbf{v}_{P2} d\mathbf{x}_1 \mathbf{v}_{P2} [f_S(\mathbf{x}, \mathbf{v}'_{S2}) f_P^{\text{II}}(\mathbf{x}_1, \mathbf{x}, \mathbf{v}_{P1}, \mathbf{v}'_{P2}) - f_S(\mathbf{x}, \mathbf{v}_S, t) f_P^{\text{II}}(\mathbf{x}_1, \mathbf{x}, \mathbf{v}_{P1}, \mathbf{v}_{P2})] \omega_2 \\
& = m_B \int d\mathbf{v}_S d\mathbf{v}'_{S1} d\mathbf{v}_{P1} d\mathbf{v}'_{P1} [\mathbf{v}_P - \mathbf{v}'_P] f_S(\mathbf{x}, \mathbf{v}'_{S1}) f_P^{\text{I}}(\mathbf{x}, \mathbf{v}'_{P1}) \omega_1,
\end{aligned} \tag{7.29}$$

where once again the symmetry of transition probability with respect to pre and post collisional velocity is utilized in the loss term and the impulse \mathbf{I} is defined as:

$$\mathbf{I}(\mathbf{x}, t) = \int F(\mathbf{x}_2 - \mathbf{x}) \psi(\mathbf{x}, \mathbf{x}_2, t) d\mathbf{x}_2 - \int F(\mathbf{x} - \mathbf{x}_1) \psi(\mathbf{x}_1, \mathbf{x}, t) d\mathbf{x}_1, \tag{7.30}$$

where the property of force $\mathbf{F}_1 = -\mathbf{F}_2 \equiv \mathbf{F}$ is used and configuration distribution function is defined as:

$$\psi(\mathbf{x}_1, \mathbf{x}_2, t) = \int d\mathbf{v}_1 d\mathbf{v}_2 f_P^{\text{II}}(\mathbf{x}_1, \mathbf{x}_2, \mathbf{v}_1, \mathbf{v}_2, t). \tag{7.31}$$

Physically, stretching of the spring provides a non-local mode of momentum transport and thus \mathbf{I} should be expressed as divergence of a stress term related to the stretching. The divergence form is apparent, by integrating out space argument, which shows that

$$\int d\mathbf{x} \mathbf{I}(\mathbf{x}, t) = \int d\mathbf{x} d\mathbf{x}_2 F(\mathbf{x}_2 - \mathbf{x}) \psi(\mathbf{x}, \mathbf{x}_2, t) - \int d\mathbf{x} d\mathbf{x}_1 F(\mathbf{x} - \mathbf{x}_1) \psi(\mathbf{x}_1, \mathbf{x}, t) = 0, \tag{7.32}$$

and thus global conservation is not affected by impulse term \mathbf{I} . In other words, \mathbf{I} can be defined as a divergence of a second order tensor as:

$$\mathbf{I} = \frac{\partial}{\partial \mathbf{r}} \cdot \boldsymbol{\Theta}. \tag{7.33}$$

In (\mathbf{r}, \mathbf{Q}) coordinate system, it is easy to see that this second order tensor is nothing but the elastic stress contribution to the stress tensor. In this representation, the impulse (Eq. (7.30)), can be re-written as

$$\mathbf{I}(\mathbf{r}, t) = \int \mathbf{F}_\nu(\mathbf{Q}) \psi(\mathbf{r} - \mathbf{R}_\nu, \mathbf{Q}, t) d\mathbf{Q}, \tag{7.34}$$

Further, by expanding the configuration distribution function ψ in a Taylor series (Öttinger & Petrillo (1996)) as

$$\psi(\mathbf{r} - \mathbf{R}_\nu, \mathbf{Q}, t) = \psi(\mathbf{r}, \mathbf{Q}, t) - \mathbf{R}_\nu \cdot \frac{\partial}{\partial \mathbf{r}} \psi(\mathbf{r}, \mathbf{Q}, t) + \frac{\mathbf{R}_\nu \mathbf{R}_\nu}{2} : \frac{\partial}{\partial \mathbf{r}} \frac{\partial}{\partial \mathbf{r}} \psi(\mathbf{r}, \mathbf{Q}, t) + \dots, \tag{7.35}$$

which gives back Eq.(7.33) with

$$\boldsymbol{\Theta}(\mathbf{r}, t) = \int \psi(\mathbf{r}, \mathbf{Q}, t) \mathbf{Q} \mathbf{F} d\mathbf{Q}. \quad (7.36)$$

Finally, the evolution equation for the total momentum $\mathbf{J} = \mathbf{J}_P + \mathbf{J}_S$, obtained by adding the component momentum Eqns. (7.19),(7.23) is

$$\frac{\partial \mathbf{J}}{\partial t} + \frac{\partial}{\partial \mathbf{r}} \cdot (\mathbf{P}_P + \mathbf{P}_S - \boldsymbol{\Theta}) = 0, \quad (7.37)$$

This conservation form for the total momentum density also implies that the evolution of momentum density of solvent and polymer (Eqns. (7.19),(7.23)) can be re-written as

$$\begin{aligned} \frac{\partial \mathbf{J}_S}{\partial t} + \frac{\partial}{\partial \mathbf{r}} \cdot \mathbf{P}_S(\mathbf{r}, t) &= \frac{1}{\tau} \mathbf{V}_D \\ \frac{\partial \mathbf{J}_P}{\partial t} + \frac{\partial}{\partial \mathbf{r}} \cdot \mathbf{P}_P(\mathbf{r}, t) &= -\frac{1}{\tau} \mathbf{V}_D + \frac{\partial}{\partial \mathbf{r}} \cdot \boldsymbol{\Theta}, \end{aligned} \quad (7.38)$$

where the \mathbf{V}_D using Eqns. (7.26) is defined as

$$\mathbf{V}_D = \tau \left(m_S \int d\mathbf{v}_S d\mathbf{v}'_{S1} d\mathbf{v}_{P1} d\mathbf{v}'_{P1} [\mathbf{v}_S - \mathbf{v}'_S] f_S(\mathbf{x}, \mathbf{v}'_{S1}, t) f_P^I(\mathbf{x}, \mathbf{v}'_{P1}, t) \omega_1 \right), \quad (7.39)$$

and τ can be understood as a time scale associated with the drag force which resists the velocity difference between the two component (Milner 1991, 1993). To conclude, in this section starting from a Boltzmann-like kinetic description of the solvent-polymer mixture in phase space, a set of conservation laws are obtained for the polymer solution (Eq. (7.38)). These equations must be reproduced by any model equation written for this system. In subsequent sections, a BGK type model is developed, where these equations are used as consistency conditions.

7.5 Collision Modeling for polymer-solvent mixture

As discussed in the previous section, the polymer dumbbell collides with the solvent molecule only if the location of the solvent coincides with the location of either of the beads of dumbbell. Thus, any collision model of polymer-solvent interaction has to be non-local. Furthermore, as discussed in the previous section, the natural description is in terms of single particle distribution function for solvent and two particle distribution function for the polymer dynamics. In this section, we look for model kinetic equations of the form

$$\begin{aligned} \left(\frac{\partial}{\partial t} + \mathbf{v}_S \cdot \frac{\partial}{\partial \mathbf{r}} \right) f_S^I(\mathbf{r}, \mathbf{v}_S, t) &= \Omega_S, \\ \left(\frac{\partial}{\partial t} + \mathbf{v}_P \frac{\partial}{\partial \mathbf{r}} + \dot{\mathbf{Q}} \frac{\partial}{\partial \mathbf{Q}} \right) f_P^{II}(\mathbf{r}, \mathbf{Q}, \mathbf{v}_P, \dot{\mathbf{Q}}, t) &= \Omega_P, \end{aligned} \quad (7.40)$$

where the collision operator Ω_S , Ω_P should be such that the continuum level description, given by (7.38), is recovered. The conservation of mass density of the polymer as well as the solvent

phase of the mixture enforces the following condition on collision term:

$$\int d\mathbf{v}_S m_S \Omega_S(\mathbf{r}, \mathbf{v}_S, t) + \sum_{\nu} \int d\mathbf{Q} d\mathbf{v}_P d\dot{\mathbf{Q}} \Omega_P(\mathbf{r} + \mathbf{R}_{\nu}, \mathbf{Q}, \mathbf{v}_P + \dot{\mathbf{R}}_{\nu}, \dot{\mathbf{Q}}, t) = 0. \quad (7.41)$$

In present approach, in order to obtain the correct total momentum equation (Eq. (7.37)), both the momentum exchange occurring via drag terms as well as impulse generated due to stretching of the spring are considered in the momentum conservation equation as

$$\int d\mathbf{v}_S m_S \Omega_S(\mathbf{r}, \mathbf{v}_S, t) \mathbf{v}_S + \sum_{\nu} m_B \int d\mathbf{Q} d\mathbf{v}_P d\dot{\mathbf{Q}} \Omega_P(\mathbf{r} + \mathbf{R}_{\nu}, \mathbf{Q}, \mathbf{v}_P + \dot{\mathbf{R}}_{\nu}, \dot{\mathbf{Q}}, t) \mathbf{v}_P - \tau \mathbf{I} = 0. \quad (7.42)$$

We would like to point out here that similar to the mixture model, the relaxation mechanism with two relaxation times is needed in order to have tunable viscosity as well as diffusivity. On using the quasi-equilibrium based relaxation method, we model the collision term in the following manner:

$$\Omega_S = \frac{1}{\tau_1} [f_S^{\text{MB}}(\rho_S, \mathbf{u}_S, T_S) - f_S] + \frac{1}{\tau_2} [f_S^{\text{MB}}(\rho_S, \mathbf{U}, T) - f^{\text{MB}}(\rho_S, \mathbf{u}_S, T_S)], \quad (7.43)$$

where, the Maxwell-Boltzmann distribution around any velocity, \mathbf{u} , is given as:

$$f^{\text{MB}}(\rho_S, \mathbf{u}, T) = \rho_S \sqrt{\frac{m_S}{2\pi k_B T}} \exp\left(-\frac{m_S(\mathbf{v}_S - \mathbf{u})^2}{2k_B T}\right). \quad (7.44)$$

Similarly, we write the evolution equation for two particle distribution as

$$\Omega_P(\mathbf{r} + \mathbf{R}_{\nu}, \mathbf{Q}, \mathbf{v}_P + \dot{\mathbf{R}}_{\nu}, \dot{\mathbf{Q}}, t) = \frac{1}{\tau_1} [f_P^{*II} - f_P^{\text{II}}] + \frac{1}{\tau_2} [f_P^{\text{eqII}} - f_P^{*II}], \quad (7.45)$$

where the equilibrium distributions are

$$\begin{aligned} f_P^{\text{eqII}}\left(\mathbf{r} + \frac{\mathbf{Q}}{2}, \mathbf{Q}, \mathbf{v}_P + \frac{\dot{\mathbf{Q}}}{2}, \dot{\mathbf{Q}}\right) &= \psi\left(\mathbf{r} + \frac{\mathbf{Q}}{2}, \mathbf{Q}\right) \left(\frac{m^B}{2\pi k_B T}\right)^3 \times \\ &\quad \exp\left[-\left(\frac{m^B(\mathbf{v} - \mathbf{U}(\mathbf{r}) - \frac{\mathbf{F}_1}{\zeta})^2}{2k_B T}\right) - \left(\frac{m^B(\mathbf{v} + \dot{\mathbf{Q}} - \mathbf{U}(\mathbf{r} + \mathbf{Q}) - \frac{\mathbf{F}_2}{\zeta})^2}{2k_B T}\right)\right], \\ f_P^{\text{eqII}}\left(\mathbf{r} - \frac{\mathbf{Q}}{2}, \mathbf{Q}, \mathbf{v}_P - \frac{\dot{\mathbf{Q}}}{2}, \dot{\mathbf{Q}}\right) &= \psi\left(\mathbf{r} - \frac{\mathbf{Q}}{2}, \mathbf{Q}\right) \left(\frac{m^B}{2\pi k_B T}\right)^3 \times \\ &\quad \exp\left[-\left(\frac{m^B(\mathbf{v} - \dot{\mathbf{Q}} - \mathbf{U}(\mathbf{r} - \mathbf{Q}) - \frac{\mathbf{F}_1}{\zeta})^2}{2k_B T}\right) - \left(\frac{m^B(\mathbf{v} - \mathbf{U}(\mathbf{r}) - \frac{\mathbf{F}_2}{\zeta})^2}{2k_B T}\right)\right], \end{aligned} \quad (7.46)$$

and the quasi-equilibrium distributions are

$$\begin{aligned}
f_P^{*II}(\mathbf{r} + \frac{\mathbf{Q}}{2}, \mathbf{Q}, \mathbf{v}_P + \frac{\dot{\mathbf{Q}}}{2}, \dot{\mathbf{Q}}) &= \psi(\mathbf{r} + \frac{\mathbf{Q}}{2}, \mathbf{Q}) \left(\frac{m^B}{2\pi k_B T} \right)^3 \times \\
&\quad \exp \left[- \left(\frac{m^B [\mathbf{v} - \mathbf{u}^r(\mathbf{r} + \frac{\mathbf{Q}}{2})]^2}{2k_B T} \right) - \left(\frac{m^B [\mathbf{v} + \dot{\mathbf{Q}} - (\mathbf{u}^r(\mathbf{r} + \frac{\mathbf{Q}}{2}) + \mathbf{u}^Q(\mathbf{r} + \frac{\mathbf{Q}}{2}))]^2}{2k_B T} \right) \right], \\
f_P^{*II}(\mathbf{r} - \frac{\mathbf{Q}}{2}, \mathbf{Q}, \mathbf{v}_P - \frac{\dot{\mathbf{Q}}}{2}, \dot{\mathbf{Q}}) &= \psi(\mathbf{r} - \frac{\mathbf{Q}}{2}, \mathbf{Q}) \left(\frac{m^B}{2\pi k_B T} \right)^3 \times \\
&\quad \exp \left[- \left(\frac{m^B [\mathbf{v} - \dot{\mathbf{Q}} - (\mathbf{u}^r(\mathbf{r} - \frac{\mathbf{Q}}{2}) - \mathbf{u}^Q(\mathbf{r} - \frac{\mathbf{Q}}{2}, \mathbf{Q}))]^2}{2k_B T} \right) - \left(\frac{m^B [\mathbf{v} - \mathbf{u}^r(\mathbf{r} - \frac{\mathbf{Q}}{2})]^2}{2k_B T} \right) \right],
\end{aligned} \tag{7.47}$$

where f^{eqII} and f^{*II} are the factorized Maxwellian in \mathbf{r} and \mathbf{Q} space and

$$\begin{aligned}
\mathbf{J}^r &= \psi \mathbf{u}^r = \langle \langle m_B \dot{\mathbf{Q}}, f_P^{\text{II}} \rangle \rangle, \\
\mathbf{J}^Q &= \psi \mathbf{u}^Q = \langle \langle m_B \dot{\mathbf{Q}}, f_P^{\text{II}} \rangle \rangle,
\end{aligned} \tag{7.48}$$

with

$$\langle \langle \phi_1, \phi_2 \rangle \rangle = \int d\mathbf{v}_P d\dot{\mathbf{Q}} \phi_1 \phi_2, \tag{7.49}$$

where ϕ_1 and ϕ_2 are any arbitrary quantities defined at bead location.

A more stricter requirement on the model is that it should recover Smoluchowski equation for the configuration distribution function. In order to show that the model in long time leads to expected form of Smoluchowski equation, we define bead averaged version of any quantity ϕ as:

$$\hat{\phi}(\mathbf{r}, \mathbf{Q}, t) = \sum_{\nu} \phi(\mathbf{r} - \mathbf{R}_{\nu}, \mathbf{Q}, t), \tag{7.50}$$

In Appendix A, the Chapman-Enskog expansion is used to show that, in dilute limit, the desired Smoluchowski equation for homogeneous case and diffusion equation (for the polymer concentration) for inhomogeneous case are recovered. Using this definition, the evolution equation for the lower order moments for Eq. (7.45) is

$$\begin{aligned}
\frac{\partial}{\partial t} \psi(\mathbf{r}, \mathbf{Q}, t) + \frac{\partial}{\partial \mathbf{r}} \cdot \mathbf{J}^r + \frac{\partial}{\partial \mathbf{Q}} \cdot \mathbf{J}^Q &= 0, \\
\frac{\partial}{\partial t} \mathbf{J}^r(\mathbf{r}, \mathbf{Q}, t) + \frac{\partial}{\partial \mathbf{r}} \cdot \mathbf{P}^r + \frac{\partial}{\partial \mathbf{Q}} \cdot \mathbf{P}^{rQ} &= \frac{1}{\tau_2} \left[\psi \mathbf{U}(\mathbf{r}, t) + \sum_{\nu} \left(\frac{\mathbf{F}_{\nu}}{\zeta} \psi(\mathbf{r} - \mathbf{R}_{\nu}, \mathbf{Q}, t) \right) - \mathbf{J}^r \right], \\
\frac{\partial}{\partial t} \mathbf{J}^Q(\mathbf{r}, \mathbf{Q}, t) + \frac{\partial}{\partial \mathbf{r}} \cdot \mathbf{P}^{rQ} + \frac{\partial}{\partial \mathbf{Q}} \cdot \mathbf{P}^Q &= \frac{1}{\tau_2} \left[\psi(\mathbf{r}, \mathbf{Q}, t) \mathbf{Q} \cdot \frac{\partial \mathbf{U}}{\partial \mathbf{r}} - \psi \frac{2\mathbf{F}}{\zeta} - \mathbf{J}^Q(\mathbf{r}, \mathbf{Q}, t) \right].
\end{aligned} \tag{7.51}$$

where

$$\begin{aligned}
\mathbf{P}^r &= \langle \langle m_B \mathbf{v}_P \mathbf{v}_P, f_P^{\text{II}} \rangle \rangle, \\
\mathbf{P}^Q &= \langle \langle m_B \dot{\mathbf{Q}} \dot{\mathbf{Q}}, f_P^{\text{II}} \rangle \rangle, \\
\mathbf{P}^{rQ} &= \langle \langle m_B \mathbf{v}_P \dot{\mathbf{Q}}, f_P^{\text{II}} \rangle \rangle.
\end{aligned} \tag{7.52}$$

The polymer mass density ρ_P and the momentum density \mathbf{J}_P , given by Eq. (7.9) and Eq. (7.10), can be redefined as

$$\rho_P(\mathbf{r}, t) = \int d\mathbf{Q} \psi(\mathbf{r}, \mathbf{Q}, t), \quad \mathbf{J}_P(\mathbf{r}, t) = \int d\mathbf{Q} \mathbf{J}^r(\mathbf{r}, \mathbf{Q}, t). \quad (7.53)$$

These quasi-equilibrium model is constructed such that, the conservation law takes the following expected form:

$$\begin{aligned} \frac{\partial \rho_S}{\partial t} + \frac{\partial \rho_S}{\partial \mathbf{r}} &= 0, \\ \frac{\partial \rho_P}{\partial t} + \frac{\partial \rho_P}{\partial \mathbf{r}} &= 0, \\ \frac{\partial \mathbf{J}_S}{\partial t} + \frac{\partial \mathbf{P}_S}{\partial \mathbf{r}} &= \frac{\mathbf{V}_D}{\tau}, \\ \frac{\partial \mathbf{J}_S}{\partial t} + \frac{\partial}{\partial \mathbf{r}}(\mathbf{P}_P - \boldsymbol{\Theta}) &= -\frac{\mathbf{V}_D}{\tau}. \end{aligned} \quad (7.54)$$

It should be noted that the above model will limit the maximum attainable Sc to be equal to mass ratio in the limit of dilute solution, as mentioned in the previous chapter. In order to avoid this limitation, the relevant collision model for single particle distribution function is

$$\begin{aligned} \Omega_S &= \frac{1}{\tau_1} [f_S^*(\rho_S, \mathbf{U}, \mathbf{P}_S) - f_S] + \frac{1}{\tau_2} [f_S^{\text{MB}}(\rho_S, \mathbf{U}, T) - f_S^*(\rho_S, \mathbf{U}, \mathbf{P}_S)], \\ \Omega_P &= \frac{1}{\tau_1} [f_P^{**II} - f_P^{\text{II}}] + \frac{1}{\tau_2} [f_P^{\text{eqII}} - f_P^{**II}]. \end{aligned} \quad (7.55)$$

where

$$f_S^* = \rho_S \sqrt{\frac{m_S}{2\pi k_B \det(\mathbf{T}_S)}} \exp\left(-\frac{m_S(\mathbf{v}_S - \mathbf{U}) \cdot \mathbf{T}_S^{-1} \cdot (\mathbf{v}_S - \mathbf{U})}{2k_B T}\right) \quad (7.56)$$

giving $\langle f_S^*, v_{S\alpha} v_{S\beta} \rangle = \rho_S T_{S\alpha\beta} + \rho_S u_{S\alpha} u_{S\beta}$ and $f_P^{**II}(\mathbf{r} + \mathbf{R}_\nu, \mathbf{Q}, \mathbf{v}_P + \dot{\mathbf{R}}_\nu, t)$ is such that

$$\int d\mathbf{Q} d\mathbf{v}_P d\dot{\mathbf{Q}} v_{P\alpha} v_{P\beta} f_P^{**II} = \rho_P T_{P\alpha\beta} + \rho_P u_{P\alpha} u_{P\beta} \quad (7.57)$$

This model will give the moment-chain same as Eq. (7.51) but with the relaxation time τ_1 instead of τ_2 and therefore the lower limit on Sc will become Sc^* for dilute solution, which was the upper limit in the previous model. Physically, the two models differ in terms of the fixed quasi variables. In the first model where Sc^* is the upper limit, the velocity of individual component is a quasi variable. It means that the system first relaxes to a state with a fixed component velocity and then relaxes to a state that has fixed mass averaged velocity. In the model where Sc^* is the lower limit, the quasi variable is the pressure tensor of the individual component.

7.6 Numerical validation via one way coupling

In this section, we validate our scheme by showing its ability to capture inhomogeneous effects. A restricted version of inhomogeneity is tested. It has been assumed that while polymer dynamics get affected by homogeneity of the flow, there is no feedback to the flow. This is justified in the

dilute limit case. As a concrete setup, we consider two-dimensional plane Poiseuille flow with the parabolic velocity profile:

$$u_{xS} = U_m \left(1 - \frac{y^2}{L^2}\right), \quad u_{yS} = 0. \quad (7.58)$$

where U_m is the velocity at the center of the channel and $2L$ ($-L$ to L) is the length of the channel. On using L, l_0, U_m and L/U_m to scale $\mathbf{r}, \mathbf{Q}, \mathbf{u}_S$ and t respectively, we get the following non-dimensional Smoluchowski Equation:

$$\begin{aligned} \frac{\partial \psi}{\partial t} + \frac{\partial}{\partial \mathbf{r}} \cdot \left[\mathbf{u}_S(\mathbf{r})\psi + \frac{l_0^2}{4L^2 \text{Wi}} \frac{\mathbf{Q}}{1 - \frac{Q^2}{b}} \mathbf{Q} \cdot \frac{\partial}{\partial \mathbf{r}} \psi \right] + \frac{\partial}{\partial \mathbf{Q}} \cdot \left[\mathbf{Q} \cdot \nabla \mathbf{u}_S - \frac{1}{2\text{Wi}} \frac{\mathbf{Q}}{1 - \frac{Q^2}{b}} \right] \psi \\ = \frac{l_0^2}{4L^2 \text{Wi}} \frac{\partial \psi}{\partial r^2} + \frac{1}{2\text{Wi}} \frac{\partial^2 \psi}{\partial Q^2} \end{aligned} \quad (7.59)$$

where $\text{Wi} = (\zeta U_m)/(4HL)$. With the following choice of imposed velocity,

$$\begin{aligned} \mathbf{v}_r &= \left[\mathbf{u}_S(\mathbf{r}) + \frac{l_0^2}{4L^2 \text{Wi}} \frac{\mathbf{Q}}{1 - \frac{Q^2}{b}} \mathbf{Q} \cdot \frac{\partial}{\partial \mathbf{r}} \psi \right], \\ \mathbf{v}_Q &= \left[\mathbf{Q} \cdot \nabla \mathbf{u}_S - \frac{1}{2\text{Wi}} \frac{\mathbf{Q}}{1 - \frac{Q^2}{b}} \right], \end{aligned} \quad (7.60)$$

and using a multi-scale Chapman-Enskog expansion, the Eq. (7.59) is recovered as the slow dynamics of the following kinetic equation:

$$\left(\frac{\partial}{\partial t} + v_\alpha \frac{\partial}{\partial r_\alpha} + \dot{Q}_\alpha \frac{\partial}{\partial Q_\alpha} \right) f_P^{\text{II}}(\mathbf{r}, \mathbf{Q}, \mathbf{v}, \dot{\mathbf{Q}}, t) = \frac{1}{\tau} [f_P^{\text{eqII}}(\psi, \mathbf{v}_r, \mathbf{v}_Q, t) - f_P^{\text{II}}(\mathbf{r}, \mathbf{Q}, \mathbf{v}, \dot{\mathbf{Q}}, t)], \quad (7.61)$$

In the Sec. 7.6.1, we discuss the LB based discrete scheme in four dimensional space to solve Eq. (7.61).

7.6.1 Discrete formulation

The discrete formulation is similar as discussed in Chapter 3 with the exception that in order to solve two dimensional problems in real physical space we need to deal with four dimensional $\mathbf{r} - \mathbf{Q}$ space as shown in Fig. 7.5. Therefore, proper choice of discrete velocity is needed. Here, D4Q25 velocity model is used whose discrete velocities $(v_x, v_y, \dot{Q}_x, \dot{Q}_y)$ are given in Table 7.1 (Qian *et al.* 1992).

Using the following conditions,

$$\sum_i w_i = 1, \quad \sum_i w_i c_{i\alpha} c_{i\beta} = c_{\text{SP}}^2 \delta_{\alpha\beta}, \quad \sum_i w_i c_{i\alpha} c_{i\beta} c_{i\gamma} c_{i\theta} = c_{\text{SP}}^4 \Delta_{\alpha\beta\gamma\theta}, \quad (7.62)$$

the associated weights can be found as $w_0 = 1/3$ and $w_{24} = 1/36$ with $c^2 = 3c_{\text{SP}}^2$ where Δ is used to denote symmetrized tensor generated from the Kronecker-delta δ . Recall that the dynamics

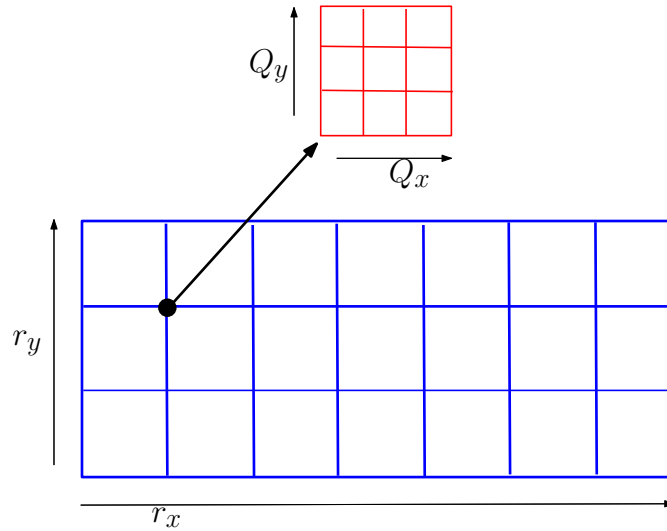


Figure 7.5: Four dimensional configuration space for polymer dumbbell

r_x	r_y	Q_x	Q_y
$\pm c$	$\pm c$	0	0
$\pm c$	0	$\pm c$	0
$\pm c$	0	0	$\pm c$
0	$\pm c$	$\pm c$	0
0	$\pm c$	$\pm c$	0
0	0	$\pm c$	$\pm c$

Table 7.1: Discrete velocity set

of discrete population f_i corresponding to discrete velocity is

$$\frac{\partial f_{Pi}^{\text{II}}}{\partial t} + v_{i\alpha} \frac{\partial f_{Pi}^{\text{II}}}{\partial r_\alpha} + \dot{Q}_{i\alpha} \frac{\partial f_{Pi}^{\text{II}}}{\partial Q_\alpha} = \frac{1}{\tau} \left(f_{Pi}^{\text{eqII}}(\psi, \mathbf{v}_r, \mathbf{v}_Q) - f_{Pi}^{\text{II}} \right), \quad (7.63)$$

where $\psi = \sum_i f_i$ and $\mathbf{v}_r, \mathbf{v}_Q$ are given by Eq. (7.60). The linear discrete equilibrium distribution is:

$$f_{Pi}^{\text{eqII}} = w_i \psi \left[1 + \frac{\mathbf{v}_r \cdot \mathbf{v}}{c_s^2} + \frac{\mathbf{v}_Q \cdot \dot{\mathbf{Q}}}{2c_s^2} \right]. \quad (7.64)$$

The discrete time space evolution equation is similar to Eq. (4.6). In the \mathbf{r} -space, the bounce-back boundary condition is applied to the top and bottom boundary to mimic wall, and periodic boundary condition is applied at the inlet and outlet. In \mathbf{Q} -space, the periodic boundary condition is applied in both the directions but the contribution in ψ is neglected if it leaves the FENE sphere whose radius is \sqrt{b} . The initial condition on $\psi(\mathbf{r}, \mathbf{Q}, t)$ at every location in \mathbf{r} is similar as given by Eq. (4.9).

7.6.2 Results

It is well known that the flexible polymers in dilute solution migrate across streamlines in pressure-driven flows (Jendrejack *et al.* 2004; Ma & Graham 2005; Park *et al.* 2007). The shear rate stretches and aligns the polymer along the flow direction in a pressure driven flow, reducing its configurational entropy. Thermodynamic arguments therefore suggest that the polymer will migrate to the centerline where the local shear rate is minimum (Usta *et al.* 2006). In order to capture the same effect in the present scheme, a parabolic velocity profile (given by Eq. (7.58)) is imposed. The width of the channel L is chosen to be 10 times larger than the equilibrium extension length l_0 ($L = 10 \times l_0$). The extensibility parameter b is chosen to be 4. We plot the polymer density at a given x as a function of y . As can be seen from the Fig. 7.6, the method is capable of capturing the the phenomena of migration of polymer towards the center of the channel. The figure also depicts that as the Wi increases, the concentration profile becomes sharper, which indicates a stronger migration effect at higher Wi .

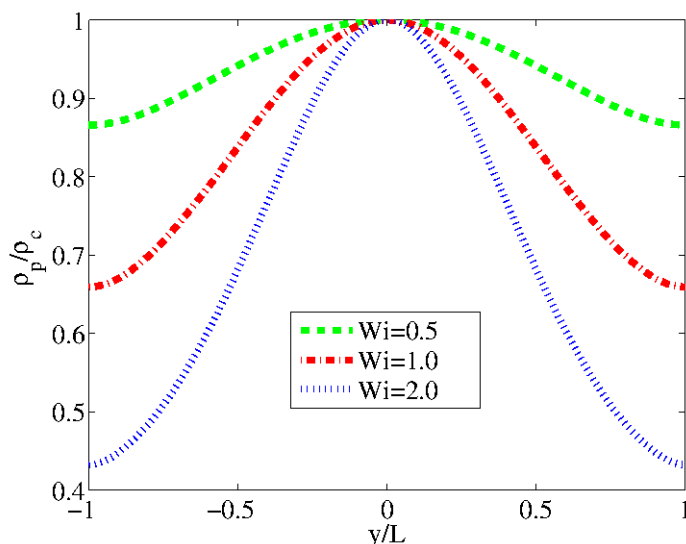


Figure 7.6: The polymer density profiles at $Wi= 0.5, 1$ and 2 in plane Poiseuille flow in a channel of width $L= 10 \times l_0$ and a given x . The polymer density ρ_P is scaled by its value at the centerline of the channel ρ_c . The number of grid point taken in Q -space is 20×20 .

7.7 Conclusion

An extension of the Boltzmann equation for gaseous mixture is proposed for polymer solvent mixture. Motivating from Boltzmann collision description for polymer dumbbell and solvent molecule, a quasi-equilibrium based relaxation mechanism for collision kernel is proposed. The model is shown to reproduce the desired macroscopic equations for the polymer-solvent mixture. Further, simulation of an imposed plane Poiseuille flow is used to show that the method is capable of capturing the effect of shear induced migration in polymers.

7.8 Appendix A: Chapman-Enskog Expansion

In this section, using a multi-scale Chapman-Enskog expansion, it is shown that in the present BGK type collision model (Eq. (7.45)), the correct slow dynamics of configuration distribution function is recovered in the dilute limit for both homogeneous as well as inhomogeneous case. In the Chapman-Enskog multi-scale expansion, f_P^{II} is expanded as

$$f_P^{\text{II}} = f^{\text{eqII}} + \tau f_P^{(1)\text{II}} + \tau^2 f_P^{(2)\text{II}} + \dots \quad \text{such that} \quad \int f^{(n)\text{II}} d\dot{\mathbf{Q}} d\mathbf{v} = 0 \quad \text{for} \quad n > 1, \quad (7.65)$$

The consequence of this is that the non-conserved moments are also expanded in powers of smallest time scale τ_1 around their equilibrium values. For example, the momentum and the second-order moments have the following expansions,

$$\begin{aligned} \mathbf{J}^{\text{r}} &= \mathbf{J}^{\text{req}} + \tau \mathbf{J}^{\text{r}(1)} + \dots \\ \mathbf{J}^{\text{Q}} &= \mathbf{J}^{\text{Qeq}} + \tau \mathbf{J}^{\text{Q}(1)} + \dots \\ \mathbf{P}^{\text{r}} &= \mathbf{P}^{\text{req}} + \tau \mathbf{P}^{\text{r}(1)} + \dots \\ \mathbf{P}^{\text{rQ}} &= \mathbf{P}^{\text{rQeq}} + \tau \mathbf{P}^{\text{rQ}(1)} + \dots \\ \mathbf{P}^{\text{Q}} &= \mathbf{P}^{\text{Qeq}} + \tau \mathbf{P}^{\text{Q}(1)} + \dots \end{aligned} \quad (7.66)$$

where the equilibrium values are:

$$\begin{aligned} \mathbf{J}^{\text{req}} &= \psi(\mathbf{r}, \mathbf{Q}, t) \mathbf{U} + \sum_{\nu} \left(\frac{\mathbf{F}_{\nu}}{\zeta} \psi(\mathbf{r} - \mathbf{R}_{\nu}, \mathbf{Q}, t) \right), \\ \mathbf{J}^{\text{Qeq}} &= \psi(\mathbf{r}, \mathbf{Q}, t) \mathbf{Q} \cdot \frac{\partial \mathbf{U}}{\partial \mathbf{r}} - \psi(\mathbf{r}, \mathbf{Q}, t) \frac{2\mathbf{F}}{\zeta}, \\ \mathbf{P}^{\text{req}} &= \psi(\mathbf{r}, \mathbf{Q}, t) \frac{k_{\text{B}} T}{m_{\text{B}}} \boldsymbol{\delta} + H.O.T., \\ \mathbf{P}^{\text{rQeq}} &= \sum_{\nu} (-1)^{\nu} \psi(\mathbf{r} - \mathbf{R}_{\nu}, \mathbf{Q}, t) \boldsymbol{\delta} + H.O.T., \\ \mathbf{P}^{\text{Qeq}} &= 2\psi(\mathbf{r}, \mathbf{Q}, t) \frac{k_{\text{B}} T}{m_{\text{B}}} \boldsymbol{\delta} + H.O.T., \end{aligned} \quad (7.67)$$

The time derivative is also expanded as:

$$\frac{\partial \phi}{\partial t} = \frac{\partial^{(0)} \phi}{\partial t} + \tau \frac{\partial^{(1)} \phi}{\partial t} + \dots \quad (7.68)$$

The moment equation (7.51) at the zeroth order gives:

$$\begin{aligned} -\mathbf{J}^{\text{r}(1)} &= \left[\frac{\partial}{\partial \mathbf{r}} \cdot \left(\psi(\mathbf{r}, \mathbf{Q}, t) \frac{k_{\text{B}} T}{m_{\text{B}}} \boldsymbol{\delta} \right) + \frac{\partial}{\partial \mathbf{Q}} \mathbf{P}^{\text{rQeq}} \right] + \tau_{1,2} \frac{\partial^{(0)}}{\partial t} \mathbf{J}^{\text{req}}, \\ -\mathbf{J}^{\text{Q}(1)} &= \left[\frac{\partial}{\partial \mathbf{r}} \cdot \mathbf{P}^{\text{rQeq}} + \frac{\partial}{\partial \mathbf{Q}} \cdot \left(2\psi(\mathbf{r}, \mathbf{Q}, t) \frac{k_{\text{B}} T}{m_{\text{B}}} \boldsymbol{\delta} \right) \right] + \tau_{1,2} \frac{\partial^{(0)}}{\partial t} \mathbf{J}^{\text{Qeq}}. \end{aligned} \quad (7.69)$$

The configuration distribution evolution is

$$\frac{\partial}{\partial t} \psi(\mathbf{r}, \mathbf{Q}, t) + \frac{\partial}{\partial \mathbf{r}} (\mathbf{J}^{\text{req}}(\mathbf{r}, \mathbf{Q}, t) + \tau_1 J_\alpha^{\text{r}(1)}) + \frac{\partial}{\partial \mathbf{Q}} (\mathbf{J}^{\text{Qeq}}(\mathbf{r}, \mathbf{Q}, t) + \tau_1 J_\alpha^{\text{Q}(1)}) = 0. \quad (7.70)$$

Homogeneous flow in dilute limit

In dilute limit $\mathbf{U}(\mathbf{r}, t) \approx \mathbf{u}_S(\mathbf{r}, t)$ and for homogeneous flows the elements of velocity gradient tensor $\nabla \mathbf{u}_S$ can be taken as constant. Therefore on integrating the \mathbf{r} degrees of freedom from Eq. (7.70), one gets

$$\frac{\partial}{\partial t} \psi(\mathbf{Q}, t) + \frac{\partial}{\partial \mathbf{Q}} \cdot \left(\psi(\mathbf{Q}, t) \mathbf{Q} \cdot \frac{\partial \mathbf{u}_S}{\partial \mathbf{r}} - \psi(\mathbf{r}, \mathbf{Q}, t) \frac{2\mathbf{F}}{\zeta} + \tau \frac{2k_B T}{m_B} \frac{\partial \psi}{\partial \mathbf{Q}} \right) = 0, \quad (7.71)$$

which is the desired Smoluchowski Equation in the homogeneous flow scenario with $\tau = m_B/\zeta$.

Density diffusion equation in dilute limit

In order to obtain the polymer density equation, \mathbf{Q} degrees are integrated out from the Eq. (7.70), which gives

$$\frac{\partial}{\partial t} \rho_P(\mathbf{r}, t) + \frac{\partial}{\partial \mathbf{r}} \cdot \left[\rho_P \mathbf{U} + \frac{m_B}{\zeta} \frac{\partial}{\partial \mathbf{r}} \Theta_{\alpha\beta} + \tau \int d\mathbf{Q} J_\alpha^{\text{r}(1)} \right] = 0, \quad (7.72)$$

where

$$- \int d\mathbf{Q} J_\alpha^{\text{r}(1)} = \tau \left[\frac{\partial}{\partial r_\beta} \left(\rho_P(\mathbf{r}, t) \frac{k_B T}{m_B} \delta_{\alpha\beta} + \underbrace{\hat{D}_{\alpha\beta}(\mathbf{r}, t)}_{\text{higher-order}} \right) \right] + \frac{\partial^{(0)}}{\partial t} (\rho_P(\mathbf{r}, t) U_\alpha) \quad (7.73)$$

At macroscopic level:

$$\frac{\partial \mathbf{J}}{\partial t} + \frac{\partial}{\partial \mathbf{r}} \cdot \mathbf{P}(\mathbf{r}, t) = \frac{m_B}{\zeta \tau} \frac{\partial}{\partial \mathbf{r}} \cdot \Theta, \quad (7.74)$$

which gives:

$$\begin{aligned} \rho \frac{\partial^{(0)} U_\alpha}{\partial t} + \underbrace{U_\alpha \frac{\partial^{(0)} \rho}{\partial t}}_{\text{higher-order}} &= \frac{\partial}{\partial r_\beta} \left(\frac{m_B}{\zeta \tau} \Theta_{\alpha\beta} - P_{\alpha\beta}^{\text{eq}} \right), \\ \frac{\partial^{(0)} U_\alpha}{\partial t} &= \frac{1}{\rho} \frac{\partial}{\partial r_\beta} \left(\frac{m_B}{\zeta \tau} \Theta_{\alpha\beta} - nk_B T \delta_{\alpha\beta} + H.O.T \right), \\ \frac{\partial^{(0)} U_\alpha}{\partial t} &= \frac{1}{\rho} \frac{\partial}{\partial r_\beta} \left(\frac{m_B}{\zeta \tau} \Theta_{\alpha\beta} - nk_B T \delta_{\alpha\beta} \right). \end{aligned} \quad (7.75)$$

Therefore,

$$\begin{aligned}
-\int d\mathbf{Q} J_\alpha^{r(1)} &= \tau_{1,2} \left[\frac{\partial}{\partial r_\beta} \left(\rho_P(\mathbf{r}, t) \frac{k_B T}{m_B} \delta_{\alpha\beta} \right) \right] + \frac{\rho_P}{\rho} \frac{\partial}{\partial r_\beta} \left(\frac{m_B}{\zeta \tau_{1,2}} \Theta_{\alpha\beta} - n k_B T \delta_{\alpha\beta} \right) + H.O.T \\
&= \frac{\partial}{\partial r_\beta} \left(\rho_P(\mathbf{r}, t) \frac{k_B T}{m_B} \delta_{\alpha\beta} \right) + \underbrace{\frac{\rho_P}{\rho} \frac{\partial}{\partial r_\beta} \left(\frac{m_B}{\zeta \tau_{1,2}} \Theta_{\alpha\beta} - n k_B T \delta_{\alpha\beta} \right)}_{\Xi}
\end{aligned} \tag{7.76}$$

In the dilute limit $\rho_P/\rho \rightarrow 0$, therefore the term $\Xi \rightarrow 0$,

$$-\int d\mathbf{Q} J_\alpha^{r(1)} = \frac{\partial}{\partial r_\beta} \left(\rho_P(\mathbf{r}, t) \frac{k_B T}{m_B} \delta_{\alpha\beta} \right). \tag{7.77}$$

Finally,

$$\frac{\partial}{\partial t} \rho_P(\mathbf{r}, t) + \frac{\partial}{\partial \mathbf{r}_\alpha} \left[\rho_P U_\alpha + \frac{m_B}{\zeta \tau} \frac{\partial}{\partial r_\beta} \Theta_{\alpha\beta} - \tau \frac{\partial}{\partial r_\beta} \left(\rho_P(\mathbf{r}, t) \frac{k_B T}{m_B} \delta_{\alpha\beta} \right) \right] = 0, \tag{7.78}$$

which is the required density equation with $\tau = m_B/\zeta$ (Beris & Mavrantzas 1994; Öttinger & Petrillo 1996; Apostolakis *et al.* 2002).

Chapter 8

Outlook

In this thesis, a BGK type relaxation formulation for the inertial Fokker-Planck equation governing the dynamics of FENE dumbbell in phase space, is proposed. A multi-scale Chapman-Enskog procedure is used to show that this momentum relaxation dynamics in phase space does not affect the slow dynamics in configuration space. A discrete numerical scheme based on LB method is developed for such a formulation which is benchmarked for steady and unsteady shear and extensional flows. This approach is further modified to include an additional inherent physics, that is the effects of hydrodynamic interaction between the beads. The method requires very less computational time as compared to its stochastic counterpart and is at-least an order of magnitude faster than it. Further, the approach is extended for the case of inhomogeneous flows by treating the polymer solution as a two component mixture. A Boltzmann description is used to describe the collision between the polymer dumbbell and solvent molecule. A quasi-equilibrium based relaxation collision kernel is proposed, which reproduces the desired continuum description. In order to benchmark this approach, simulation using one way coupling with plane Poiseuille flow is presented, which show that the method is capable of capturing the shear induced migration in polymers.

The natural extension of this work is to investigate the flows where not only the polymer shares information of the solvent velocity but also the feedback of the polymer dumbbell is communicated to the solvent. For such a case, the realistic memory requirement in three dimensional system of size $100^3 \times 24^3$ is around 5-7 TB. A typical computing cluster of 32 nodes, (assuming 24 cores per node) and assuming memory of 8 GB per core, will have around 6.0 TB RAM. Thus, due to intrinsic parallel nature of current algorithm such simulations are quite feasible.

It is seen that the present numerical scheme is quite fast for a dumbbell model as compared to BD simulations. However, the RAM requirement grows dramatically as the number of beads increase because like any other grid based method, the memory requirement drastically increases with dimension of the problem. This suggests that the application of the present approach is restricted to lower dimensional Fokker Planck Equations which are often encountered in colloidal suspensions, crystallization processes and many other fields.

References

- ABE, T. 1997 Derivation of the lattice Boltzmann method by means of the discrete ordinate method for the Boltzmann equation. *Journal of Computational Physics* **131** (1), 241–246.
- AHLRICHS, P. & DÜNWEIG, B. 1998 Lattice-Boltzmann simulation of polymer-solvent systems. *International Journal of Modern Physics C* **9** (8), 1429–1438.
- AHLRICHS, P. & DÜNWEIG, B. 1999 Simulation of a single polymer chain in solution by combining lattice Boltzmann and molecular dynamics. *The Journal of chemical physics* **111** (17), 8225–8239.
- AIDUN, C. & CLAUSEN, J. 2010 Lattice-Boltzmann method for complex flows. *Annual Review of Fluid Mechanics* **42**, 439–472.
- AMMAR, A. 2010 Lattice Boltzmann method for polymer kinetic theory. *Journal of Non-Newtonian Fluid Mechanics* **165** (19-20), 1082–1092.
- ANDRIES, P., AOKI, K. & PERTHAME, B. 2002 A consistent BGK-type model for gas mixtures. *Journal of Statistical Physics* **106** (5-6), 993–1018.
- ANSUMALI, S., ARCIDIACONO, S., CHIKATAMARLA, S., PRASIANAKIS, N., GORBAN, A. & KARLIN, I. 2007 Quasi-equilibrium lattice Boltzmann method. *The European Physical Journal B-Condensed Matter and Complex Systems* **56** (2), 135–139.
- ANSUMALI, S. & KARLIN, I. V. 2002 Kinetic boundary conditions in the lattice Boltzmann method. *Physical Review E* **66** (2), 026311.
- ANSUMALI, S. & KARLIN, I. V. 2005 Consistent lattice Boltzmann method. *Physical review letters* **95** (26), 260605.
- ANSUMALI, S., KARLIN, I. V. & ÖTTINGER, H. C. 2003 Minimal entropic kinetic models for hydrodynamics. *Europhys. Lett.* **63**, 798–804.
- ANSUMALI, S., KARLIN, I. V. & ÖTTINGER, H. C. 2005 Thermodynamic theory of incompressible hydrodynamics. *Physical review letters* **94** (8), 080602.
- APOSTOLAKIS, M. V., MAVRANTZAS, V. G. & BERIS, A. N. 2002 Stress gradient-induced migration effects in the Taylor–Couette flow of a dilute polymer solution. *Journal of non-newtonian fluid mechanics* **102** (2), 409–445.

- ARCIDIACONO, S., MANTZARAS, J., ANSUMALI, S., KARLIN, I., FROUZAKIS, C. & BOULOUCHOS, K. 2006 Simulation of binary mixtures with the lattice boltzman method. *Physical Review E* **74** (5), 056707.
- BERIS, A. N. & MAVRANTZAS, V. G. 1994 On the compatibility between various macroscopic formalisms for the concentration and flow of dilute polymer solutions. *Journal of Rheology (1978-present)* **38** (5), 1235–1250.
- BHATNAGAR, P., GROSS, E. & KROOK, M. 1954 A model for collision processes in gases. I. Small amplitude processes in charged and neutral one-component systems. *Physical review* **94** (3), 511.
- BIRD, R., CURTISS, C., ARMSTRONG, R. & HASSAGER, O. 1987a *Dynamics of polymeric liquids. Vol. 1.* Wiley.
- BIRD, R., CURTISS, C., ARMSTRONG, R. & HASSAGER, O. 1987b *Dynamics of Polymeric Liquids. Vol. 2.* Wiley.
- BIRD, R., DOTSON, P. & JOHNSON, N. 1980 Polymer solution rheology based on a finitely extensible bead–spring chain model. *Journal of Non-Newtonian Fluid Mechanics* **7** (2-3), 213–235.
- BIRD, R. B., STEWART, W. E. & LIGHTFOOT, E. N. 2007 *Transport phenomena.* John Wiley & Sons.
- BOGHOSIAN, B. M., YEPEZ, J., COVENEY, P. V. & WAGER, A. 2001 Entropic lattice Boltzmann methods. *Proceedings of the Royal Society of London. Series A: Mathematical, Physical and Engineering Sciences* **457** (2007), 717–766.
- BONVIN, J. & PICASSO, M. 1999 Variance reduction methods for CONNFESSIT-like simulations. *Journal of non-newtonian fluid mechanics* **84** (2), 191–215.
- BRUNEAU, C.-H. & SAAD, M. 2006 The 2D lid-driven cavity problem revisited. *Computers & Fluids* **35** (3), 326–348.
- CERCIGNANI, C. 1988 *The Boltzmann equation.* Springer.
- CHAPMAN, S. & COWLING, T. 1991 *The Mathematical Theory of Non-Uniform Gases: An Account of the Kinetic Theory of Viscosity, Thermal Conduction, and Diffusion in Gases.* Cambridge Univ Pr.
- CHAUVIÈRE, C. & LOZINSKI, A. 2004 Simulation of dilute polymer solutions using a Fokker–Planck equation. *Computers & Fluids* **33** (5), 687–696.
- CHEN, S. & DOOLEN, G. 1998 Lattice Boltzmann method for fluid flows. *Annual Review of Fluid Mechanics* **30** (1), 329–364.
- CHIKATAMARLA, S., ANSUMALI, S. & KARLIN, I. 2006 Entropic lattice Boltzmann models for hydrodynamics in three dimensions. *Physical Review Letters* **97** (1), 10201.

- CHILCOTT, M. & RALLISON, J. 1988 Creeping flow of dilute polymer solutions past cylinders and spheres. *Journal of Non-Newtonian Fluid Mechanics* **29**, 381–432.
- CHOKSHI, P. & KUMARAN, V. 2007 Stability of the flow of a viscoelastic fluid past a deformable surface in the low Reynolds number limit. *Physics of Fluids (1994-present)* **19** (10), 104103.
- CHRISTAINSEN, R. & BIRD, R. 1977 Dilute solution rheology: experimental results and finitely extensible nonlinear elastic dumbbell theory. *Journal of Non-Newtonian Fluid Mechanics* **3** (2), 161–177.
- CURTISS, C. & BIRD, R. B. 1996 Multicomponent diffusion in polymeric liquids. *Proceedings of the National Academy of Sciences* **93** (15), 7440–7445.
- DE GENNES, P. 1974 Coil-stretch transition of dilute flexible polymers under ultrahigh velocity gradients. *The Journal of Chemical Physics* **60** (12), 5030–5042.
- DEGOND, P., LIU, H. *et al.* 2009 Kinetic models for polymers with inertial effects. *Networks and Heterogeneous Media* **4** (4), 625–647.
- DELLAR, P. J. 2002 Nonhydrodynamic modes and a priori construction of shallow water lattice Boltzmann equations. *Physical Review E* **65** (3), 036309.
- DIMITROPOULOS, C., DUBIEF, Y., SHAQFEH, E., MOIN, P. & LELE, S. 2005 Direct numerical simulation of polymer-induced drag reduction in turbulent boundary layer flow. *Physics of Fluids* **17**, 011705.
- DOI, M. & EDWARDS, S. 1988 *The Theory of Polymer Dynamics*, , vol. 73. Oxford University Press, USA.
- DOI, M. & ONUKI, A. 1992 Dynamic coupling between stress and composition in polymer solutions and blends. *Journal de Physique II* **2** (8), 1631–1656.
- DOYLE, P., SHAQFEH, E. & GAST, A. 1997 Dynamic simulation of freely draining flexible polymers in steady linear flows. *Journal of Fluid Mechanics* **334** (1), 251–291.
- DOYLE, P. S., SHAQFEH, E. S., MCKINLEY, G. H. & SPIEGELBERG, S. H. 1998 Relaxation of dilute polymer solutions following extensional flow. *Journal of non-newtonian fluid mechanics* **76** (1), 79–110.
- FEIGL, K., LASO, M. & ÖTTINGER, H. C. 1995 CONNFFESSIT approach for solving a two-dimensional viscoelastic fluid problem. *Macromolecules* **28** (9), 3261–3274.
- FREDRICKSON, G. H. 2002 Dynamics and rheology of inhomogeneous polymeric fluids: A complex Langevin approach. *The Journal of chemical physics* **117** (14), 6810–6820.
- GARZÓ, V., SANTOS, A. & BREY, J. 1989 A kinetic model for a multicomponent gas. *Physics of Fluids A: Fluid Dynamics (1989-1993)* **1** (2), 380–383.

- GHOSH, I., MCKINLEY, G. H., BROWN, R. A. & ARMSTRONG, R. C. 2001 Deficiencies of FENE dumbbell models in describing the rapid stretching of dilute polymer solutions. *Journal of Rheology* **45** (3), 721–758.
- GIRAUD, L., D'HUMIÈRES, D. & LALLEMAND, P. 1998 A lattice Boltzmann model for Jeffreys viscoelastic fluid. *EPL (Europhysics Letters)* **42**, 625.
- GOLDMAN, E. & SIROVICH, L. 2004 Equations for gas mixtures. *Physics of Fluids (1958-1988)* **10** (9), 1928–1940.
- GORBAN, A. N. & KARLIN, I. V. 1994 General approach to constructing models of the Boltzmann equation. *Physica A: Statistical Mechanics and its Applications* **206** (3), 401–420.
- GRAD, H. 1949 On the kinetic theory of rarefied gases. *Communications on Pure and Applied Mathematics* **2** (4), 331–407.
- GROSS, E. P. & KROOK, M. 1956 Model for collision processes in gases: Small-amplitude oscillations of charged two-component systems. *Physical Review* **102** (3), 593.
- HAMEL, B. B. 1965 Kinetic model for binary gas mixtures. *Physics of Fluids (1958-1988)* **8** (3), 418–425.
- HE, X. & LUO, L.-S. 1997*a* A priori derivation of the lattice Boltzmann equation. *Physical Review E* **55** (6), R6333.
- HE, X. & LUO, L.-S. 1997*b* Theory of the lattice Boltzmann method: From the Boltzmann equation to the lattice Boltzmann equation. *Physical Review E* **56** (6), 6811.
- HELFAIND, E. & FREDRICKSON, G. H. 1989 Large fluctuations in polymer solutions under shear. *Physical review letters* **62** (21), 2468.
- HERRCHEN, M. & ÖTTINGER, H. C. 1997 A detailed comparison of various FENE dumbbell models. *Journal of Non-Newtonian Fluid Mechanics* **68** (1), 17–42.
- HINCH, E. J. 1977 Mechanical models of dilute polymer solutions in strong flows. *Physics of Fluids* **20**, S22.
- HUA, C., SCHIEBER, J. & VENERUS, D. 1999 Segment connectivity, chain-length breathing, segmental stretch, and constraint release in reptation models. iii. shear flows. *Journal of Rheology* **43**, 701.
- HULSEN, M., VAN HEEL, A. & VAN DEN BRULE, B. 1997 Simulation of viscoelastic flows using brownian configuration fields. *Journal of Non-Newtonian Fluid Mechanics* **70** (1), 79–101.
- HUR, J. S., SHAQFEH, E. S. & LARSON, R. G. 2000 Brownian dynamics simulations of single DNA molecules in shear flow. *Journal of rheology* **44**, 713.
- ISPOLATOV, I. & GRANT, M. 2002 Lattice Boltzmann method for viscoelastic fluids. *Physical Review E* **65** (5), 56704.

- JAIN, A., SUNTHAR, P., DUENWEG, B. & PRAKASH, J. R. 2012 Optimization of a Brownian-dynamics algorithm for semidilute polymer solutions. *Physical Review E* **85** (6), 066703.
- JENDREJACK, R., SCHWARTZ, D., DE PABLO, J. & GRAHAM, M. 2004 Shear-induced migration in flowing polymer solutions: Simulation of long-chain DNA in microchannels. *The Journal of Chemical Physics* **120**, 2513.
- JENDREJACK, R. M., GRAHAM, M. D. & DE PABLO, J. J. 2000 Hydrodynamic interactions in long chain polymers: Application of the Chebyshev polynomial approximation in stochastic simulations. *The Journal of Chemical Physics* **113** (7), 2894–2900.
- JENDREJACK, R. M., DE PABLO, J. J. & GRAHAM, M. D. 2002 Stochastic simulations of DNA in flow: Dynamics and the effects of hydrodynamic interactions. *The Journal of chemical physics* **116** (17), 7752–7759.
- JOU, D., CASAS-VÁZQUEZ, J. & LEBON, G. 1996 *Extended irreversible thermodynamics*. Springer.
- KARLIN, I. V., FERRANTE, A. & ÖTTINGER, H. C. 1999 Perfect entropy functions of the lattice Boltzmann Method. *Europhys. Lett.* **47**, 182–188.
- KEUNINGS, R. 1997 On the peterlin approximation for finitely extensible dumbbells. *Journal of Non-Newtonian Fluid Mechanics* **68** (1), 85–100.
- KIRKWOOD, J. G. & RISEMAN, J. 1948 The intrinsic viscosities and diffusion constants of flexible macromolecules in solution. *The Journal of Chemical Physics* **16** (6), 565–573.
- KOPPOL, A., SURESHKUMAR, R. & KHOMAMI, B. 2007 An efficient algorithm for multi-scale flow simulation of dilute polymeric solutions using bead-spring chains. *Journal of Non-Newtonian Fluid Mechanics* **141** (2), 180–192.
- KRAMERS, H. 1944 Het gedrag van macromoleculen in een stroomende vloeistof. *Physica* **11** (1), 1–19.
- KRAMERS, H. A. 1946 The behavior of macromolecules in inhomogeneous flow. *The Journal of Chemical Physics* **14** (7), 415–424.
- LADD, A. 1994 Numerical simulations of particulate suspensions via a discretized Boltzmann equation. part 2. numerical results. *Journal of Fluid Mechanics* **271** (1), 311–339.
- LARSON, R. 1988 *Constitutive Equations for Polymer melts and Solutions*. Butterworths, 1988,.
- LASO, M. & ÖTTINGER, H. C. 1993 Calculation of viscoelastic flow using molecular models: the CONNFESSIT approach. *Journal of Non-Newtonian Fluid Mechanics* **47**, 1–20.
- LEVERMORE, C., WONG, J. & POMRANING, G. 1988 Renewal theory for transport processes in binary statistical mixtures. *Journal of mathematical physics* **29** (4), 995–1004.

- LIELENS, G., HALIN, P., JAUMAIN, I., KEUNINGS, R. & LEGAT, V. 1998 New closure approximations for the kinetic theory of finitely extensible dumbbells. *Journal of Non-Newtonian Fluid Mechanics* **76** (1-3), 249–279.
- LIELENS, G., KEUNINGS, R. & LEGAT, V. 1999 The FENE-L and FENE-LS closure approximations to the kinetic theory of finitely extensible dumbbells. *Journal of Non-Newtonian Fluid Mechanics* **87** (2-3), 179–196.
- LOZINSKI, A. & CHAUVIÈRE, C. 2003 A fast solver for fokker–planck equation applied to viscoelastic flows calculations: 2d FENE model. *Journal of Computational Physics* **189** (2), 607–625.
- MA, H. & GRAHAM, M. 2005 Theory of shear-induced migration in dilute polymer solutions near solid boundaries. *Physics of Fluids* **17**, 083103.
- MAVRANTZAS, V. G. & BERIS, A. N. 1992 Modeling of the rheology and flow-induced concentration changes in polymer solutions. *Physical review letters* **69** (2), 273.
- MAZUR, P. & DE GROOT, S. R. 1963 *Non-equilibrium thermodynamics*. North-Holland.
- MELCHIONNA, S., SUCCI, S. & HANSEN, J.-P. 2006 Simulation of single-file ion transport with the lattice fokker-planck equation. *Physical Review E* **73** (1), 017701.
- MELCHIOR, M. & ÖTTINGER, H. C. 1996 Variance reduced simulations of polymer dynamics. *The Journal of Chemical Physics* **105**, 3316.
- MILNER, S. 1991 Hydrodynamics of semidilute polymer solutions. *Physical review letters* **66** (11), 1477.
- MILNER, S. T. 1993 Dynamical theory of concentration fluctuations in polymer solutions under shear. *Physical Review E* **48** (5), 3674.
- MORONI, D., HANSEN, J.-P., MELCHIONNA, S. & SUCCI, S. 2006a On the use of lattice Fokker-Planck models for hydrodynamics. *EPL (Europhysics Letters)* **75** (3), 399.
- MORONI, D., ROTENBERG, B., HANSEN, J., SUCCI, S. & MELCHIONNA, S. 2006b Solving the Fokker-Planck kinetic equation on a lattice. *Physical Review E* **73** (6), 66707.
- NOURGALIEV, R., DINH, T., THEOFANOUS, T. & JOSEPH, D. 2003 The lattice Boltzmann equation method: theoretical interpretation, numerics and implications. *International Journal of Multiphase Flow* **29** (1), 117–169.
- ÖTTINGER, H., VAN DEN BRULE, B. & HULSEN, M. 1997 Brownian configuration fields and variance reduced CONNFESSIT. *Journal of non-newtonian fluid mechanics* **70** (3), 255–261.
- ÖTTINGER, H. C. 1985 Consistently averaged hydrodynamic interaction for Rouse dumbbells in steady shear flow. *The Journal of chemical physics* **83** (12), 6535–6536.
- ÖTTINGER, H. C. 1987 Consistently averaged hydrodynamic interaction for Rouse dumbbells: translational diffusivity. *The Journal of chemical physics* **87** (10), 6185–6190.

- ÖTTINGER, H. C. 1987 A model of dilute polymer solutions with hydrodynamic interaction and finite extensibility. i. basic equations and series expansions. *Journal of Non-Newtonian Fluid Mechanics* **26** (2), 207–246.
- ÖTTINGER, H. C. 1994 Variance reduced brownian dynamics simulations. *Macromolecules* **27** (12), 3415–3423.
- ÖTTINGER, H. C. 1996 *Stochastic Processes in Polymeric fluids: Tools and Examples for Developing Simulation Algorithms*. Springer Berlin,, New York.
- ÖTTINGER, H. C. & PETRILLO, F. 1996 Kinetic theory and transport phenomena for a dumbbell model under nonisothermal conditions. *Journal of Rheology (1978-present)* **40** (5), 857–874.
- PARK, J., BRICKER, J. M. & BUTLER, J. E. 2007 Cross-stream migration in dilute solutions of rigid polymers undergoing rectilinear flow near a wall. *Physical Review E* **76** (4), 040801.
- PHAM, T., SCHILLER, U., PRAKASH, J. & DÜNWEIG, B. 2009 Implicit and explicit solvent models for the simulation of a single polymer chain in solution: Lattice Boltzmann versus brownian dynamics. *The Journal of Chemical Physics* **131**, 164114.
- QIAN, Y., D’HUMIERES, D. & LALLEMAND, P. 1992 Lattice BGK models for navier-stokes equation. *EPL (Europhysics Letters)* **17** (6), 479.
- RISKEN, H. 1996 *The Fokker-Planck equation: Methods of Solution and Applications*, , vol. 18. Springer Verlag.
- ROTNE, J. & PRAGER, S. 1969 Variational treatment of hydrodynamic interaction in polymers. *The Journal of Chemical Physics* **50**, 4831.
- RUDISILL, J. & CUMMINGS, P. 1992 Brownian dynamics simulation of model polymer fluids in shear flow. i. Dumbbell models. *Journal of non-newtonian fluid mechanics* **41** (3), 275–288.
- SCHIEBER, J. & ÖTTINGER, H. C. 1988 The effects of bead inertia on the rouse model. *The Journal of Chemical Physics* **89** (11), 6972–6981.
- SCHROEDER, C., BABCOCK, H., SHAQFEH, E. & CHU, S. 2003 Observation of polymer conformation hysteresis in extensional flow. *Science* **301** (5639), 1515–1519.
- SHAN, X. & HE, X. 1998 Discretization of the velocity space in the solution of the Boltzmann equation. *Physical Review Letters* **80** (1), 65–68.
- SHET, A. G., SIDDHARTH, K., SORATHIYA, S. H., DESHPANDE, A. M., SHERLEKAR, S. D., KAUL, B. & ANSUMALI, S. 2013a On vectorization for Lattice Based Simulations. *International Journal of Modern Physics C* **24** (12).
- SHET, A. G., SORATHIYA, S. H., KRITHIVASAN, S., DESHPANDE, A. M., KAUL, B., SHERLEKAR, S. D. & ANSUMALI, S. 2013b Data structure and movement for lattice-based simulations. *Physical Review E* **88** (1), 013314.

- SINGH, S., KRITHIVASAN, S., KARLIN, I. V., SUCCI, S. & ANSUMALI, S. 2013a Energy conserving lattice Boltzmann models for incompressible flow simulations. *Commun Comput Phys* **13**, 603–13.
- SINGH, S., SUBRAMANIAN, G. & ANSUMALI, S. 2011 A lattice Boltzmann method for dilute polymer solutions. *Philosophical Transactions of the Royal Society A: Mathematical, Physical and Engineering Sciences* **369** (1944), 2301–2310.
- SINGH, S., SUBRAMANIAN, G. & ANSUMALI, S. 2013b Lattice fokker planck for dilute polymer dynamics. *Physical Review E* **88** (1), 013301.
- SOMASI, M., KHOMAMI, B., WOO, N., HUR, J. & SHAQFEH, E. 2002 Brownian dynamics simulations of bead-rod and bead-spring chains: numerical algorithms and coarse-graining issues. *Journal of Non-Newtonian Fluid Mechanics* **108** (1), 227–255.
- SUBRAMANIAN, G. & BRADY, J. 2004 Multiple scales analysis of the Fokker–Planck equation for simple shear flow. *Physica A: Statistical Mechanics and its Applications* **334** (3), 343–384.
- SUCCI, S. 2001 *The Lattice Boltzmann method for Fluid Dynamics and Beyond*. Oxford University Press, USA.
- SUCCI, S., BENZI, R. & VERGASSOLA, M. 1992 The lattice Boltzmann-equation -theory and applications. *phys. Rep.* **222**, 145–197.
- SUCCI, S., KARLIN, I. V. & CHEN, H. 2002 Colloquium: Role of the H theorem in lattice Boltzmann hydrodynamic simulations. *Reviews of Modern Physics* **74** (4), 1203.
- SURESHKUMAR, R., BERIS, A. & HANDLER, R. 1997 Direct numerical simulation of the turbulent channel flow of a polymer solution. *Physics of Fluids* **9**, 743.
- TITULAER, U. M. 1978 A systematic solution procedure for the Fokker-Planck equation of a Brownian particle in the high-friction case. *Physica A: Statistical Mechanics and its Applications* **91** (3), 321–344.
- USTA, O., BUTLER, J. & LADD, A. 2006 Flow-induced migration of polymers in dilute solution. *Physics of fluids* **18**, 031703.
- VAN KAMPEN, N. G. 1992 *Stochastic processes in physics and chemistry*, , vol. 1. North holland.
- VIRK, P. 1975 Drag reduction fundamentals. *AIChE Journal* **21** (4), 625–656.
- WAGNER, A. 2001 Derivation of a non-objective Oldroyd model from the Boltzmann equation. *Arxiv preprint cond-mat/0105067* .
- WARNER, H. R. 1972 Kinetic theory and rheology of dilute suspension of finitely extendible dumbbells. *Industrial & Engineering Chemistry Fundamentals* **11**, 379–387.

- WEDGEWOOD, L. & ÖTTINGER, H. 1988 A model of dilute polymer solutions with hydrodynamic interaction and finite extensibility. ii. Shear flows. *Journal of non-newtonian fluid mechanics* **27** (2), 245–264.
- YAMAKAWA, H. 1970 Transport properties of polymer chains in dilute solution: hydrodynamic interaction. *The Journal of Chemical Physics* **53** (1), 436–443.
- YUDISTIAWAN, W. P., KWAK, S. K., PATIL, D. V. & ANSUMALI, S. 2010 Higher-order Galilean-invariant lattice Boltzmann model for microflows: Single-component gas. *Phys. Rev. E* **82**, 046701.
- ZYLKA, W. & ÖTTINGER, H. C. 1989 A comparison between simulations and various approximations for Hookean dumbbells with hydrodynamic interaction. *The Journal of chemical physics* **90** (1), 474–480.

Curriculum Vitae

Personal

- Name: Shiwani Singh
- Sex: Female
- Nationality: Indian
- Date of birth: 25/04/1987

Education

- **Ph. D** 2009-2015
 - Title: Lattice Fokker Planck Method for Complex Fluids
 - Advisor: Prof. Santosh Ansumali
 - Department: Engineering Mechanics Unit
 - Institute: Jawaharlal Nehru Centre for Advanced Scientific Research, Bangalore (India)
- **M.Sc.** in Physical Sciences 2007-2009
 - Department: School of Physical Sciences
 - Institute: Jawaharlal Nehru University, New Delhi (India)
- **B.Sc.** 2004-2007
 - Department: Physical Science
 - Institute: Lucknow University (India)

List of publications

- **Shiwani Singh**, Ganesh Subramanian and Santosh Ansumali. Lattice Fokker Planck for dilute polymer dynamics.
Phys. Rev. E **88**, 013301 (2013)
- Chakradhar Thantanapally, **Shiwani Singh**, Dhiraj V Patil, Sauro Succi, and Santosh Ansumali. Quasi-equilibrium lattice Boltzmann models with tunable Prandtl number for incompressible hydrodynamics.
Int. J. Mod. Phys. C **24**, 1340004 (2013)
- **Shiwani Singh**, Siddharth Krithivasan, Iliya V. Karlin, Sauro Succi and Santosh Ansumali. Energy Conserving Lattice Boltzmann Models for Incompressible Flow Simulations.
Commun. Comput. Phys. **13**, 603-613 (2013)

- **Shiwani Singh**, Ganesh Subramanian and Santosh Ansumali. A lattice Boltzmann Method for dilute polymer solutions.
Phil. Trans. Roy. Soc. A **369**, 2301 (2011)